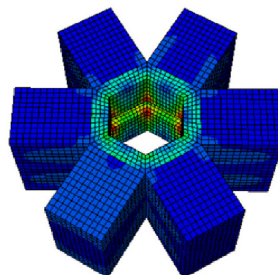
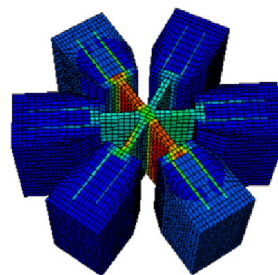


Ragnhild Myrnes
Kristin Kilvik Skeide

Parametric Structural Analysis and Development of Aluminium Connectors in Timber Gridshells

Master's thesis in Civil and Environmental Engineering
Supervisor: Anders Rønnquist, Steinar H. Dyvik, Marcin Luczkowski
June 2020



Ragnhild Myrnes
Kristin Kilvik Skeide

Parametric Structural Analysis and Development of Aluminium Connectors in Timber Gridshells

Master's thesis in Civil and Environmental Engineering
Supervisor: Anders Rønnquist, Steinar H. Dyvik, Marcin Luczkowski
June 2020

Norwegian University of Science and Technology
Faculty of Engineering
Department of Structural Engineering





MASTER THESIS 2020

SUBJECT AREA: Conceptual Structural Design	DATE: 10.06.2020	NO. OF PAGES: XIV + 144
---	---------------------	----------------------------

TITLE:

Parametric Structural Analysis and Development of Aluminium Connectors in Timber Gridshells

Parametrisk Konstruksjonsanalyse og Utvikling av Aluminiumsforbindere i Gitterskall av Tre

BY:

Kristin Kilvik Skeide and Ragnhild Myrnes



SUMMARY:

Gridshell structures have traditionally been constructed with steel members welded together or bolted to steel connectors. Due to matters such as environmental aspects, developments of timber products and an increased focus on timber as a building material, both regarding aesthetics and material qualities, more gridshells are now being constructed with timber products. The design of the connections in gridshells can be complicated due to loading conditions and comprehensive geometries. This thesis investigates the possibility of developing aluminium connectors as a substitute to steel connectors, since aluminium is recyclable, has low density and is easier to form compared to steel.

Finite element analyses of two gridshell connectors in aluminium are presented. These are the "Glued Finger" (GF) connector, where the material meets in the centre, and the "Split Ring" (SR) connector, where the material is placed around the centre. Two main design challenges have been identified and checked structurally: the core part, and the timber-to-metal part. To make the design process of gridshell connectors more effective, finite element analyses (FEA) in a parametric environment have been explored. Custom components in the Rhino/Grasshopper software have successfully been developed to analyse the structural behaviour of connectors parametrically. The components enable the designer to make a parametric finite element 3D model in Rhino/Grasshopper, and scripts the input file (INP), which can be directly imported as a model to be submitted for analysis in Abaqus.

From the results in the parametric structural analysis, it was concluded that the SR connector is the best design regarding volume efficiency and thus also cost efficiency. When assessing whether the connectors are susceptible to buckling and how they handle eccentric loads, the SR connector seems to be the better design due to its high bending stiffness about both axes. To improve the performance of the GF connector regarding eccentric loads and buckling, it is proposed to add plates perpendicular to the middle of its inner plates. Nevertheless, the rotational stiffness of the GF joints is found to be about twice as high as the rotational stiffness of the SR joints. Furthermore, the GF connector is argued to be the most practical design when assembling the structure at building site, as it consists of less parts that connects the timber members together.

RESPONSIBLE TEACHER: Nils Erik Anders Rønnquist

SUPERVISOR(S): Steinar Hillersøy Dyvik and Marcin Luczkowski

CARRIED OUT AT: Department of Structural Engineering, NTNU, Trondheim

Abstract

Gridshell structures have traditionally been constructed with steel members welded together or bolted to steel connectors. Due to matters such as environmental aspects, developments of timber products and an increased focus on timber as a building material, both regarding aesthetics and material qualities, more gridshells are now being constructed with timber products. The design of the connections in gridshells can be complicated due to loading conditions and comprehensive geometries. This thesis investigates the possibility of developing aluminium connectors as a substitute to steel connectors, since aluminium is recyclable, has low density and is easier to form compared to steel.

Finite element analyses of two gridshell connectors in aluminium are presented. These are the “Glued Finger” (GF) connector, where the material meets in the centre, and the “Split Ring” (SR) connector, where the material is placed around the centre. Two main design challenges have been identified and checked structurally: the core part, and the timber-to-metal part. To make the design process of gridshell connectors more effective, finite element analyses (FEA) in a parametric environment have been explored. Custom components in the Rhino/Grasshopper software have successfully been developed to analyse the structural behaviour of connectors parametrically. The components enable the designer to make a parametric finite element 3D model in Rhino/Grasshopper, and scripts the input file (INP), which can be directly imported as a model to be submitted for analysis in Abaqus.

From the results in the parametric structural analysis, it was concluded that the SR connector is the best design regarding volume efficiency and thus also cost efficiency. When assessing whether the connectors are susceptible to buckling and how they handle eccentric loads, the SR connector seems to be the better design due to its high bending stiffness about both axes. To improve the performance of the GF connector regarding eccentric loads and buckling, it is proposed to add plates perpendicular to the middle of its inner plates. Nevertheless, the rotational stiffness of the GF joints is found to be about twice as high as the rotational stiffness of the SR joints. Furthermore, the GF connector is argued to be the most practical design when assembling the structure at building site, as it consists of less parts that connects the timber members together.

Sammendrag

Gitterskallkonstruksjoner har tradisjonelt blitt bygd opp av rette stålelementer, sveiset eller boltet til stålforbindere. På grunn av miljøaspekter, utvikling av trelastprodukter, økt fokus på tre som byggemateriale både med hensyn til estetikk og materialegenskaper, bygges flere gitterskall nå i tre. Design av forbindere i gitterskall kan være komplisert på grunn av lastforholdene og omfattende geometrier. Med bakgrunn i at aluminium er et resirkulerbart materiale, har lav tetthet og er lettere å forme sammenlignet med stål, undersøkes muligheten for å utvikle forbindere i aluminium som en erstatning til forbindere i stål.

Elementanalyser av to gitterskallforbindere i aluminium er presentert. Den ene er “Glued Finger” (GF)-forbinderen, hvor alt materialet møtes i senteret. Den andre er “Split Ring” (SR)-forbinderen, hvor alt materialet er flyttet ut fra senteret. To hovedutfordringer med designet er identifisert og dimensjonert; kjernedelen og tre-til-metall-delen. For å gjøre dimensjoneringsprosessen av gitterskallforbindere mer effektiv, har elementanalyser blitt etterforsket i et parametrisk miljø. Tilpassede komponenter har med suksess blitt utviklet i programmene Rhino/Grasshopper, for å analysere den konstruksjonsmessige oppførselen til forbindere parametrisk. Komponentene muliggjør at designeren kan lage parametriske elementmodeller i 3D i Rhino/Grasshopper, og genererer input-filen (INP) som kan importeres som en modell og deretter sendes inn for analyse direkte i Abaqus.

Fra resultatene i den parametriske konstruksjonsanalysen ble det konkludert med at SR-forbinderen har det beste designet med tanke på volumeffektivitet og dermed også kostnadseffektivitet. Ved vurdering av om forbindere er utsatt for knekking og hvordan de takler eksentriske laster, ser SR-forbinderen ut til å være et bedre design, på grunn av dens høye bøyestivhet om begge akser. For å forbedre opptreden til GF-forbinderen i forhold til eksentriske laster og knekking, er det foreslått å legge til plater rettvisklet på midten av de indre platene. Derimot er rotasjonsstivheten til GF-forbinderen funnet å være rundt dobbelt så høy som rotasjonsstivheten til SR-forbinderen. Videre er det argumentert for at GF-forbinderen ser ut til å ha det mest praktiske designet ved montering av konstruksjonen på byggeplass, siden den består av færre deler som skal binde sammen treelementene.

Preface and acknowledgements

This master thesis concludes our Master of Science degree and is written in the spring semester of 2020 on behalf of the Department of Structural Engineering at the Norwegian University of Science and Technology (NTNU). The process of writing our thesis has been very interesting and educational as we have learnt a lot about the topics that are discussed. It has been particularly inspiring to work with, and get more insight into, parametric design through visual programming, as it was one of the reasons why we chose to specialise in the field of Conceptual Structural design. As we had limited prior experience of programming, this is one of the subject fields where we have increased our knowledge the most.

We start by thanking Professor Nils Erik Anders Rønnquist for introducing us to the subject field of Conceptual Structural Design and for his feedback and comments on our structural analyses. Next, we express our sincere gratitude to PhD candidate Steinar Hillersøy Dyvik for introducing us to the topic of aluminium connectors in timber gridshells and his continuous guidance throughout the whole semester. It has been interesting and educational to have gotten an insight to the problem from an architectural point of view. Furthermore, we give special thanks to Marcin Luczkowski for setting the course for us in our thesis, keeping us on the right track and for finding time for us in his busy schedule as his help has been greatly appreciated.

In addition, we thank Haris Stamatopoulos for giving us valuable information about newly performed research within timber-metal connections, and we also thank Katarzyna Ostapska for introducing us to important aspects in finite element analyses of timber structures. Furthermore, we thank Bunji Izumi for pointing out important concerns regarding structural connections. In the end, we have to thank each other for inspiring and motivating one another to work hard and learn more throughout the whole semester. Thanks to our families and friends for the pinned support to keep us grounded but allowing for some flexibility. No thanks to the corona virus.

Trondheim, June 10, 2020

Kristin Kilvik Skeide

Kristin Kilvik Skeide

Ragnhild Myrnes

Ragnhild Myrnes

Problem description

The topic of timber gridshells with aluminium connectors is part of the PhD project of Steinar Hillersøy Dyvik. Three master theses, including this, have investigated relevant and related aspects of the topic. One group, consisting of Håkon J. K. Brun, Erlend Hansen and Edvard H. Zimmer, has investigated design tools and optimisation options for discrete timber gridshells in a parametric environment. The second group, consisting of Sverre M. Haakonsen, Daniel M. Instanes and June-Marie J. Esjeholm, has implemented Thrust network analysis (TNA) in Grasshopper and tested the method's performance on discrete gridshells, especially regarding the global stability and how it is affected by the joint's stiffness. This thesis, on the other hand, investigates the connector itself, the connection between the timber and the connector, and how this can be analysed with finite element modelling parametrically.

The aim of this thesis is to present Finite Element Analysis (FEA) of the GF and SR connector, which is developed by Steinar Hillersøy Dyvik, and analyse different dimensions of the connectors by changing the geometrical parameters, to find an optimal shape. To provide numerical FEA, Abaqus CAE is to be used. It is also desired to compare the two connector designs by looking at their strengths and weaknesses, and to get an understanding of how stresses will be distributed in each design.

Furthermore, a goal is also to develop components in Grasshopper so the structural behaviour of connectors can be analysed rapidly, this to make the design process of gridshell connectors more effective and part of the gridshell design as a whole. Current add-ons in Grasshopper does not provide the possibility to perform FEA of 3D solids. To construct a model in Abaqus can be time consuming since one manually need to define all aspects of the model, step by step. Therefore, Abaqus is not well suited for parametric structural analyses. Thus, to create a link between the Rhino/Grasshopper environment and Abaqus so that one in an efficient way can analyse 3D models parametrically, is favourable.

Contents

Abstract	I
Sammendrag	II
Preface and acknowledgements	III
Problem description	IV
List of figures	VIII
List of tables	XII
Abbreviations and acronyms	XIV
1 Introduction	1
1.1 Timber gridshells	1
1.2 Aluminium structural design	3
1.3 Design of connections in timber gridshells	6
1.4 Designing connectors for the British Museum Great Court as a timber gridshell	12
1.5 Software for parametric design and structural analyses	16
2 Comparing connectors in aluminium and steel	18
2.1 Necessary cross-section of connector in aluminium	19
2.2 Necessary cross-section of connector in steel	21
3 Structural design of timber-to-metal connections	24
3.1 Difference in weight of connector in aluminium and steel	24
3.2 Necessary glue surface in Glued Finger connector	33
3.3 Diameter and penetration length of threaded rods in Split Ring connector	38
4 Benchmarks - comparing structural behaviours	45
4.1 Case 1 - Cantilever	47
4.2 Case 2 - Column	50
4.3 Case 3 - Bonded connection	52
4.4 Case 4 - Bonded connection with eccentricity	54
4.5 Case 5 - Screwed connection	57

5	Establishing a parametric finite element model	59
5.1	The input file	59
5.2	FEM with Grasshopper components	62
6	Parametric finite element analyses of connectors	81
6.1	Glued Finger connector	82
6.2	Split Ring connector	100
6.3	Comparing necessary volumes of Glued Finger and Split Ring connector	104
6.4	Comparing rotational stiffness of Glued Finger and Split Ring joints . .	108
7	Discussion	113
7.1	Choice of material - steel vs. aluminium	113
7.2	The efficiency and functionality of the parametric workflow	113
7.3	Structural behaviour of Glued Finger connector	115
7.4	Structural behaviour of Split Ring connector	116
7.5	Comparing the designs of Glued Finger and Split Ring connector . . .	117
8	Conclusion	120
9	Recommendations for further work	122
	Bibliography	124
	Appendices	128
A	Comparing connectors in aluminium and steel	128
A.1	Detailed calculation of necessary aluminium cross-section	128
A.2	Detailed calculation of necessary steel cross-section	129
B	Structural design of timber-to-metal connections	130
B.1	Difference in weight of connector in aluminium and steel	130
B.2	Necessary glue surface in Glued Finger connector	132
B.3	Diameter and penetration length of threaded rods in Split Ring connector	133
C	Benchmarks - comparing structural behaviours	134
C.1	Case 1 - Cantilever	134
C.2	Case 2 - Column	137

D Parametric FEM model examples	140
D.1 I-Beam	140
D.2 Shell	142
E Grasshopper files attached	144
E.1 Components	144
E.2 ModelExamples.gh	144
E.3 GFConnector.gh	144
E.4 SRConnector.gh	144

List of figures

1.1	Discrete timber gridshell under construction at Crossrail Place in London, Photo: ©Arup (2013)	2
1.2	Trondheim Pavilion, Photo: Labonnote (2015)	2
1.3	Printshell, Photo: Labonnote (2016)	6
1.4	Different inclinations and angles of the connecting members in free form gridshells. Figure: Steinar Hillersøy Dyvik	7
1.5	Examples of end-face connectors	8
1.6	Examples of splice connectors	9
1.7	Queen Elisabeth II Great Court, British Museum (London UK)	13
1.8	Solution proposals for aluminium connectors in timber gridshells.	14
1.9	Similar connector design concepts	14
1.10	Parametric model in GH with geometries displayed in Rhino for different input values	17
2.1	Necessary cross-section of aluminium connector	21
2.2	Comparison of the dimensions of necessary cross-sections for a connector consisting of steel and a connector consisting of aluminium	23
3.1	Connector design for weight calculations, (Dome of visions, 2017)	25
3.2	Connector dimensions of one metal plate	26
3.3	Failure modes for steel-timber connections (Standard Norge, 2010 <i>c</i> , fig. 8.3)	27
3.4	Symbols for spacing of fasteners in steel and aluminium, (Standard Norge, 2009 <i>b</i> , fig. 8.1)	28
3.5	Symbols for spacing of fasteners in timber (Standard Norge, 2010 <i>c</i> , fig. 8.7)	29
3.6	Block shear (Standard Norge, 2010 <i>c</i> , fig. A1)	31
3.7	Shear stress distribution and load capacity for different bond-line stiffnesses (Stamatopoulos, 2019)	33
3.8	Influence of bond-line length on load capacity in a lap joint (Stamatopoulos, 2019)	34
3.9	Influence of bond-line length on shear stress distribution in a lap joint (Stamatopoulos, 2019)	35
3.10	Definitions of edge and end distances for threaded rods (Stamatopoulos, 2016, fig.2.3)	42
3.11	Definitions for spacings and distances in SR connector.	42
3.12	Flow chart of calculation procedure	43
4.1	The axis system and stress notations in Abaqus	45
4.2	Benchmark, Case 1 - Cantilever	47
4.3	U case 1	48

4.4	Principal stresses case 1	48
4.5	Shear stresses case 1	49
4.6	Benchmark, Case 2 - Column	50
4.7	Buckling mode	51
4.8	Buckling coefficient and S11	51
4.9	Benchmark, Case 3 - bonded	52
4.10	Comparison of principal stresses in bonded contact	53
4.11	Benchmark, Case 4 - Bonded type with eccentricity	54
4.12	Shear stress distributions of bond-lines	54
4.13	Comparison of stresses in bonded contact with eccentricity. The left part of the cross-section is closer to the fixed support, whereas the right part is closer to the applied load.	55
4.14	Shear distribution of S12 in isotropic material at the top in bonded contact	56
4.15	Shear distribution of S12 in orthotropic material at the top in bonded contact	56
4.16	Benchmark, Case 5 - Connection	57
4.17	The withdrawal capacity increases as the angle increases	58
4.18	Mises stress in steel rod	58
5.1	The input file in listing 1 describes this model geometry with boundary conditions and loading	61
5.2	Default coordinate systems in Rhino and Abaqus	62
5.3	<i>SortPts</i> sorts points automatically to reduce errors while creating new meshes from part in model	64
5.4	Stages of the MeshPointsSweep component	65
5.5	Output of the MeshPointsSweep component	65
5.6	Geometry made in Grasshopper from 8 corner points, and assigned divi- sion of 2x2x2, 8 elements in total	66
5.7	Imported, mirrored geometry in Abaqus. Note that Abaqus' numbering starts with 1, while Grasshopper starts with 0	66
5.8	Example of making a more smooth mesh by approximating curves be- tween corner points using NURBS curves in the MeshPointsNurbsSweep component	68
5.9	Hexagon mesh	68
5.10	Ring mesh	69
5.11	Twisted model	69
5.12	Orientation of elements with orthotropic material	71
5.13	Possible Load types; Pressure and Surface traction	73

5.14	Examples using the different load types	73
5.15	Possible element types; C3D8, C3D8R and C3D8I	75
5.16	Example of joining three meshes together into one part	76
5.17	15 surfaces numbered from 0-14	76
5.18	Grasshopper data tree of example	78
5.19	A flowchart which shows the workflow of a GH script which has the INP-file as the last output.	79
5.20	An example of assembling the different components to create a similar model to that of figure 5.1.	79
5.21	Model examples that are found in appendix E.2	80
6.1	the GF connector	82
6.2	Applied load and boundary conditions to one connector	83
6.3	Demonstration of how FEA results are given in Abaqus	84
6.4	FEA Mises stress results of four splices with a length of 350 mm. The two inner splices transfer most of the stresses, making the two exterior inner splices appear to be redundant.	85
6.5	Length of inner splices	85
6.6	Width of inner splices	86
6.7	Angle between inner and outer splice	86
6.8	Length of outer splice	87
6.9	Width of mid plate	87
6.10	Length of inner plate	88
6.11	Width of inner plate	88
6.12	Whole GF connector with proposed geometry as stated in table 6.1. As seen, the connectors do not collide.	89
6.13	Displacement and Mises stress in the optimised GF connector	90
6.14	Displacement and Mises stress in the proposed solution of simplified GF connector with shear force applied in the horizontal direction	90
6.15	GF connector applied to pure compression	91
6.16	GF connector with eccentricity in the vertical direction	91
6.17	GF connector with eccentricity in the horizontal direction	91
6.18	GF connector with stiffening plates	92
6.19	Boundary conditions and loading for buckling analysis of one leg	93
6.20	Buckling modes	93
6.21	GF whole connector	94
6.22	Whole GF connector applied to different pressures on the ends of the timber members	95

6.23	Mises stress in whole simplified GF connector applied to pressure	96
6.24	Whole GF connector applied to different surface tractions at the ends of the timber parts	97
6.25	Mises stress of connectors applied to surface traction	98
6.26	Applied loading for checking the buckling capacity of the whole connector	98
6.27	Buckling modes with buckling of fixed leg	99
6.28	Buckling modes	99
6.29	Simplified SR connector with parameters	100
6.30	The yellow circles marks the surfaces that are tied in a tied connection	100
6.31	SR connector applied to different pressures on the ends of the timber members	101
6.32	SR connector with pure compression	101
6.33	SR connector with eccentricity in the vertical direction	102
6.34	SR connector with eccentricity in the horizontal direction	102
6.35	Whole simplified SR connector applied to shear	103
6.36	Comparison of GF and SR connector when decreasing the volumes . . .	104
6.37	Pressure of 20 MPa applied to all timber members in the GF connection	105
6.38	Pressure of 20 MPa applied to all timber members in the SR connection	105
6.39	Shear load of 2 MPa applied to all timber members in GF connection .	106
6.40	Shear load of 2 MPa applied to all timber members in SR connection .	106
6.41	Loading and for estimating rotational stiffness of GF joints	108
6.42	Plot of displacement in the middle of one leg of the GF connector . . .	109
6.43	Model to estimate the rotational stiffness of SR joints	110
6.44	Plot of displacement in the middle of one leg of the SR connector . . .	110
6.45	Comparison of displacements, where the dashed lines represent straight lines from the initial point, through the transition point, to the end points.	112
7.1	Whole Grasshopper assembly model for the GF connector	114
7.2	Example of an inconsistent and consistent mesh	115
B.1	Weight calculation of aluminium connector	130
B.2	Weight calculation of steel connector	131
B.3	Necessary glue surface and splice lengths in GF connector	132
B.4	Estimated calculations of diameter and penetration length of threaded rods in SR connector	133
C.1	Principal stresses case 2	138
C.2	Shear stresses case 2	139
D.1	I-Beam	141
D.2	Parametric FE Shell model	143

List of tables

2.1	Maximum forces and moments in most utilized cross-section	18
2.2	Strength values from Standard Norge (2010 <i>a</i>)	18
2.3	Result of necessary cross-section	20
2.4	Result of necessary cross-section	22
3.1	Spacing requirements for bolts in steel and aluminium plates	28
3.2	Spacing requirements for steel and aluminium bolts	28
3.3	Spacing requirements for bolts in timber members	29
3.4	Weight difference of connector in steel and aluminium	32
3.5	Values for the necessary parameters	36
3.6	Estimation of necessary cross section and splice lengths in GF connector	37
3.7	Minimum spacing and distance requirements for threaded rods in timber members	41
3.8	Necessary diameter and penetration length of threaded rods in SR-connector with four rods.	44
4.1	Chosen system of units in Abaqus	45
4.2	Material properties for orthotropic material	46
4.3	Material properties for isotropic material	46
5.1	Components that create and/or sort geometry	63
5.2	MeshPointsSweep	64
5.3	MeshPointsNurbsSweep	67
5.4	Materials	70
5.5	Boundary conditions	72
5.6	Load	73
5.7	AbaqusPart	74
5.8	Tie	75
5.9	INPAssembly	78
6.1	Values which gives an optimised solution for the simplified GF connector	89
6.2	Pressures applied to the ends of the timber members, calculated from connector number 1125 which are subjected to biggest axial force . . .	95
6.3	Surface tractions applied to the ends of the different timber members, calculated from connector number 1 which are subjected to the biggest shear force	97
6.4	Estimated rotational stiffness of GF connector	109
6.5	Estimated rotational stiffness of SR connector	111
6.6	Comparing rotational stiffnesses of the GF and SR connector	111
C.1	Cantilever stresses for orthotropic material	134

C.2	Cantilever stresses for isotropic material	135
C.3	Comparison of cantilever displacement	136
C.4	Column stresses for orthotropic material	137
C.5	Column stresses for isotropic material	137
C.6	Comparison of buckling coefficient	138

Abbreviations and acronyms

AD Adhesive Dowels

AM Additive Manufacturing

BC Boundary Conditions

BESO Bi-directional Evolutionary Structural Optimization

CAD Computer Aided Design

CAE Complete Abaqus Environment

ETA European Technical Approval

FEA Finite Element Analysis

GF Glued Finger

GH Grasshopper

HAZ Heat Affected Zone

HPDC High Pressure Die Casting

HSK Holz-Stahl-Komposit-Systeme

IDE Integrated Development Environment

INP Input file

LPDC Low Pressure Die Casting

LVL Laminated Veneer Lumber

NURBS Non Uniform Rational B Splines

SR Split Ring

1 Introduction

Designing connections for gridshell structures can be challenging and it demands progressive research and investigations to accomplish innovative solutions. Due to the irregular geometries of most gridshells, the connectors should be investigated as part of the gridshell as a whole. To introduce the topic of timber gridshells with aluminium connectors, timber gridshells in general are investigated as well as theory behind aluminium structural design. Furthermore, the design of the connections are considered with existing designs of connections of timber gridshells. Then, the complexity of NURBS- and free form surfaces is discussed in addition to numerical analysis and experimental testing of connectors. In the end, the two different connector designs which has been developed for the British Museum as a timber gridshell is introduced, and the software used in this thesis.

1.1 Timber gridshells

Shell structures are characterised by curved surfaces, where the thickness of the surface is small compared to the other dimensions of the structure. In addition, shell structures carry their loads mainly through membrane action; by tension forces, compression forces and shear in the plane of the shell (Harris, 2011).

In Chilton and Tang (2016), a simple and wide definition of a gridshell is that “a gridshell is essentially a shell with holes, but with its structure concentrated into strips”. A more detailed definition is that a gridshell is a spatially curved framework of rods and rigid joints. The effectiveness of the load-bearing capacities of shells and gridshells eliminates the need of additional columns and beams, which may be a preferred choice to create open and inviting structures and areas.

Historically, shells have generally been constructed in concrete or masonry whereas gridshells have predominantly been constructed in steel. The first timber gridshell, the *Deubau Pavilion* in Essen, was realised in 1962 (Chilton and Tang, 2016, p. 14), but timber gridshells back then were designed largely by highly intricate physical hanging chain models. Due to subsequent developments of timber engineering products and advances in digital design, analysis, parametry and fabrication along with a greater focus on sustainable materials, timber gridshells in various forms are emerging as structures that were previously impossible to build.

1.1 Timber gridshells

Timber gridshells can generally be divided in two categories; discrete timber gridshells, where straight timber members are connected by using metal connectors, and kinematic timber gridshells, where the grid is built flat and then post-formed into the desired curved shell shape. A built example of a discrete timber gridshell in London can be seen in figure 1.1, and is more thoroughly described in section 1.3.1.

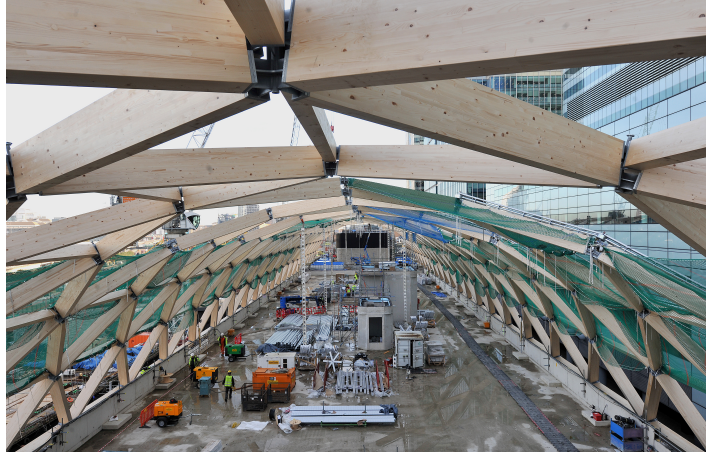


Figure 1.1: Discrete timber gridshell under construction at Crossrail Place in London, Photo: ©Arup (2013)

One example of a kinematic gridshell is the Trondheim Pavilion in figure 1.2. Laths with straight and slotted holes are bolted together in a grid, creating kinematic connections that are tightened when the gridshell is formed and lifted to its desired shape. Unlike the straight members of discrete timber gridshells, the timber members are bent in kinematic gridshells due to the shape forming method.



Figure 1.2: Trondheim Pavilion, Photo: Labonnote (2015)

1.2 Aluminium structural design

Aluminium is not just one material, but it is the base for many groups of alloys with different material properties. The material properties can vary both between and within the groups of alloys. It is critical to have good knowledge about which alloys that are available and their material properties, to choose the most suitable alloy in the design. The reason for using aluminium alloys is primarily because of the increase in strength, corrosion resistance and toughness that the alloying gives (Dyvik et al., 2019). However, the history of using aluminium alloys in structural design is quite short, but the usage has increased in recent years (Mazzolani, 2008).

There exists several reasons for using aluminium as a structural material. Firstly, when it comes to manufacturing, aluminium is easy to form, due to its softness (Müller, 2010). It is a more preferred material of the fabricator compared to steel, as aluminium is simpler to saw, drill and cut. Secondly, it is a lightweight material as well as it is completely recyclable without weakening any material properties. With an environmental point of view, the recycling ability makes aluminium a material with a high potential in the future. By finding approaches where recycled aluminium is beneficial, one could lower the environmental impact. Remelting of aluminium only demands 5 % of the energy necessary in the primary production of aluminium, which is an easy and cost-effective process. However, the emissions due to remelting, transportation and collection, is a disadvantage of the recycling process of aluminium. Furthermore, aluminium alloys have good tensile and compressive strength. In addition, aluminium is corrosion resistant, even in aggressive environments, which means that aluminium structures need less maintenance work. This makes the material suitable to use in for example gridshell structures, due to the bad accessibility. Unlike steel, with lower temperatures, the aluminium behaviour remains ductile and the tensile strength increases.

On the other hand, the usage of aluminium also has some challenges in structural design. Aluminium have for instance lower modulus of elasticity than steel (Müller, 2010). In addition, aluminium has a low melting point and the strength weakens when exposed to heat. This leads to the term of Heat Affected Zone (HAZ). HAZs are areas which are weakened due to material heating, and arise mostly adjacent to welds. It is important to be aware of that not all alloys can be welded or heat treated. Due to the risk of heat exposure, aluminium structures should be fire protected. However, the relevance of this for gridshells could be discussed, due to the high distance between a potential fire and the gridshell surface.

When designing aluminium structures, it is critical to think smart and take advantage of the benefits of the material and have as few weak spots, for example welds, as possible. Smart design will also be to utilise the tensile and compressive strength, and minimise the exposure of bending moments in the structure. Moreover, the possible methods to manufacture structural components in aluminium alloys, are extrusion, rolling, drawing and casting (Mazzolani, 2008). Furthermore, in the production of aluminium alloy products, there is two principal classifications; cast alloys and wrought alloys (Dyvik et al., 2019).

Since casting alloys can have a larger amount of other elements than alloy products produced in other ways, it is a common opinion that casting is the most suitable method for producing products of recycled aluminium alloys. Therefore, the aluminium casting alloys and the main casting methods will be given a special attention. The most popular aluminium alloy for casting, is the Al-Si alloys. Such alloys can produce a wide amount of different properties, as silicon contributes to satisfactory castability (Otarawanna and Dahle, 2011). The resulting mechanical properties of the aluminium alloy products manufactured by the different casting techniques, will vary as the techniques gives different results. One parameter that will influence the mechanical properties of the final product, is the porosity. Porosity will reduce the mechanical properties. This may arise since most aluminium alloys will shrink about 3-6 %, and if not the mould will be refilled with extra liquid, porosity will be a problem.

The main casting methods for aluminium alloy products are High Pressure Die Casting (HPDC), Low Pressure Die Casting (LPDC), Sand Casting and Permanent Mould Casting (Otarawanna and Dahle, 2011). For large production volumes, HPDC is the most suitable method. Whilst for small production volumes, the other three casting techniques are more usual. In both HPDC, LPDC and permanent mould casting, the metal die can be reused. HPDC is a rapid, automated method and are used to produce thin-walled, comprehensive products. The aluminium alloy liquid are poured into the die with high speed, and solidified under high pressure. However, the main problem with traditional HPDC, is porosity due to air being entrapped in the shrinking and filling process during solidification. This affects the mechanical property of the final product in addition to the pressure tightness of parts.

LPDC is a technique where the filling of aluminium alloy liquid into the die, is done with a low speed in comparison to the filling in HPDC (Otarawanna and Dahle, 2011). Due to the low speed, the amount of entrapped air and turbulence is minimized, and

thus this method can produce casting products with low porosity. By using LPDC, finishing of surfaces is possible and an excellent dimensional accuracy is within the reach.

According to section 3.3.2 in Standard Norge (2010*b*), sand casting is the process in which molten metal is poured into a sand mould and solidified at atmospheric temperature. Due to automation in the process of making sand moulds, sand casting has in the recent years also become cost effective for large production volumes, and not only for small production volumes as in the past (Otarawanna and Dahle, 2011). Components made from sand casting, do often have a rough surface, sometimes with variations or impurities. There are different sand types and moulding processes, and the choice of these is affecting the dimensional accuracy.

The permanent mould casting is a mix of sand casting and lost-foam casting. In this casting method, a mould of foamed polymer is lying in a loose sand bed and the aluminium alloy, in a liquid form, is poured into the polymer mould (Shivkumar et al., 1990). This will cause the foam to evaporate, and the mould will be filled with the aluminium alloy. Permanent mould casting is most often used for making simple metal products with uniform wall thickness.

1.3 Design of connections in timber gridshells

The design of gridshell connectors and connections is complicated because of loading conditions and comprehensive geometries (Seifi et al., 2020). Therefore, it is essential to develop flexible connectors which can handle the switching structural behaviour and the variations in the geometrical parameters of the connector (Stephan et al., 2004). In this thesis, the focus will be on timber gridshells and connectors for single layer discrete free-form surfaces. Such gridshells are often referred to as discrete or reticulated gridshells, and have straight members between the connectors. An example of a connector design in a discrete gridshell structure can be found in figure 1.3.



Figure 1.3: Printshell, Photo: Labonnote (2016)

The reason why the design of gridshell connectors is complicated in discrete free form gridshells, has to do with the different inclinations and angles of the connecting members, see figure 1.4. Both the angles between the members, horizontal angles, and the inclinations of the members, vertical angles, in addition to the twisting angles, will most often vary in each connector, which means that each connector in the gridshell will be unique. Therefore, it is important to develop methods to design and produce such connectors in an efficient way.

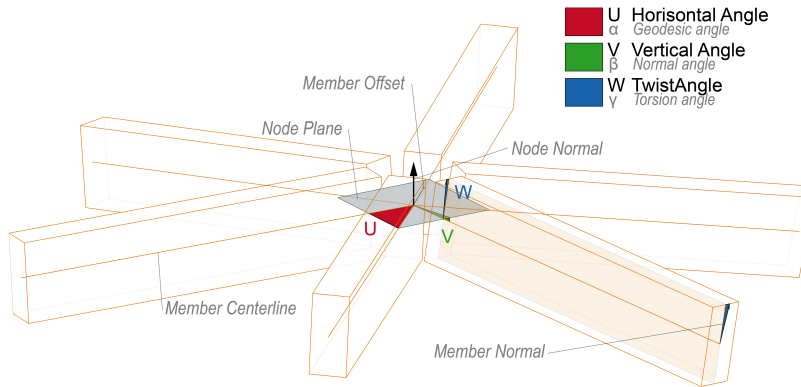


Figure 1.4: Different inclinations and angles of the connecting members in free form gridshells.
Figure: Steinar Hillersøy Dyvik

1.3.1 Status of connections in timber gridshells

Connectors for discrete gridshells can generally be divided in two categories; end-face connectors and splice connectors. In end-face connectors, the contact surface between the connector and the end-face of the connected structural member is transverse to the longitudinal axis of the structural member (Stephan et al., 2004). At Canary Wharf in London, a 310 m long timber lattice roof, with typical beam lengths of 6 meters, encapsulates a public roof garden (Worsfold et al., 2018). The roof is continuous, with moment resisting connections, which can be seen in figure 1.5a. The structure is therefore highly indeterminate, and thus the sensitivity of the roof to varying stiffness assumptions had to be considered. The connectors consists of welded steel plates with glued threaded rods connected with nuts at the end-face to the timber. To minimise the amount of temporary support of the members during construction, the connections were designed to enable the timber beams to cantilever off one connector temporarily.

Another built example of a timber gridshell with an end-face connector is the Pods Sports Academy, located in Scunthorpe, England. Here, the connection between the main member elements and the connector is also made with glued, threaded rods and can be seen in figure 1.5b. However, in this case the steel meets and forms a cylinder rather than meeting in the middle as in figure 1.5a. M16 and M20 rods, with effective bonding lengths of 300-500 mm were considered during initial testing (Harris et al., 2012), and inserted and tested parallel to grain. The rods proved to be sufficient for the case.

1.3 Design of connections in timber gridshells

A not yet built, but an interesting example of emerging technology is the 3D printed structural steel connector by MX3D and Japanese construction company Takenaka, seen in figure 1.5c. Here they have used additive manufacturing together with topology optimisation to generate an efficient shape. The steel joint is printed to be hollow, and thereafter filled with mortar, which is considered to be more economical than having solid steel (MX3D, 2020). By using mortar in substitute of steel, the joint will also be more lightweight. Filling the core will prevent local buckling of the steel, and let the outer steel handle bending and tensile forces. The next step is to implement the design in an actual building projector. However, it is not stated clearly how they plan to connect the steel joint to the timber itself.



(a) Connector detail at the Crossrail Place in London. The connectors consists of welded steel plates connected to the timber by glued threaded rods. Photo: ©Nigel Young (Seele, 2014).



(b) Connectors at the Pods Sports Academy. Here the steel forms a hollow cylinder to where members meet. Photo: Westmuckett Hawkes Ltd (2010)



(c) A hollow steel joint in development by MX3D and Takenaka. The shape is created using topology optimisation and thereafter 3D printed before filling the core with mortar. Photo: ©Leonard Fäustle (MX3D, 2020)

Figure 1.5: Examples of end-face connectors

In splice connectors, the contact surface between the connector and the connected structural member runs along splice plates in the longitudinal axis of the member (Stephan et al., 2004). The splice plates can either be inserted horizontally or vertically according to the member's alignment and are glued and/or bolted to the timber members.

Dome of visions 1.0 was a 10.5 meter tall and 21 meter wide transportable dome erected for the first time in 2013 in Copenhagen (Dome of Visions, 2013). 3.4 meter long Laminated Veneer Lumber (LVL) beams are connected by 91 steel connectors using splices aligned vertically to the longitudinal axis of the beams and bolted to the beams, as seen in figure 1.6a. The splices are welded together to a hollow steel cylinder. A slightly bigger dome was erected in Aarhus in 2016, called dome of visions 3.0 (Dome of visions, 2017). Here the splices are aligned horizontally, as seen in figure 1.6b, making the steel itself rather hidden.

The Herbert Art Gallery and Museum in Coventry, England, was renovated and expanded in 2009 with a 50 meter long and 12 metres high gridshell atrium. The connector detail can be seen in figure 1.6c. The splices are welded to a sphere in the centre. However, it is noted that the splices in fact acts as flitch plates since they are continuous along the timber beams. Hence, in this case, the structure itself is a hybrid gridshell with flitch beams of timber and steel.



(a) *Dome of visions 1.0 in Copenhagen, Denmark. The splices are inserted vertically and welded to a hollow cylinder. Photo: Paul Nybo Andersen (Dome of Visions, 2013)*



(b) *Dome of visions 3.0 in Aarhus, Denmark. The splices are inserted horizontally to the timber elements. Photo: Kristoffer Tejlgaard (Dome of visions, 2017)*



(c) *Connector Detail at The Herbert Art Gallery & Museum in Coventry, England. The splices are welded to a sphere in the centre. Photo: Cmglee (2011)*

Figure 1.6: Examples of splice connectors

1.3.2 NURBS- and free form surfaces

Free form surfaces are surfaces with geometries based on the mathematics and techniques of Non Uniform Rational B Splines (NURBS) (Stephan et al., 2004). By using NURBS surfaces, any imaginable geometry can be constructed. The construction process of such surfaces is quite complex, and compared to algebraic surfaces, such as the sphere, it cannot be described with fixed equations. On the other hand, the creation of free form surfaces demands a highly comprehensive approach, with a composition

of different geometrical objects, such as points, curves, planes and also mathematical formulas and algorithms. The designer will usually not get involved in the complex mathematical background of NURBS and uses instead programs where this has been implemented as CAD-tools, to develop the wanted free form surface.

The iteration process of designing free form surfaces is demanding and requires analyses and adjustments to improve the geometry (Stephan et al., 2004). Form-finding methods are optimisation approaches where surfaces are constructed by non-geometrical modes. Such methods can be both analytical, as the force-density method and dynamic relaxation, and experimental, by using phenomena as hanging nets which has given the conventional form of gridshells in compression.

Even though non-optimised free form surfaces has considerably complex designs, structures with such geometries has lately and is still increasing, due to architects' weakness for limitless design and the rise of CAD-programs with the possibility of NURBS surfaces (Stephan et al., 2004). This shows that development of flexible, cost-efficient and aesthetic designs of connectors, which are simple to manufacture and are user friendly at the building site, is crucial to continue the trend of free form discrete surfaces. Such connectors will make free form surfaces more applicable to build for several building companies, and not only for the big companies with many resources. The connector should be able to handle problems like varying angles between structural members and connectors and the switching structural behaviour between tension, compression and bending stresses in members.

1.3.3 Numerical analyses and experimental testing of connectors

Due to the difficulties when applying complex design loads to gridshell connectors in laboratory tests, it is difficult to confirm connector designs (Seifi et al., 2020). Gridshell connectors must transmit all loads working in the structure. Often, in experimental tests, the connector design and load conditions are simplified. This because it is hard to create the exact geometry, topology and loading conditions, which is complex in gridshells.

To know which loads that should be applied in the experimental tests, the load resisting capacities of the connectors should be predicted in advance. This could be done numerically by a linear or non-linear FEA with Abaqus CAE, for instance. Several load cases should be analysed. From the obtained maximum loads and the test setup configuration, the loads that should be applied in the experimental tests can be calculated.

A number of methods have been used in earlier years to construct a test setup for different connector designs (Seifi et al., 2020). One method has been to simplify the connector design and loading conditions. Another method has been to apply load on a certain part of the test specimen, to see how it will influence the behaviour of the connectors. In recent years, a new and innovative approach of designing connectors, has been developed which combines Bi-directional Evolutionary Structural Optimization (BESO) design and Additive Manufacturing (AM). AM is dependent on an efficient design method, such as BESO, to get the wanted structural behaviour with the minimum amount of material. The design concept of BESO is to optimise the structural element by only adding material where it is necessary and remove superfluous material. The benefit of using AM as the manufacturing method, is that it can minimise or even exclude human errors throughout the manufacturing. An AM method, which is a simpler method than casting when it comes to making small objects, is the Binder Jet method. This method bond metal particles together in layers from bottom to top, and are often used for 3D printing.

This new method of designing connectors has lead to the development of new test setups which can handle the complexity of connectors in latticed structures. One example of a recently innovative and inexpensive developed test setup, is one developed by Seifi et al. The test rig is based on three operations and can be used for both individual and combined loading conditions. To expose the connector for bending moments, the axial load is applied to the connector with appropriate eccentricities. This is the first operation. In the next operation, the goal is to expose the connector for axial load in each branch, by altering the direction of the vertical load. The last operation is to find the one vertical load that the connector should be applied to, by combining the vertical loads that are applied in all branches. The study performed by Seifi et al. shows that the concurrence of the failure modes of the connector is good, when comparing the capacity results from the numerical FE analyses with the experimental results.

1.4 Designing connectors for the British Museum Great Court as a timber gridshell

Most gridshells are traditionally constructed with straight steel members welded or bolted to steel connectors. In recent years, more gridshells are being made with timber products, as a result of environmental focus, developments of timber products and an increased focus on timber as a building material, both regarding aesthetics and material qualities. Also, since aluminium is fully recyclable and the manufacturing methods and material properties, such as low self-weight, can be beneficial for connectors in gridshells, it is interesting to explore the possibility of developing aluminium connectors to be used instead of steel connectors in gridshells. Therefore, a redesign of the British Museum Great Court, see figure 1.7a, from steel members into timber members and from steel connectors, see figure 1.7b, into aluminium connectors, have been investigated.

Brun (2019) has modelled the redesign and analysed it in Autodesk's Robot structural analysis professional software. The gridshell roof-geometry, originally made from steel rectangular hollow sections (RHS), are redesigned by replacing the sections with GL32h as the material and a cross-section of $b \cdot h = 200mm \cdot 350mm$. From the structural analysis in ROBOT, the maximum forces and moments in the most utilised timber member in the roof structure have been found. These have been used as design values in this thesis when estimating necessary dimensions of geometrical parameters of the connectors. Furthermore, the aluminium alloy material in the connector was chosen to be EN AC-43000 T6, and the important material properties are given in table 2.2.



(a) British Museum Great Court. Photo: Andrew Dunn (2005)

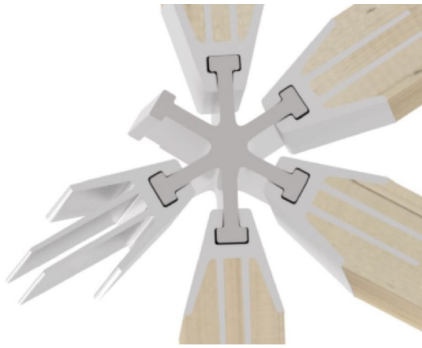


(b) Connector detail of connected steel elements. Photo: Piergiorgio Rossi (2005)

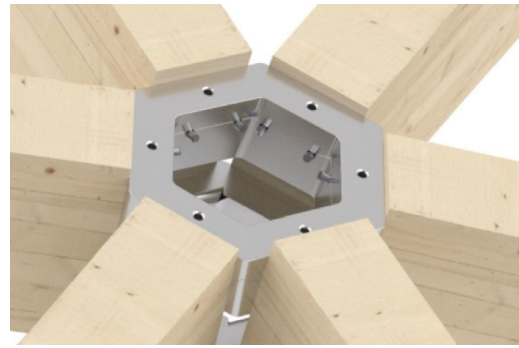
Figure 1.7: Queen Elisabeth II Great Court, British Museum (London UK)

1.4.1 Glued Finger and Split Ring connector

By studying typical timber gridshell steel connectors found in Chilton and Tang (2016), two main principles of connector designs have been developed by Steinar Hillersøy Dyvik and will be investigated further in this thesis. The first principle is connectors where all aluminium material meet in the centre point to ensure best load transfer. The second one is connectors where the material is moved away from the centre to ensure better space for the meeting members. Based on this, two solutions was found; the Glued Finger (GF) connector, see figure 1.8a, and Split Ring (SR) connector, see figure 1.8b. When looking at the two principles of connector design, two main challenges were identified; the gripper and the core. Chapter 2 investigates cores, the metal part where all members meet, by using rules of structural design from the Eurocodes. Chapter 3 investigates grippers, the connection between timber and metal, for threaded rods and glued connections.



(a) *Glued Finger (GF) connector design. Figure: Steinar Hillersøy Dyvik*



(b) *Split Ring (SR) connector design. Figure: Steinar Hillersøy Dyvik*

Figure 1.8: Solution proposals for aluminium connectors in timber gridshells.

The GF connector, can be put into the category of splice connectors, as the timber members are attached to the connector by aluminium splices. Furthermore, the timber members and the aluminium splices are glued together. This connector design is inspired by the timber-aluminium joints designed by Renzo Piano Building Workshop for the IBM Travelling Pavilion, see figure 1.9a. The design of the GF connector consists of one core, which is unique for all connectors, and six grippers, equal for all connectors and suitable for mass production, which is attached to each timber member. The grippers can be attached to the core either by self-locking or by bolts, see figure 1.9b for bolt holes.



(a) *Timber-aluminium joint in IBM Travelling Pavilion, Photo: ©Gianno Berengo Gardin (Fondazione Renzo Piano, n.d.)*



(b) *GF connector seen from above. Figure: Steinar Hillersøy Dyvik*

Figure 1.9: Similar connector design concepts

On the other hand, the SR connector is an end-face connector, since the end-face of the timber member is perpendicular to the grain direction. The SR connector is connected

to the timber members by screwed-in threaded rods. Such connectors, have proved to be a good solution in moment resisting connections, by ensuring high stiffness and withdrawal capacity (Stamatopoulos and Malo, 2015*b*). To prevent the arise of cracks, the rods must be inserted with an angle to the grain. Compared to glued-in rods, screwed-in rods can provide better fire-protection in addition to being less brittle and less exposed to issues with the construction quality. Also, connections with screwed-in threaded rods can be designed for having a ductile behaviour. When it comes to the split ring, it consists of an upper- and lower-ring, as is suggested by Monasterio et al. (2018), to save material but still keep the height of the beams. On the other hand, a disadvantage with such design may be that the shear capacity is less than for a solid connector and in addition it leads to more difficulties when assembling the structure. These rings are again divided into a top-part and a bottom-part. Also, the width of one side of the ring is equal to the width of the timber member.

1.5 Software for parametric design and structural analyses

Parametric structural design is a design method to analyse connector designs for grid-shell connectors in an efficient way, by changing the dimensions of different geometrical parameters. The benefit of parametric design is that it is a design method which gives architects and engineers the possibility to optimise structures by exploring more options and making more efficient designs. This, because parametric design enables the designer to define the main parameters in the design and make adjustments in the design interactively. The model will update and adapt to these adjustments automatically. In this section, the software used in this thesis to solve the problem are presented.

1.5.1 Rhinoceros 3D and Grasshopper

Rhinoceros 3D, hereby abbreviated as Rhino, is a command-driven 3D-modelling CAD program. It can create, edit, analyse, document, render, animate, and translate NURBS curves, surfaces, and solids, point clouds, and polygon meshes with no limits on complexity, degree, or size beyond those of the designated hardware (R. McNeel & Associates, 2020).

Grasshopper (GH) is a graphical algorithm editor tightly integrated with Rhino's 3D modelling tools (Davidson, 2020) and is written using both Visual Basic.NET and C#, both object-oriented programming languages. By making parametric geometry using GH components and visualise this in Rhino, one can establish parametric models. Since GH is an intuitive visual programming tool, the user does not need any prior knowledge of programming to use existing components. Furthermore, the desire to achieve something specific out of scope of the existing plugin or possible add-ons can be addressed by scripting own components, either directly using C# in GH or through an Integrated Development Environment (IDE) such as Microsoft Visual studio.

Unlike CAD models, where small changes can turn into a complex action, the Rhino/GH environment enables the designer to make small changes and get an update of the adjusted model automatically. In figure 1.10a, an arch which is repeated several times is modelled parametrically in GH. The arch consists of three input points. The Z-coordinate of the arch mid point and the number of arches are set as a number slider which has a value which can be easily adjusted. In figure 1.10b, the resulting geometry which are displayed in Rhino from the GH model, is shown. The lower geometry is created only by increasing the values in the number sliders for the Z-coordinate of the arch mid point and the number of arches.

1.5 Software for parametric design and structural analyses

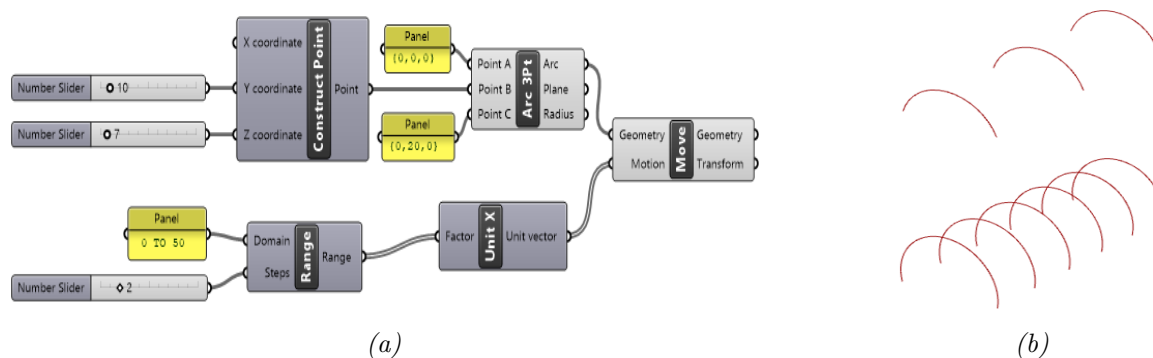


Figure 1.10: Parametric model in GH with geometries displayed in Rhino for different input values

There exists fully embedded software packages in Grasshopper that provides analysis of spatial trusses, frames and shells, such as Karamba3D (Karamba3D, 2020). However, current add-ons does not provide the possibility to thoroughly analyse solids in 3D.

1.5.2 Abaqus CAE

Abaqus CAE is a complete Abaqus environment that provides an interface for creating, editing, submitting, monitoring and visualising results from advanced Abaqus FEA (Dassault Systèmes, 2020). Abaqus CAE is divided into modules, where each module defines an aspect of the modelling process; for example, defining the geometry, defining material properties, and generating a mesh. As you move from module to module, you build the model from which Abaqus/CAE generates an input file that you submit to the Abaqus/Standard or Abaqus/Explicit analysis product. The analysis product performs the analysis, sends information to Abaqus CAE to allow you to monitor the progress of the job, and generates an output database to read and view the result of the analysis (Dassault Systèmes, 2014). Abaqus CAE is hereby abbreviated as Abaqus.

2 Comparing connectors in aluminium and steel

As stated in the introduction, aluminium has lower modulus of elasticity than steel. Therefore, it is interesting to investigate the difference between the necessary dimension of a rectangular cross-section in aluminium compared to in steel, when applied to a given set of loading. The design values that are used to estimate the necessary dimensions, can be found in table 2.1 and are taken from the structural analysis of the British Museum Great Court case project, which were explained more closely in section 1.4. The moment about the z-axis and the shear force in the y-direction is neglected in the calculations. In the case project, the gridshell roof-geometry, originally made from steel rectangular hollow sections (RHS), was redesigned by replacing the steel members with timber members with GL32h as material and a cross section of 200·350 mm².

Table 2.1: Maximum forces and moments in most utilized cross-section

$N_{Ed}[kN]$	$V_{z,Ed}[kN]$	$V_{y,Ed}[kN]$	$M_{y,Ed}[kNm]$	$M_{z,Ed}[kNm]$
68.60	3.04	0.08	15.79	0.45

The chosen aluminium alloy to use in the design is EN AC-43000 T6, and the strength values from section 7.1 in Standard Norge (2010a), can be found in table 2.2.

Table 2.2: Strength values from Standard Norge (2010a)

	Yield strength [MPa]	Ultimate Tensile strength [MPa]
EN AC-43000 T6	180	220

2.1 Necessary cross-section of connector in aluminium

To find an estimation of the necessary dimension of cross-section for a aluminium connector, the Eurocode is used to check for combined load; axial load, shear and moment. Buckling is not taken into account.

According to section 6.2.9.2 in Standard Norge (2009b), solid cross-sections and hollow sections in aluminium, should satisfy the following criterion:

$$\left(\frac{N_{Ed}}{\omega_0 \cdot N_{Rd}}\right)^\psi + \left[\left(\frac{M_{y,Ed}}{\omega_0 \cdot M_{y,Rd}}\right)^{1.7} + \left(\frac{M_{z,Ed}}{\omega_0 \cdot M_{z,Rd}}\right)^{1.7}\right]^{0.6} \leq 1.0 \quad (2.1)$$

where

$\psi = 2$ for solid cross-sections;

$\omega_0 = 1$, for sections without localised welds or holes, which is assumed for this connector.

The expressions for the design resistances are given in section 6.2.9 in Standard Norge (2009b) as:

$$N_{Rd} = \frac{A \cdot f_o}{\gamma_{M1}} \quad (2.2)$$

$$M_{y,Rd} = \alpha_y \cdot \frac{W_{y,el} \cdot f_o}{\gamma_{M1}} \quad (2.3)$$

$$M_{z,Rd} = \alpha_z \cdot \frac{W_{z,el} \cdot f_o}{\gamma_{M1}} \quad (2.4)$$

where

$\gamma_{M1} = 1.1$, according to NA.6.1.3(1) in Standard Norge (2009b);

α_y , and α_z is equal to 1.0, when assuming no welds and cross-section class 3, conservatively;

f_o is the yield strength of the aluminium alloy, which is 180 MPa.

Furthermore, according to section 6.2.10(2) in Standard Norge (2009b), if $V_{Ed} \leq 0.5 \cdot V_{Rd}$, there should be no reduction of the resistances defined for axial force and bending. This

2.1 Necessary cross-section of connector in aluminium

criteria, was firstly assumed to be fulfilled, and was checked with the calculated cross-section afterwards.

A width of 30 mm is assumed to find the necessary cross-section, and was used in the equations for the design resistances above. The obtained values of the design resistances was then inserted in equation 2.1, to find the necessary height with the given width.

Solving equation 2.1 for the height, gives a necessary height of 141 (140.92) mm. The necessary cross-section is then

$$A = b \cdot h = 30mm \cdot 141mm = 4230mm^2$$

In the end, it was checked that $V_{Ed} \leq 0.5 \cdot V_{Rd}$. The equation for the shear design resistance is given in section 6.2.6 as:

$$V_{Rd} = A_v \cdot \frac{f_o}{\sqrt{3} \cdot \gamma_{M1}} \quad (2.5)$$

The shear area, for a solid bar is given as:

$$A_v = \eta_v \cdot A_e \quad (2.6)$$

where

A_e is the full section area of an unwelded section;

$\eta_v = 0.8$ for a solid bar.

The criteria was by calculation found to be fulfilled, and the result is given in table 2.3. The detailed calculation of this verification can be found in appendix A.1.

Table 2.3: Result of necessary cross-section

Width [mm]	Height [mm]	Area of cross-section [mm²]
30	141	4230

The calculation procedure above was calculated for several widths, and the result is given in figure 2.1 below.

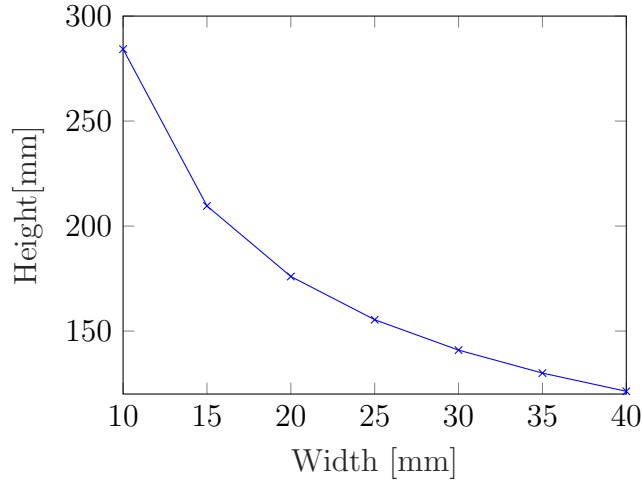


Figure 2.1: Necessary cross-section of aluminium connector

2.2 Necessary cross-section of connector in steel

To find an estimation of the necessary dimension of cross-section for a steel connector, the Eurocode was used to check for combined load; axial load, shear and moment. Buckling is not taken into account.

According to section 6.2.9.1(3) in Standard Norge (2015), rectangular solid cross-sections in steel, should satisfy the following criterion:

$$\left(\frac{N_{Ed}}{N_{Rd}}\right)^2 + \left(\frac{M_{y,Ed}}{M_{y,Rd}}\right) + \left(\frac{M_{z,Ed}}{M_{z,Rd}}\right) \leq 1.0 \quad (2.7)$$

The expressions for the design resistances are given as:

$$N_{Rd} = \frac{A \cdot f_{yk}}{\gamma_{M0}} \quad (2.8)$$

$$M_{y,Rd} = \frac{W_{y,pl} \cdot f_{yk}}{\gamma_{M0}} \quad (2.9)$$

$$M_{z,Rd} = \frac{W_{z,pl} \cdot f_{yk}}{\gamma_{M0}} \quad (2.10)$$

where

$\gamma_{M0} = 1.05$, according to NA.6.1(1)2B (Standard Norge, 2015);

f_{yk} is the yield strength of steel, which is 355 MPa.

2.2 Necessary cross-section of connector in steel

Furthermore, according to section 6.2.10(2) in Standard Norge (2015), if $V_{Ed} \leq 0.5 \cdot V_{Rd}$, there should be no reduction of the resistances defined for axial force and bending. This criteria, was firstly assumed to be fulfilled, and was checked with the calculated cross-section afterwards.

A width of 30 mm is assumed to find the necessary cross-section, and was used in the equations for the design resistances above. The obtained values of the design resistances was then inserted in equation 2.7, to find the necessary height with the given width. Solving equation 2.7 for the height, gives a necessary height of 82.23 mm. The necessary cross-section is then

$$A = b \cdot h = 30mm \cdot 83mm = 2490mm^2$$

In the end, it was checked that $V_{Ed} \leq 0.5 \cdot V_{Rd}$. The equation for the shear design resistance is given in section 6.2.6(2) as:

$$V_{Rd} = A_v \cdot \frac{f_{yk}}{\sqrt{3} \cdot \gamma_{M0}} \quad (2.11)$$

The criteria was by calculation found to be fulfilled, and the result is found in table 2.4.

Table 2.4: Result of necessary cross-section

Width [mm]	Height [mm]	Area of cross-section [mm²]
30	83	2490

The necessary cross-section in steel was also calculated for several widths, see figure 2.2 below with comparison to necessary cross-section in aluminium calculated in section 2.1.

2.2 Necessary cross-section of connector in steel

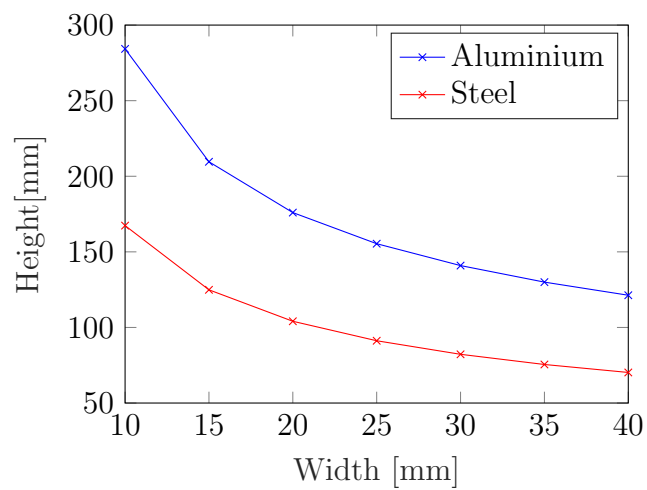


Figure 2.2: Comparison of the dimensions of necessary cross-sections for a connector consisting of steel and a connector consisting of aluminium

From the result it can be found that the necessary cross-section in aluminium is around 40 % bigger than the necessary cross-section in steel.

3 Structural design of timber-to-metal connections

When designing timber structures, the most critical factors are joints that connect the structural members (Vallè et al., 2017). The composition and structure of the joint is determining the structural behaviour of the whole structure. In the GF and SR connector, two different connection types are chosen as described in section 1.4; a glued joint for the GF connector and a connection with screwed-in threaded rods for the SR connector. Thus, how these connections types should be designed structurally is investigated. However, at first, the difference between a connector in aluminium and steel, for a timber-to-metal connection, is looked more closely into.

3.1 Difference in weight of connector in aluminium and steel

When looking at the difference of a connector in steel and aluminium, it is not only the size of the cross-section that is different, but also the weight, as the density for the chosen aluminium alloy is 2700 kg/m^3 and for steel it is 7850 kg/m^3 . Therefore, the difference in weight of a metal connector in steel and aluminium, when connected to timber, is investigated. The detailed calculation of this problem can be found in section B.1, in the appendix. In the calculations, the necessary dimensions for the cross-section for each material, given in table 2.2, is taken into account. At first, the assumptions assumed is described, before the important equations for the necessary failure modes and spacing requirements, which should be checked for the assumed connector design, are given.

3.1.1 Assumptions

To get an estimation on the difference in weight between a connector in steel and a connector in aluminium with the same connector concept, a connector design had to be chosen as a base for the calculation. The connector design that was chosen was a design with two horizontal slotted in metal plates in the timber part connected by bolts, as can be seen in figure 3.1.



Figure 3.1: Connector design for weight calculations, (Dome of visions, 2017)

In the calculation, it was assumed that the bolts are only loaded laterally, by the moment and axial load calculated in the British Museum Great Court case study. Also, in the calculation of load transfer with Johansen's equations, the rope effect was neglected. Since the loads are taken from the case study, also the same timber material and cross section was used. In Standard Norge (2010c), the Johansen's equations are only given for connections with timber against timber and steel against timber. Therefore, the equations for connections with steel against timber was assumed to be valid for connections with aluminium against timber as well. The load with the shortest duration, was assumed to have a medium-term duration and the humidity class was assumed to be 2, which gives the modification factor $k_{mod} = 0.8$, from table 3.1 in Standard Norge (2010c).

When it comes to the chose of bolt types, the steel bolts was assumed to have the 4.8 strength class with a tensile strength of 400 N/mm^2 (Standard Norge, 2009a). For the bolts in aluminium, the material was chosen to be an alloy with the numerical designation EN AW5019, which has a characteristic ultimate tensile strength of 310 N/mm^2 (Standard Norge, 2009b). A figure of the geometry of one metal plate is given in figure 3.2. The dimensions and number of bolt holes in the figure is arbitrary and is not the result for any of the materials.

3.1 Difference in weight of connector in aluminium and steel

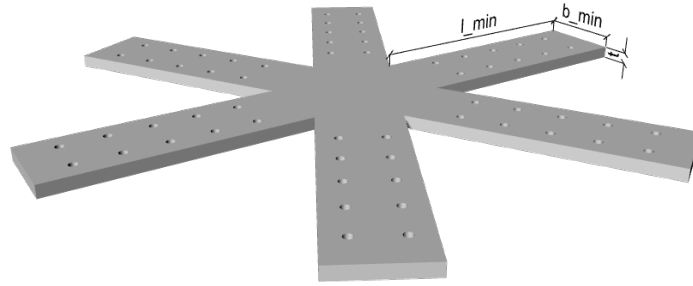


Figure 3.2: Connector dimensions of one metal plate

When finding the optimal connector dimension with lowest weight for each material, the width of the metal plates could not exceed the width of the timber beam of 200 mm. For instance, this led to that if the timber aluminium connection was having two bolt rows, the diameter of the bolts could not be bigger than 12 mm, which was assumed to be the minimum size of diameter. To find the minimum dimensions of the different parameters in each connector, the connectors were designed from having as few bolts as possible and the least possible diameter that is necessary to have sufficient capacity for all failure modes. The metal plates are assumed to have a thickness of 20 mm, which means that the width of the aluminium plate has a minimum value of 176 mm plus $2 \cdot d$, and the minimum value of the width of the steel plate is 105 mm plus $2 \cdot d$, see figure 2.2. In addition, the minimum width and length of the plates are restricted by spacing requirements.

3.1.2 Johansen's equations

To find the lateral load carrying capacity per shear plane per fastener, Johansen's equations in Standard Norge (2010c), section 8.2.3, were used. In this type of connection, there is four shear planes. For connections with multiple shear planes, the load carrying capacity for the outer members should be calculated by assuming that they are in single shear. On the other hand, the load carrying capacity for the inner members should be calculated by assuming that they are in double shear. In addition, the load carrying capacity of timber connections with multiple slotted in steel plates, should be calculated by assuming thick steel plates, regardless of plate thickness. Therefore, the following equations were used for the outer and inner members, respectively.

3.1 Difference in weight of connector in aluminium and steel

$$F_{v,Rk} = \min \begin{cases} f_{h,k} \cdot t_1 \cdot d & (c) \\ f_{h,k} \cdot t_1 \cdot d \left[\sqrt{2 + \frac{4 \cdot M_{y,Rk}}{f_{h,k} \cdot d \cdot t_1^2}} - 1 \right] + \frac{F_{ax,Rk}}{4} & (d) \\ 2.3 \sqrt{M_{y,Rk} \cdot f_{h,k} \cdot d} + \frac{F_{ax,Rk}}{4} & (e) \end{cases} \quad (3.1)$$

$$F_{v,Rk} = \min \begin{cases} 0.5 \cdot f_{h,2,k} \cdot t_2 \cdot d & (l) \\ 2.3 \sqrt{M_{y,Rk} \cdot f_{h,2,k} \cdot d} + \frac{F_{ax,Rk}}{4} & (m) \end{cases} \quad (3.2)$$

$M_{y,Rk}$ is the characteristic yield moment for connections with lateral loaded bolts, and is given as:

$$M_{y,Rk} = 0.3 \cdot f_{u,k} \cdot d^{2.6} \quad (3.3)$$

where

$f_{u,k}$ is the characteristic tensile strength.

$f_{h,k}$ is the characteristic embedment strength in the timber member. In this case, it is the embedment strength in the grain direction and is calculated as following:

$$f_{h,0,k} = 0.082(1 - 0.01 \cdot d) \rho_k \quad (3.4)$$

where

ρ_k is the characteristic timber density in kg/m³.

$F_{ax,Rk}$ is the characteristic withdrawal capacity of the bolt. $\frac{F_{ax,Rk}}{4}$ is added to some of the equations because of the rope effect, and for bolts this part is restricted to 25 % of the Johansen's part. If the withdrawal capacity is unknown, this effect could be neglected, and is neglected here.

The load carrying capacity per shear plane per fastener should be the minimum value from the expressions above. In addition, it is important that the load carrying capacity is calculated by adding the capacity of compatible failure modes. This can be checked by figure 3.3.

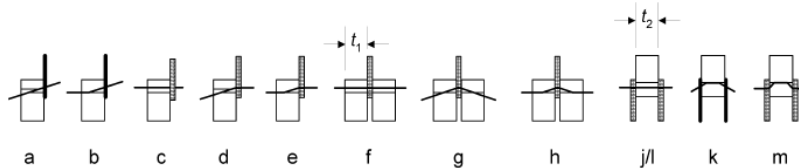


Figure 3.3: Failure modes for steel-timber connections (Standard Norge, 2010c, fig. 8.3)

3.1.3 Spacing of bolts

In (Standard Norge, 2009a, tab. 3.3), the spacing requirements for bolts in steel plates are given. These are similar to the spacing requirements for bolts in aluminium plates, given in (Standard Norge, 2009b, tab. 8.2). The spacing requirements for both steel and aluminium are given in table 3.1, below.

Table 3.1: Spacing requirements for bolts in steel and aluminium plates

e_1 [mm]	e_2 [mm]	p_1 [mm]	p_2 [mm]
$1.2 \cdot d_0$	$1.2 \cdot d_0$	$2.2 \cdot d_0$	$2.4 \cdot d_0$

The definition of the spacing symbols for fasteners in steel and aluminium are given in figure 3.4.

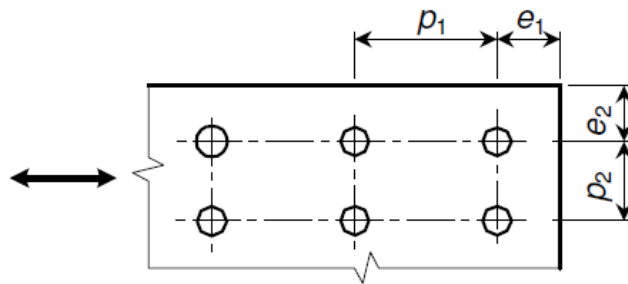


Figure 3.4: Symbols for spacing of fasteners in steel and aluminium, (Standard Norge, 2009b, fig. 8.1)

d_0 is the diameter of the bolt hole, and is given in Standard Norge (2018), as in table 3.2.

Table 3.2: Spacing requirements for steel and aluminium bolts

Bolt type	Value [mm]
M12-M14	$d_0 = d + 1$
M16-M24	$d_0 = d + 2$
M27-	$d_0 = d + 3$

When it comes to the distance requirements for bolts in timber members, these are different than those for steel and aluminium plates. The requirements are given in Standard Norge (2010c) as in table 3.3.

3.1 Difference in weight of connector in aluminium and steel

Table 3.3: Spacing requirements for bolts in timber members

a_1 [mm]	a_2 [mm]	$a_{3,t}$ [mm]	$a_{4,c}$ [mm]
$4 + \cos(\alpha) \cdot d$	$4 \cdot d$	$\max\{7 \cdot d; 80\}$	$3 \cdot d$

Figure 3.5, shows how the internal distances between fasteners and the distances to ends and edges, in timber members are defined. The end and edge distances depends on if they are loaded or not loaded, as can be seen at the bottom in the figure.

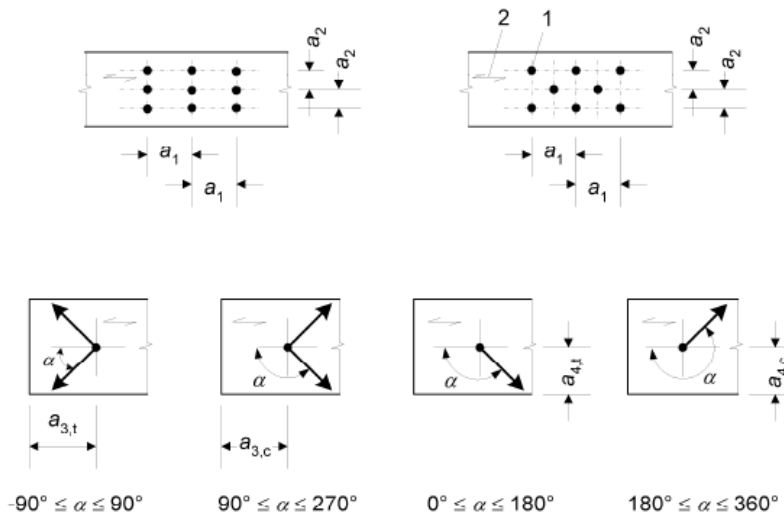


Figure 3.5: Symbols for spacing of fasteners in timber (Standard Norge, 2010c, fig. 8.7)

3.1.4 Splitting parallel to grain

Splitting parallel to grain is another failure mode that has to be checked for, when the connection has several fasteners along the grain direction. In such cases, tensile stresses will arise perpendicular to grain and can cause splitting parallel to the grain direction. To avoid this, the effective design load carrying capacity for each row of fasteners parallel to grain, should be calculated. The equation for this is given in section 8.1.2 in Standard Norge (2010c), as:

3.1 Difference in weight of connector in aluminium and steel

$$F_{v,ef,Rd} = \frac{k_{mod} \cdot n_{ef} \cdot F_{v,Rd}}{\gamma_M} \quad (3.5)$$

where

$F_{v,Rd}$ is the design capacity for each fastener in the grain direction, from Johansen's equations.

n_{ef} is the effective number of fasteners in one row in the grain direction.

$\gamma_M = 1.3$ for timber connections.

The effective number of fasteners in one row in the grain direction, is given in section 8.5.1.1(4) in Standard Norge (2009b), as:

$$n_{ef} = \min \begin{cases} n \\ n^{0.9} \sqrt[4]{\frac{a_1}{13 \cdot d}} \end{cases} \quad (3.6)$$

where

a_1 is the distance between the bolts in the grain direction.

n is number of bolts in one row in the grain direction.

d is the diameter of the bolt.

3.1.5 Block Shear

For block shear, there is two failure modes as the load transfer is either by tension parallel to grain stresses or by shear stresses. The expression for the block shear design load carrying capacity is given in annex A in Standard Norge (2010c), as:

$$F_{bs,Rd} = \frac{k_{mod}}{\gamma_M} \cdot \max \begin{cases} 1.5 \cdot A_{net,t} \cdot f_{v,k} \\ 0.7 \cdot A_{net,v} \cdot f_{t,0,k} \end{cases} \quad (3.7)$$

where

$f_{v,k}$ is the characteristic shear strength for the timber part.

$f_{t,0,k}$ is the characteristic tensile strength for the timber part.

$A_{net,t}$ is the net cross-section area perpendicular to the grain direction.

3.1 Difference in weight of connector in aluminium and steel

$A_{net,v}$ is the net shear area in the grain direction.

Furthermore, the equations for $A_{net,t}$ and $A_{net,v}$ is given as:

$$A_{net,t} = L_{net,t} \cdot t_1 \quad (3.8)$$

$$A_{net,v} = \begin{cases} L_{net,v} \cdot t_1 & \text{for the failure modes (c,f,j/l,k,m)} \\ \frac{L_{net,v}}{2} (L_{net,t} + 2 \cdot t_{ef}) & \text{in other failure modes} \end{cases} \quad (3.9)$$

where

t_{ef} is the effective width dependent on the fasteners failure mode

$L_{net,t}$ is the net width of the cross-section perpendicular to the grain direction, see figure 3.6.

$L_{net,v}$ is the total net length of the shear failure area, see figure 3.6

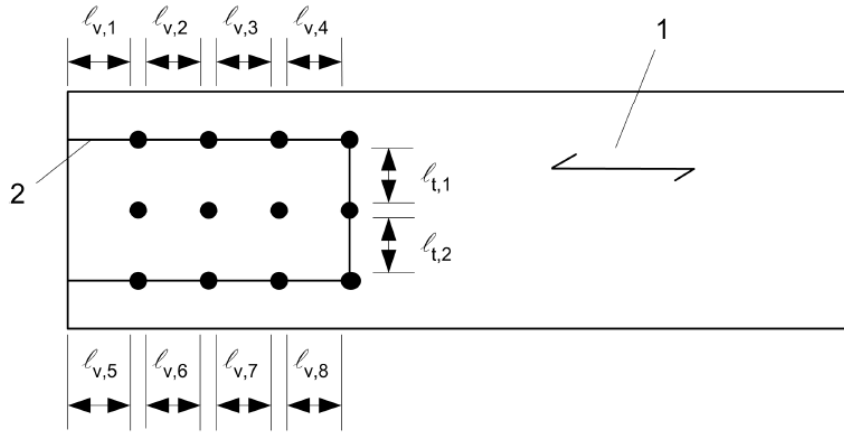


Figure 3.6: Block shear (Standard Norge, 2010c, fig. A1)

For thick steel plates, t_{ef} is given as:

$$t_{ef} = \begin{cases} 2 \cdot \sqrt{\frac{M_{y,Rk}}{f_{h,k} \cdot d}} & \text{failure modes (e and h)} \\ t_1 \left[\sqrt{2 + \frac{M_{y,Rk}}{f_{h,k} \cdot d \cdot t_1^2}} - 1 \right] & \text{failure modes (d and g)} \end{cases} \quad (3.10)$$

3.1.6 Shear resistance of bolts

For the steel bolts and aluminium bolts the expression for the shear resistance for each bolt per shear plane is the same and is given in table 3.4 in Standard Norge (2009a) and in table 8.5 in Standard Norge (2009b) respectively, as:

$$F_{v,Rd} = \frac{\alpha_v \cdot f_{ub} \cdot A}{\gamma_{M2}} \quad (3.11)$$

where

$\alpha_v = 0.5$ for steel bolts with classes 4.8 and aluminium bolts, where the shear plane passes through the threaded part of the bolt.

f_{ub} is the characteristic ultimate strength of the bolt, which is 400 N/mm² for the chosen steel bolts and 310 N/mm² for the chosen aluminium bolts.

$\gamma_{M2} = 1.25$ for both steel and aluminium design.

3.1.7 Results

By taking into account the failure modes mentioned above; block shear, splitting parallel to grain, capacity of metal plates, shear resistance of bolts and load transfer from Johansen's equations, a weight result for the optimised connector designs for both a steel connector and an aluminium connector is found. The calculations are done in Excel and can be found in appendix B.1. In section 3.1.1, the assumptions used in the calculation are explained. For both the aluminium and steel connector, the diameter became 12 mm and the number of bolts became 10, with 5 bolts in each bolt row. The result is given in table 3.4 below:

Table 3.4: Weight difference of connector in steel and aluminium

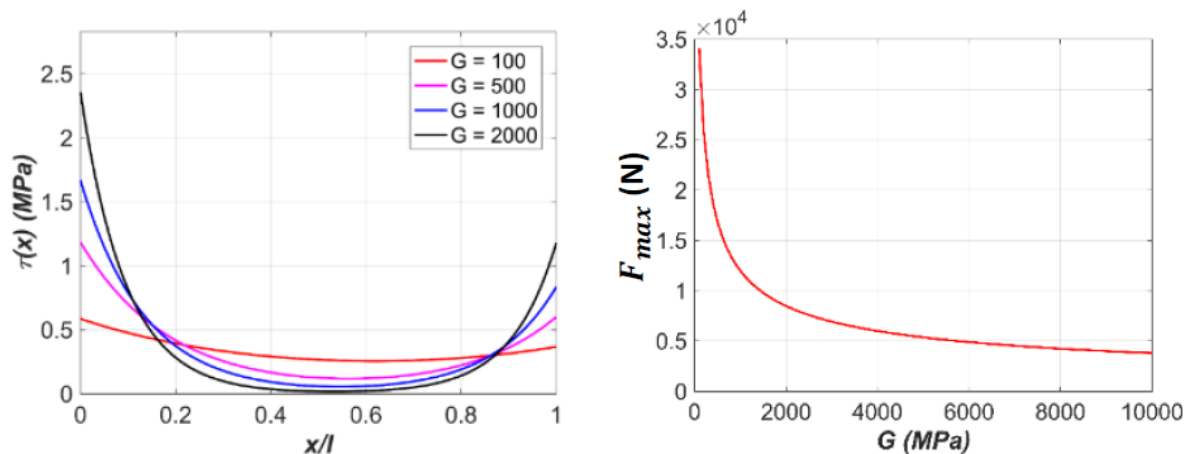
$m_{steel} [kg]$	$m_{alu} [kg]$	m_{steel}/m_{alu}
82.59	47.44	1.74

From the result, it is found that a connector in steel is 1.74 times the weight of a connector in aluminium with the same design. However, a question that should be asked is, if this difference in weight of a steel connector and a aluminium connector is big enough, so that this is a reason claiming that aluminium connectors are more preferable than steel connectors in gridshell structures.

3.2 Necessary glue surface in Glued Finger connector

In the last years, the research and development of timber connections bonded by adhesives have increased significantly (Vallée et al., 2017). This is due to the fact that traditional metal joints have limitations that lead to timber not being used in more complex structures.

When it comes to the calculation procedure of adhesively bonded timber connections, this is not straight forward as glued joints have uneven stress distributions. The most critical part for the shear stress distribution in such connections, is where the overlap ends, because there the shear stress may have sharp peaks and failure can arise. When failure occurs in one place, the whole joint will have failure, because the failure behaviour is like a zipper. There exists several methods to reduce the magnitude of the stress peaks, for instance to use ductile adhesives instead of stiff adhesives. Softer bonding results in a more uniform stress distribution which means higher capacity, see figure 3.7 below. In addition, the cohesive strength of the glue should be higher than the timber strength.



(a) Shear stress distribution for different bond-line stiffnesses

(b) Load capacity for different bond-line stiffnesses

Figure 3.7: Shear stress distribution and load capacity for different bond-line stiffnesses (Stamatopoulos, 2019)

There exists two main approaches in which a metal part can be adhesively connected to a timber part. One method is to use glued-in rods, which is a durable and effective technique. The other part is to glue-in metal plates directly in to the timber part, which is the relevant method for the GF connector. These metal plates can be either

3.2 Necessary glue surface in Glued Finger connector

solid plates or perforated plates (Vallée et al., 2017). The adhesives must have sufficient adhesion to both the timber part and the metal part. The reason for using perforated plates, is that then the strength will not rely on the adhesion between the metal part and the adhesive. This method is called Holz-Stahl-Komposit-Systeme (HSK). The benefit of this method is that the cavities are filled with adhesive, such that Adhesive Dowels (AD) are created. This technique gives a brilliant stiffness, and the yielding of the steel part, with high ductility, now becomes the critical part. In this method, it is assumed that the load transfer only happens through the ADs.

Vallée et al. (2011) have found through research that the joint capacity increase with the embedment length, but that this increase tends to flatten. This indicates an upper limit, beyond which no capacity increase should be expected. This is confirmed in other experiments of simple lap joints, see figure 3.8 for a demonstration of this effect.

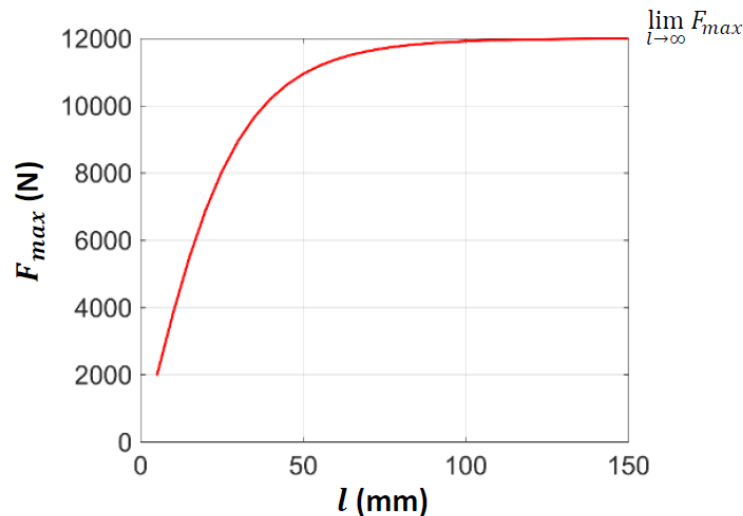


Figure 3.8: Influence of bond-line length on load capacity in a lap joint (Stamatopoulos, 2019)

In figure 3.9, the influence of bond-line length on the shear stress distribution is plotted. The figure shows that a less bond-line length, leads to a more even shear stress distribution, but on the other hand then the shear stress has a higher value.

3.2 Necessary glue surface in Glued Finger connector

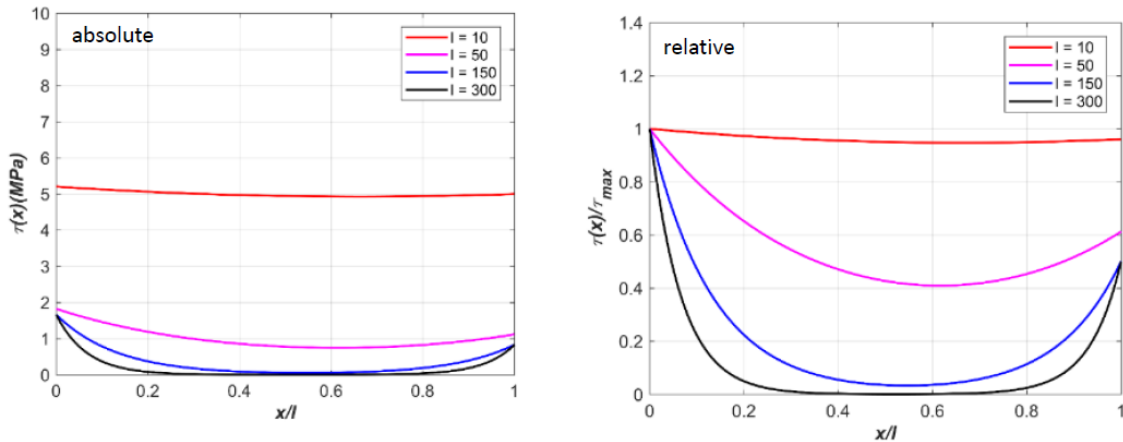


Figure 3.9: Influence of bond-line length on shear stress distribution in a lap joint (Stamatopoulos, 2019)

To give an analytical prediction of necessary glue surface for the GF-connector, Volkersen theory was used. This implicates rough assumptions and simplification of the geometry.

Assumptions in Volkersen theory:

- The adherents (timber part and aluminium part) are in pure axial stress.
- The adhesive layer is thin and it is in pure shear.
- The moment from the eccentricity between the two adherents are neglected.
- Linear elastic behaviour of glue, timber and aluminium members, until failure.

Other assumptions:

- All splices are orientated parallel to the grain direction in the timber member, creating lap joints with the timber member.
- The two outer splices take 1/5 of the total axial load of 167287.5 N together, the inner splices take 2/5 of the load each. This will imply that the outer splices will be half the length of the inner splices.
- The width of the splices is assumed to be 350 mm.

3.2 Necessary glue surface in Glued Finger connector

The values for the different parameters necessary for the calculation are given in table 3.5 below:

Table 3.5: Values for the necessary parameters

	t [mm]	E [N/mm²]	G [N/mm²]
GL32c	48.0	11200	540
Alu alloy	14.0	70000	27000
Glue	1.0	-	500

The Volkersen theory gives the following equations for the stress analysis:

$$\Gamma = \frac{G}{d_g} \quad (3.12)$$

where

d_g is the thickness of the glue.

$$\alpha = \frac{E_1 \cdot A_1}{E_2 \cdot A_2} \quad (3.13)$$

where

the parameters with notation 1 is the values for the timber part whilst the parameters with notation 2 is the values for the aluminium splices.

$$\omega = \frac{b \cdot \Gamma \cdot l^2}{E_1 \cdot A_1} \cdot (1 + \alpha) \quad (3.14)$$

$$F_{max} = \begin{cases} \frac{\tau_f \cdot \omega}{\Gamma \cdot l} \cdot \left(\frac{1}{E_1 \cdot A_1 \cdot \tanh \omega} + \frac{1}{E_2 \cdot A_2 \cdot \sinh \omega} \right)^{-1} & , \alpha \leq 0 \\ \frac{\tau_f \cdot \omega}{\Gamma \cdot l} \cdot \left(\frac{1}{E_1 \cdot A_1 \cdot \sinh \omega} + \frac{1}{E_2 \cdot A_2 \cdot \tanh \omega} \right)^{-1} & , \alpha \geq 0 \end{cases} \quad (3.15)$$

For $0 \leq x \leq l$, when failure, the stress distribution can be found from the following equation:

$$\tau(x) = \frac{F_{max} \cdot \omega}{b \cdot l \cdot (1 + \alpha) \cdot \sinh \omega} \left[\alpha \cdot \cosh \frac{\omega \cdot x}{l} + \cosh \omega \cdot \left(1 - \frac{x}{l} \right) \right] \quad (3.16)$$

3.2.1 Results

The calculations of necessary glue surface in GF connector are done in Excel, by use of the goal seek function, and the Excel sheet is given in appendix B.2. The main results can be found in table 3.6, below:

Table 3.6: Estimation of necessary cross section and splice lengths in GF connector

$L_{inn,min}[mm]$	$L_{out,min}[mm]$	$A_{min}[mm^2]$
24.46	12.23	42813.1

The estimation value of necessary glue surface is for all splices together. Since the width of the splices, of 350 mm, is quite large, the result has small values for the minimum splice lengths. One weakness is that, in the calculations, the shear force is not taken into account, only the moment and the axial force. In addition, it is important to remember that if the embedment lengths are increased, the amplification of the joint capacity will tend to flatten, as shown in figure 3.8.

3.3 Diameter and penetration length of threaded rods in Split Ring connector

When estimating the diameter and penetration length of the threaded rods in the SR connector, rules are not given directly in Eurocode 5 (EC5). Thus, equations given in EC5 and the ETA for screws and bolts, are assumed to be valid for threaded rods as well. Since, the connection is subjected to both moment, shear and axial load, these loads have to be taken into account when finding an estimation.

According to section 8.7.3 in Standard Norge (2010c), the failure criterion for a screw subjected to lateral and axial loading is:

$$\left(\frac{F_{ax,Ed}}{F_{ax,Rd}}\right)^2 + \left(\frac{F_{v,Ed}}{F_{v,Rd}}\right)^2 \leq 1 \quad (3.17)$$

3.3.1 Axial capacity

To calculate the axial capacity of the threaded rods, the failure modes that has to be checked for is, withdrawal failure, buckling failure and rod failure. In addition, it is assumed that an effective number of rods should be used as for screws. Thus, the axial capacity is given as:

$$F_{ax,Rd} = n_{ef} \cdot \min \begin{cases} (F_{ax,\alpha,Rk} \cdot k_{mod})/\gamma_M \\ F_{ki,Rk}/\gamma_{M1} \\ F_{tens,Rd} \end{cases} \quad (3.18)$$

The expression for the effective number of threaded rods, is assumed to be the same as for screws given in section 8.7.2(8) in Standard Norge (2010c), as:

$$n_{ef} = n^{0.9} \quad (3.19)$$

The characteristic withdrawal capacity for a single threaded rod is assumed to be the same as for screws given in section 8.7.2(5) in Standard Norge (2010c), as:

$$F_{ax,\alpha,Rk} = \frac{f_{ax,k} \cdot d \cdot l}{1.2 \cdot \cos^2\alpha + \sin^2\alpha} \left(\frac{\rho_k}{\rho_a}\right)^{0.8} \quad (3.20)$$

where

$f_{ax,k}$ is the characteristic withdrawal parameter perpendicular to grain in accordance with NS-EN 14592 for the corresponding density ρ_a [kg/m³];

3.3 Diameter and penetration length of threaded rods in Split Ring connector

d is the outer diameter measured on the threaded part;

l is the penetration length of the threaded rod;

ρ_k is the characteristic density, in kg/m^3 .

α is the insertion angle to the grain direction.

In Standard Norge (2010*c*), it is stated that equation 3.20 is only valid for angles over 30° , but here it is assumed that it is also valid for all angles. Stamatopoulos and Malo (2015*a*) have investigated the characteristic withdrawal capacity of threaded rods by using Norwegian spruce with a strength class of GL30c and a characteristic density of $\rho_k = 400 \text{ kg/m}^3$. It was found that the characteristic withdrawal strength parameter perpendicular to grain was $f_{ax,k} = 11.92 \text{ MPa}$.

The design tensile capacity of a threaded rod is assumed to be the same as for bolts and can be calculated from the expression for axially loaded bolts in Standard Norge (2009*a*):

$$F_{tens,Rd} = \frac{0.9 \cdot A_s \cdot f_{u,k}}{\gamma_{M2}} \quad (3.21)$$

where

A_s is the net cross-section of the rod.

$f_{u,k}$ is the characteristic ultimate strength of the rod material.

In EN 1999-1-1, the value for γ_{M2} is recommended to be 1.25 (Standard Norge, 2009*b*).

When it comes to the buckling capacity for threaded rods or screws, there are no rules in the Eurocode. But, in the European Technical Approval (ETA) for screws, rules are developed, and these are assumed to be valid for threaded rods as well. According to ETA Danmark A/S (2013) and ETA Danmark A/S (2016), the characteristic buckling capacity of screws in compression, can be calculated from the following equations:

$$F_{ki,Rk} = \kappa_c \cdot N_{pl,k} \quad (3.22)$$

$$N_{pl,k} = f_{y,k} \cdot \pi \cdot \frac{d^2}{4} \quad (3.23)$$

$$\kappa_c = \begin{cases} 1 & \bar{\lambda}_k \leq 0.2 \\ \frac{1}{(k + \sqrt{k^2 - \bar{\lambda}_k^2})} & \bar{\lambda}_k > 0.2 \end{cases} \quad (3.24)$$

$$k = 0.5[1 + 0.49 \cdot (\bar{\lambda}_k - 0.2) + \bar{\lambda}_k^2] \quad (3.25)$$

$$\bar{\lambda}_k = \sqrt{\frac{N_{pl,k}}{N_{ki,k}}} \quad (3.26)$$

$$N_{ki,k} = \sqrt{k_{v,\alpha,k} \cdot E_s \cdot I_s} \quad (3.27)$$

$$k_{v,\alpha,k} = (0.19 + 0.012 \cdot d) \cdot \rho_k \cdot \left(\frac{90^\circ + \alpha}{180^\circ} \right) \quad (3.28)$$

$$(3.29)$$

where

$f_{y,k}$ is the yielding strength of the screw.

$\bar{\lambda}_k$ is the relative slenderness.

$N_{ki,k}$ is the ideal elastic buckling load.

k_v is the foundation modulus.

E is the elastic modulus of the screw material.

I is the second moment of area of the screw.

$k_{v,\alpha,k}$ is the characteristic value of the foundation modulus as function of angle α .

3.3.2 Lateral capacity

When calculating the lateral capacity of threaded rods, an effective diameter is used as for screws given in section 8.7.1 in Standard Norge (2010c):

$$d_{ef} = 1.1 \cdot d \quad (3.30)$$

Thus, the effective diameter must be used in Johansen's equations, as well as in the expressions for the characteristic yield moment and the characteristic embedment

3.3 Diameter and penetration length of threaded rods in Split Ring connector

strength. These expressions are taken from EN 1995-1-1, and by using d_{ef} , the following expressions are obtained:

$$M_{y,Rk} = 0.3 \cdot f_{u,k} \cdot d_{ef}^{2.6} \quad (3.31)$$

$$f_{h,\alpha,k} = \frac{0.082(1 - 0.01 \cdot d_{ef})\rho_k}{k_{90} \cdot \sin^2\alpha + \cos^2\alpha} \quad (3.32)$$

For softwood, which is assumed, k_{90} is given as:

$$k_{90} = 1.35 + 0.015 \cdot d_{ef} \quad (3.33)$$

When neglecting the rope effect, the expression for the characteristic shear capacity is

$$F_{v,Rk} = \sqrt{2 \cdot f_{h,\alpha,k} \cdot d_{ef} \cdot M_{y,Rk}} \quad (3.34)$$

3.3.3 Spacing and distance requirements

The minimum requirements of spacings and distances that should be used for threaded rods, is assumed to be the same requirements as for screws. In the ETA (ETA Danmark A/S, 2013), these requirements are less strict than in EN 1995-1-1 (Standard Norge, 2010c). The requirements for both ETA and EN 1995-1-1 are given in table 3.7. See figure 3.10, for definitions of spacings and distances.

Table 3.7: Minimum spacing and distance requirements for threaded rods in timber members

	$a_1[mm]$	$a_2[mm]$	$a_{1,CG}[mm]$	$a_{2,CG}[mm]$
EN 1995-1-1	$7 \cdot d$	$5 \cdot d$	$10 \cdot d$	$4 \cdot d$
ETA-12/0114	$5 \cdot d$	$2.5 \cdot d$	$5 \cdot d$	$4 \cdot d$

3.3 Diameter and penetration length of threaded rods in Split Ring connector

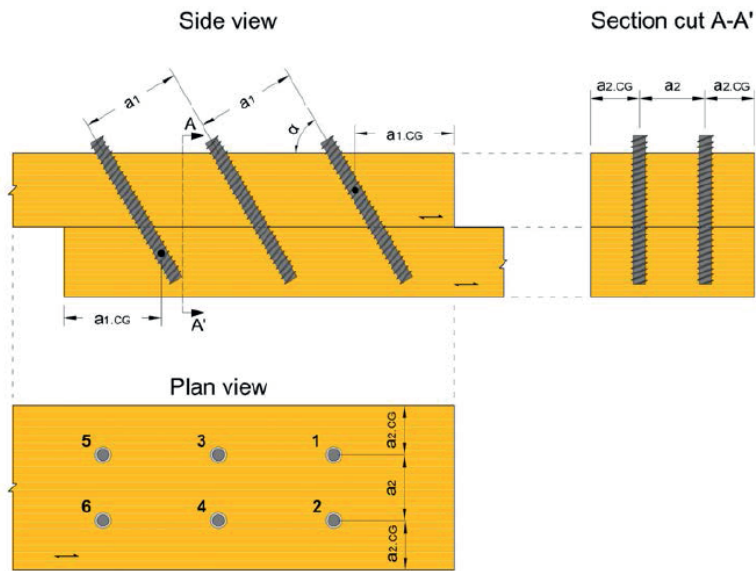


Figure 3.10: Definitions of edge and end distances for threaded rods (Stamatopoulos, 2016, fig.2.3)

Since the rods are inserted 10° to the grain direction in the end of the timber beam and not to an angle perpendicular to grain, as in figure 3.10, it is unsure if the spacing requirements given for threaded rods can be used for the SR-connector. In addition the rods are inserted against each other in the height of the cross section, such that the distance between the tip of the rods will be dependent on the penetration length, see figure 3.11.

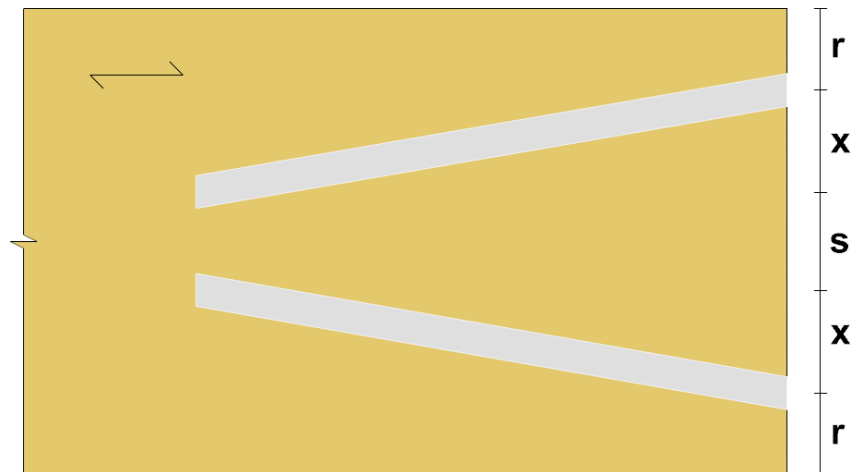


Figure 3.11: Definitions for spacings and distances in SR connector.

3.3.4 Results

The flow chart in figure 3.12 is showing the calculation procedure in this problem. Since the SR connector design consists of four threaded rods, the necessary diameter and the necessary penetration length for this diameter was calculated in Excel for four threaded rods. The calculation can be found in section B.3 in the appendix. To find a result, the goal seek function was used for two values. The failure criterion was set to the value 1.0 by changing the size of the diameter, and the necessary height of the cross section was calculated from spacing distances and set to the value 350 mm, by changing the penetration length. This was repeated until the values for failure criterion was 1.0 and the necessary height was 350 mm.

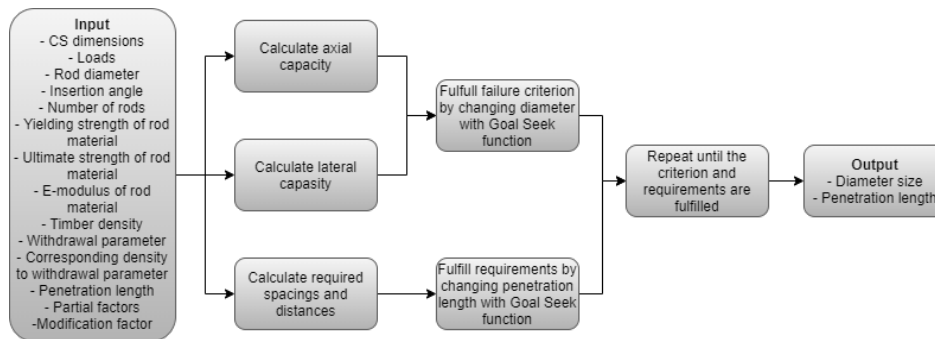


Figure 3.12: Flow chart of calculation procedure

The additional assumptions below are assumed in the calculation to be able to get a result.

- The applied loads, material and cross-section are the same as in the British Museum redesign case project.
- Four bolts are inserted in the cross-section.
- The spacing requirement between two rods in one row are assumed to be $2 \cdot d$, and the distance requirement to the edge is assumed to be $3 \cdot d$.
- The spacing requirement between the rod tip of two rods in one column is assumed to be $2 \cdot d$, and the assumed requirement for the distance to the edges is $3 \cdot d$.
- The insertion angle is set to 10° , since the angle should not be less than $5-10^\circ$.
- k_{mod} is assumed to be 0.8.

3.3 Diameter and penetration length of threaded rods in Split Ring connector

The result can be found in table 3.8, below.

Table 3.8: Necessary diameter and penetration length of threaded rods in SR-connector with four rods.

Number of rods	Diameter [<i>mm</i>]	Penetration length [<i>mm</i>]
4	22.1	498.6

As the equations that is used in this calculation are assumed to be valid for threaded rods, these equations must be verified experimentally for threaded rods. Also, this result is dependent on the assumed minimum spacing and distance requirements, which is less strict than both in the ETA and in EN 1995-1-1. They are assumed to be less strict since it is not possible with two rods in one row with the spacing and distance requirements from ETA and EN 1995-1-1. But, the definitions of the spacings and distances in this case for the SR-connector are different than in the ETA and in EN 1995-1-1. Therefore, this should be investigated further by experimental testing.

4 Benchmarks - comparing structural behaviours

The GF and SR connectors, in aluminium, are designed to connect timber members. Since aluminium is an isotropic material and timber is an orthotropic material, the behaviour of the materials will be different. To compare the behaviour and stresses of an isotropic and orthotropic material, five different benchmarks were analysed by FEA. The FEA was done in Abaqus. In Abaqus, there is no units of measurements, so one have to be consistent with the system of units to get the right output. The chosen unit system can be found in table 4.1, and the default axis system and stress notations can be seen in figure 4.1.

Table 4.1: Chosen system of units in Abaqus

Mass	Length	Force	Stress
ton	mm	N	MPa

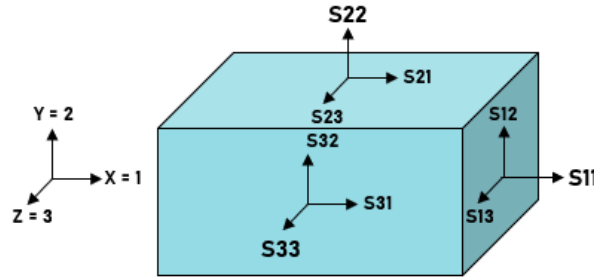


Figure 4.1: The axis system and stress notations in Abaqus

The material properties for the orthotropic material are defined by engineering constants associated with the material's principal directions, and are taken from experiments of Norwegian Spruce (Malo, 2018, p. 15). The engineering constants used are listed in table 4.2, where the Young's moduli (E_i), Poisson's ratios (ν_{ij}) and the shear moduli (G_{ij}) are stated. The material properties for the isotropic material are given in table 4.3, where the Young's modulus is equal to the orthotropic material's modulus in the stiffest direction, whereas the Poisson's ratio is taken from a typical isotropic material such as steel. In all finite element analyses in this thesis, a linear elastic material model is used for all materials. The results are given in the sections below, and more detailed tables and additional figures are given in appendix C.

Table 4.2: Material properties for orthotropic material

Engineering constants	E_1	E_2	E_3	ν_{12}	ν_{13}	ν_{23}	G_{12}	G_{13}	G_{23}
Value	10 000	800	400	0.5	0.6	0.6	600	600	30

Table 4.3: Material properties for isotropic material

Material Properties	E [MPa]	ν
Value	10 000	0.3

4.1 Case 1 - Cantilever

The first case, is a cantilever with a uniformly distributed load of 0.01 MPa, see figure 4.2. The geometry of the cantilever beam is $b \cdot h \cdot l = 100 \cdot 100 \cdot 1000 \text{ mm}^3$. Both principal stresses, shear stresses and deformation of the two different materials, are compared. The comparison of deflection is made at the top corner node at the free end, whilst the stress comparison is made at the top corner at the fixed support. Another isotropic material, with a Poisson's ratio equal to 0.495 is also modelled for comparison with the orthotropic material, as the stability criterion requires that $\nu < 0.5$ (Dassault Systèmes, 2014, 22.2.1), and ν_{12} is 0.5 for the orthotropic material. The Incompatible mode eight-node brick element (C3D8I) is used for modelling since the cantilever beam is subject to bending.

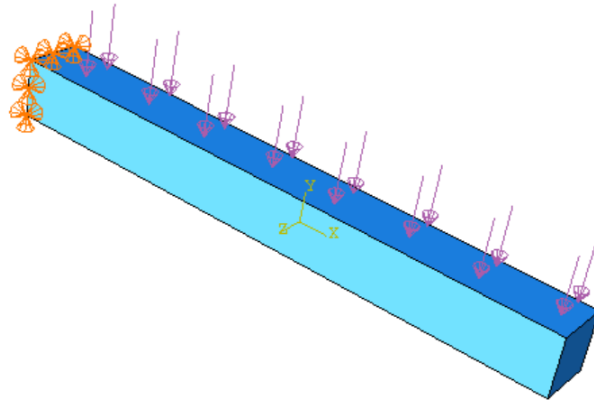


Figure 4.2: Benchmark, Case 1 - Cantilever

In figure 4.3, the displacement for the isotropic and orthotropic material is compared, and the displacement converges quickly for all the cases. The isotropic material gives less deformation than the orthotropic which corresponds well with the isotropic material being stiffer than the orthotropic material.

The Euler Bernoulli beam theory give the following displacement of the cantilever:

$$w = \frac{q \cdot L^4}{8EI} = \frac{0.01MPa \cdot 100mm \cdot (1000mm)^4}{8 \cdot 10000MPa \cdot \frac{1}{12} \cdot (100mm)^4} = 1.50mm \quad (4.1)$$

which fits well with the isotropic material with $\nu = 0.3$.

Looking at the stresses for both materials in figures 4.4 and 4.5, the isotropic stresses are a bit higher than the orthotropic stresses. With refinement of the mesh, the deformation converge in all cases whereas the stresses increase exponentially, i.e. do not

4.1 Case 1 - Cantilever

converge, due to the non-physical fixed boundary condition which induces stress concentrations at the supports. The worst case is the isotropic material with $\nu = 0.495$, where the stresses continues to increase. Values of Poisson's ratio approaching 0.5 result in nearly incompressible behaviour, and it is recommended to use solid continuum hybrid elements to avoid potential convergence problems for such materials (Dassault Systèmes, 2014, 22.2.1). Therefore, it might not be realistic to use $\nu = 0.495$ for comparison. In retrospect, one should have considered to compare the stresses at another location of the beam to experience better convergence.

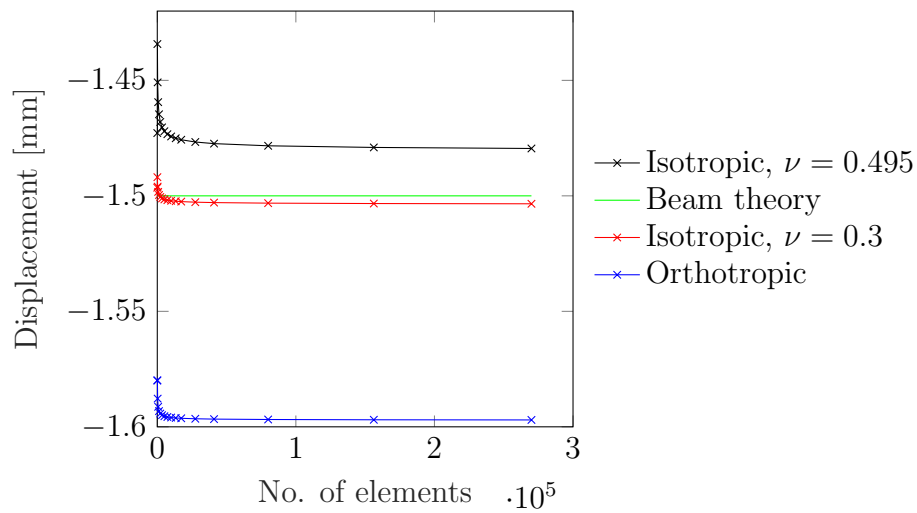


Figure 4.3: *U case 1*

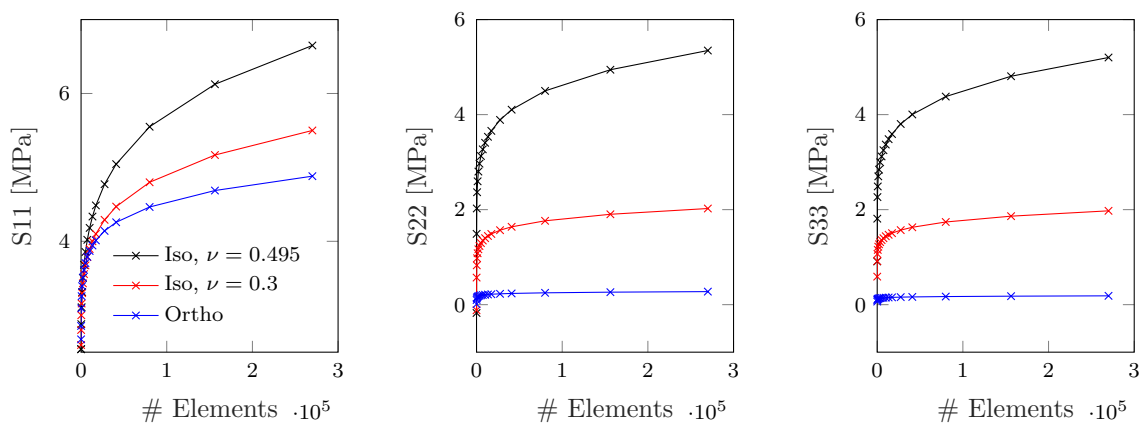


Figure 4.4: *Principal stresses case 1*

4.1 Case 1 - Cantilever

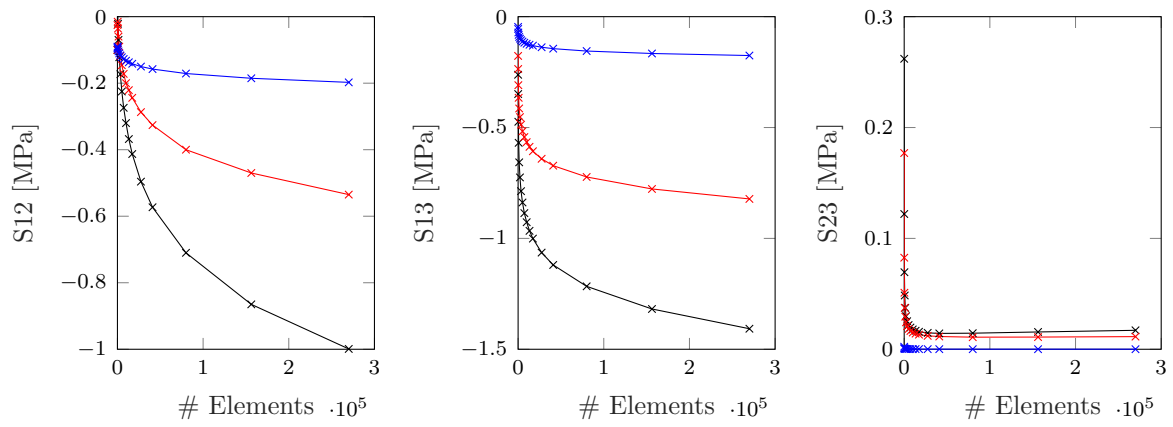


Figure 4.5: Shear stresses case 1

4.2 Case 2 - Column

The second benchmark is a column which is fixed in the bottom and applied a uniform distributed load of 0.01 MPa on the top, see figure 4.6. The dimensions of the column is $b \cdot h \cdot l = 100 \cdot 100 \cdot 2000 \text{ mm}^3$. The principal stresses in the top, left corner node in the fixed support and the buckling coefficient are compared for the two cases.

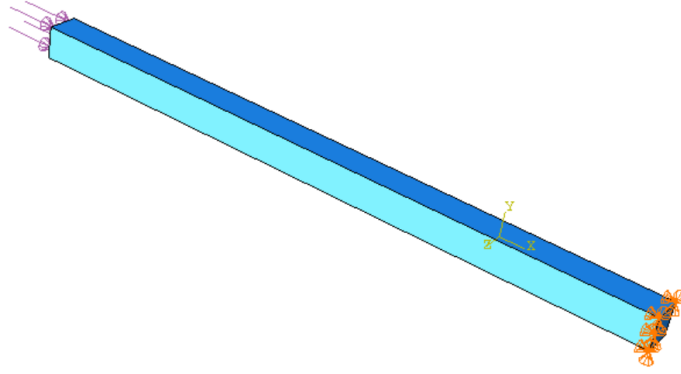


Figure 4.6: Benchmark, Case 2 - Column

Figure 4.8 shows the comparison of the buckling coefficient for the isotropic and orthotropic material. To get the buckling load, the buckling coefficient are multiplied with the applied load. So, for the isotropic and orthotropic material, the buckling loads for the biggest number of elements are respectively:

$$N_{b,iso} = 1907 \cdot 0.01 \text{MPa} \cdot (100 \text{mm})^2 = 190.70 \text{kN} \quad (4.2)$$

$$N_{b,ortho} = 1670.5 \cdot 0.01 \text{MPa} \cdot (100 \text{mm})^2 = 167.05 \text{kN} \quad (4.3)$$

The Euler load for both cases are:

$$N_{b,E} = \frac{\pi^2 \cdot 10000 \text{MPa} \cdot \frac{(100 \text{mm})^4}{12}}{(2000 \text{mm})^2} = 205.61 \text{kN} \quad (4.4)$$

The buckling length is chosen as the length of the column, since the buckling mode with the lowest positive value has the buckling shape as the one in figure 4.7.

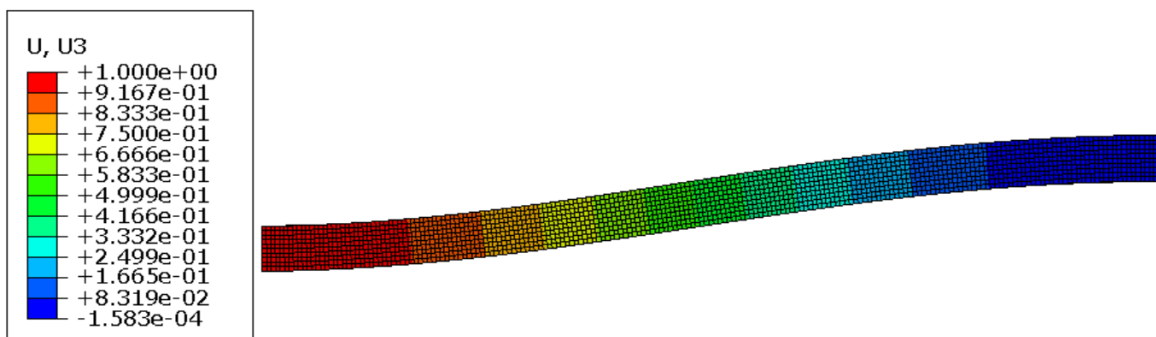


Figure 4.7: Buckling mode

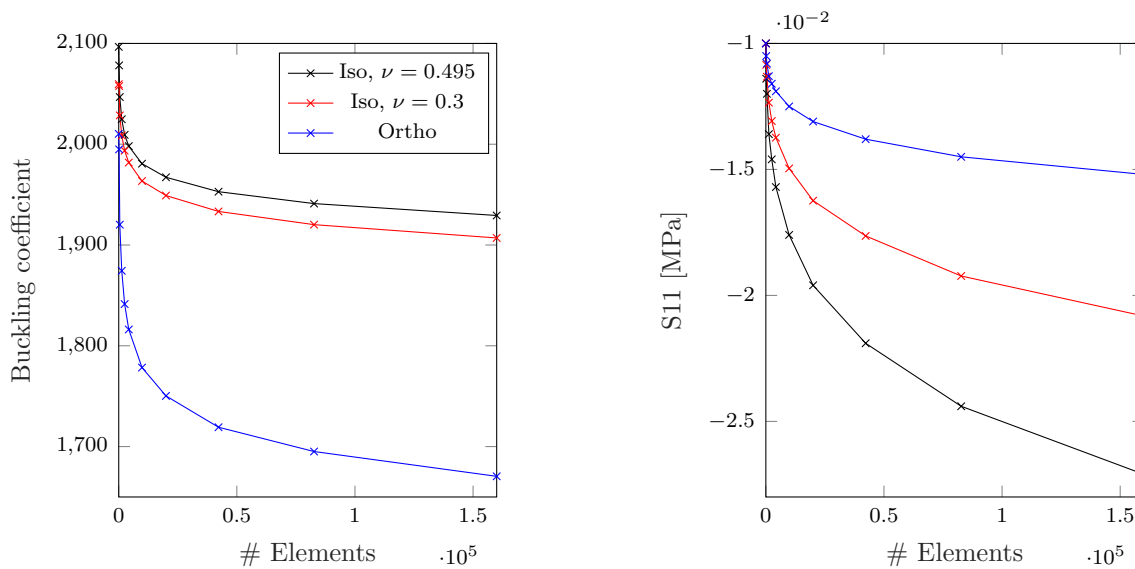


Figure 4.8: Buckling coefficient and S11

4.3 Case 3 - Bonded connection

The next benchmark, is two parts bonded together. Both parts have the dimension $b \cdot h \cdot l = 100 \cdot 100 \cdot 500 \text{ mm}^3$, and the applied tensile stress is 0.01 MPa as in the previous cases. The parts are bonded together by a 0.2 mm thick adhesive layer with a Young's modulus of 2500 MPa with a tie constraint in Abaqus. The model can be seen in figure 4.9.

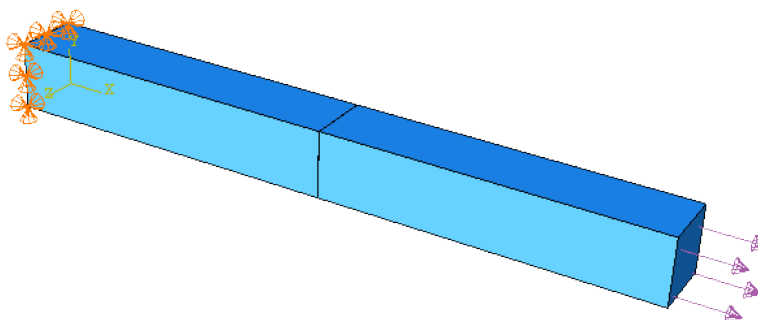
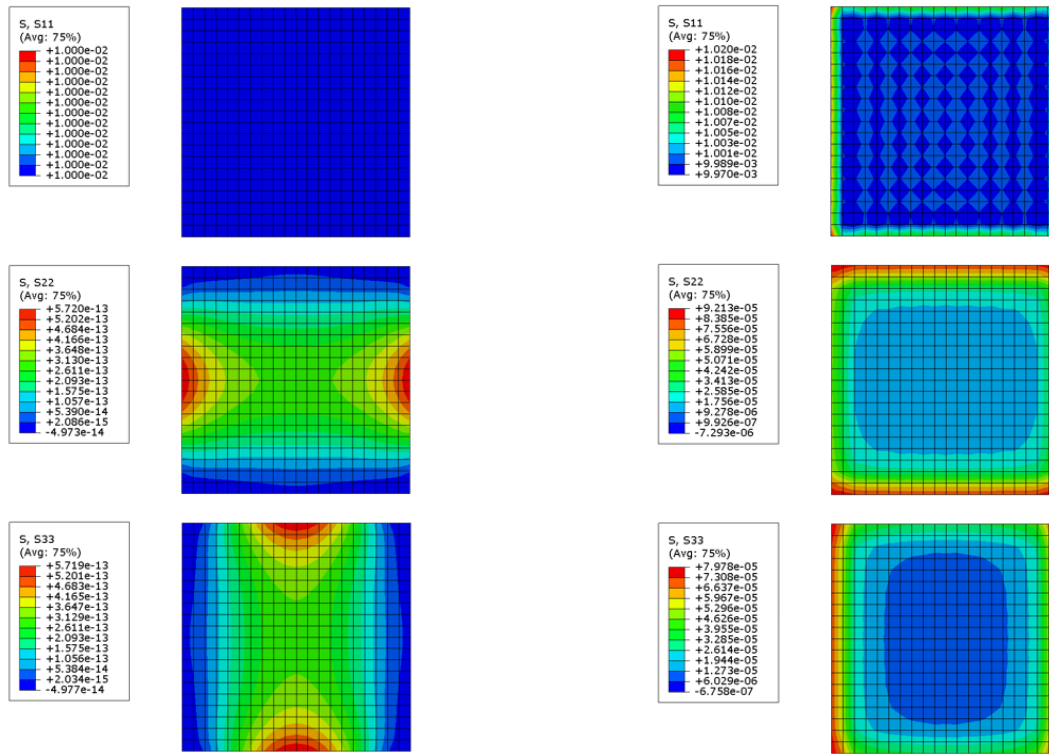


Figure 4.9: Benchmark, Case 3 - bonded

The stresses are compared in cross-sectional stress plots as shown in figure 4.10 where the parts are tied together. For the isotropic material, all the stresses are in the load direction (S11), as expected, whereas the stress in the orthotropic material is fairly more distributed in the different directions.

4.3 Case 3 - Bonded connection



(a) Isotropic (S_{11} , S_{22} , S_{33})

(b) Orthotropic (S_{11} , S_{22} , S_{33})

Figure 4.10: Comparison of principal stresses in bonded contact

4.4 Case 4 - Bonded connection with eccentricity

Similar parts to that of case 3 in section 4.3 are tied 100 mm along the length of the parts, so that the tensile stress is applied with an eccentricity to the fixed support, as seen in figure 4.11. The dimensions of the parts, the applied stress and the contact type is the same as in case 3.

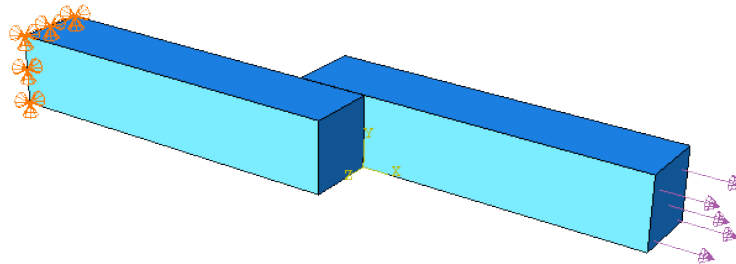


Figure 4.11: Benchmark, Case 4 - Bonded type with eccentricity

Similar to case 3, the stresses are compared along the bonded contact in stress plots, as shown in figure 4.13, where the parts are tied together. This shows that the difference in the stress magnitude between the isotropic and orthotropic material is larger when the load is applied with an eccentricity to the longitudinal axis. For lap joints, an even shear distribution, with its maximum in the middle of the glue line and not its maximum at ends, is the favourable shear distribution. The glue material should not be too stiff. If it is too stiff, large stresses will arise at the ends, see figure 4.12.

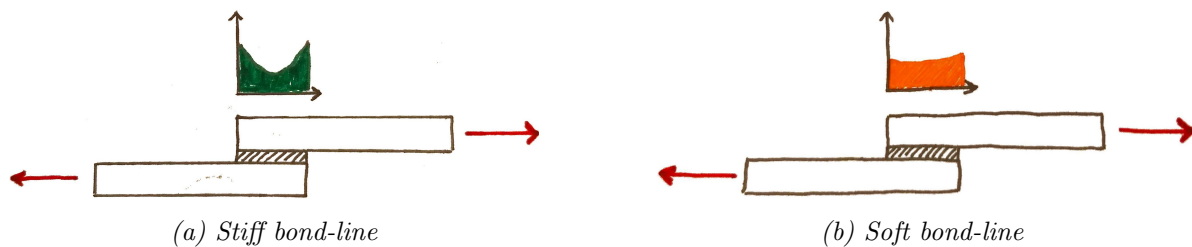
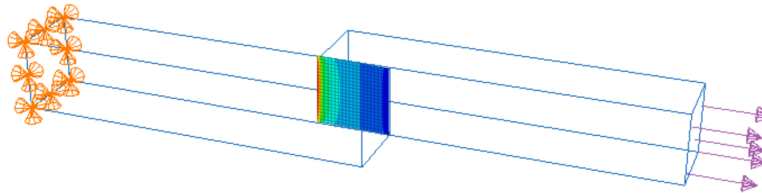


Figure 4.12: Shear stress distributions of bond-lines

4.4 Case 4 - Bonded connection with eccentricity



(a) Contact surface where the stress distribution plots are taken from

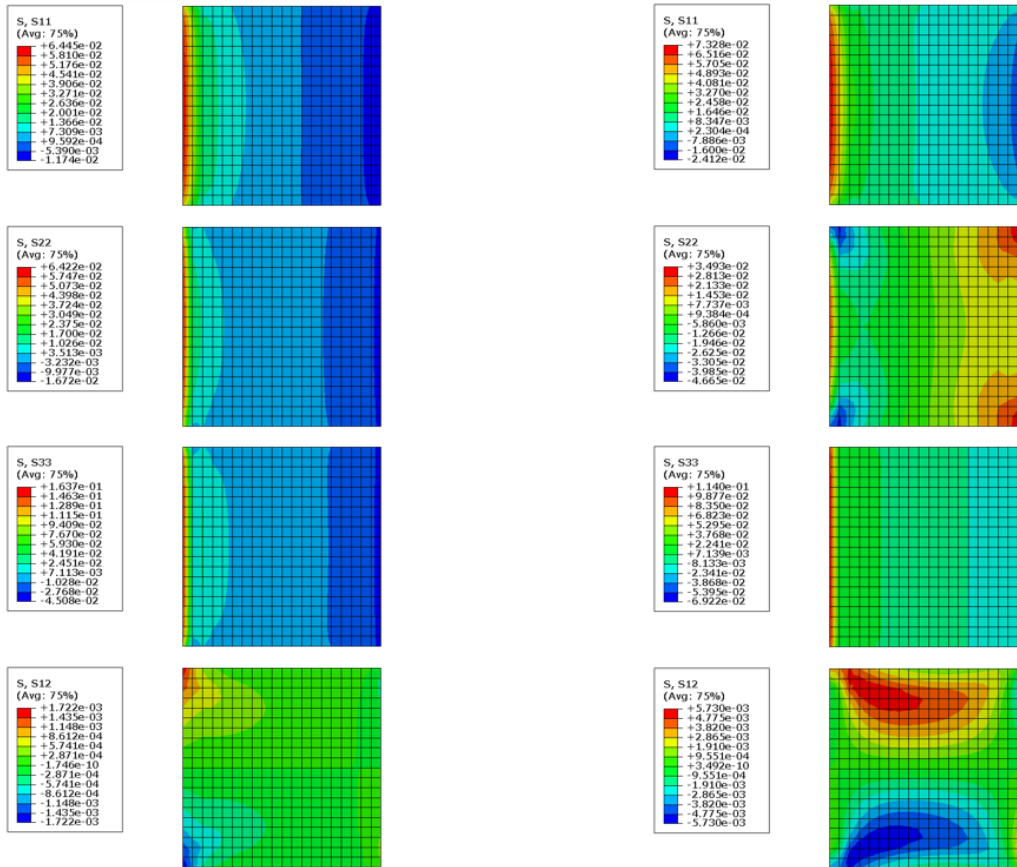


Figure 4.13: Comparison of stresses in bonded contact with eccentricity. The left part of the cross-section is closer to the fixed support, whereas the right part is closer to the applied load.

The distribution of S_{12} on the top of the glue surface connected to the fixed part, is plotted for both the isotropic and orthotropic case, see figures 4.14 and 4.15. From the plots of the shear distribution of S_{12} , it can be seen that for the isotropic material the shear stress has its highest peak at the left end. For the orthotropic material the shear stress tends to be higher at the left side, but a high shear stress peak also appears at the right side.

4.4 Case 4 - Bonded connection with eccentricity

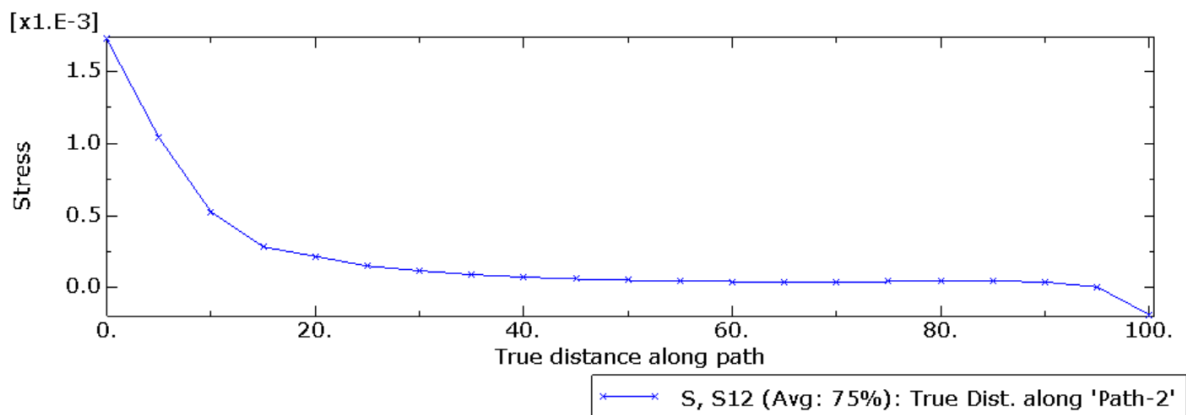


Figure 4.14: Shear distribution of S_{12} in isotropic material at the top in bonded contact

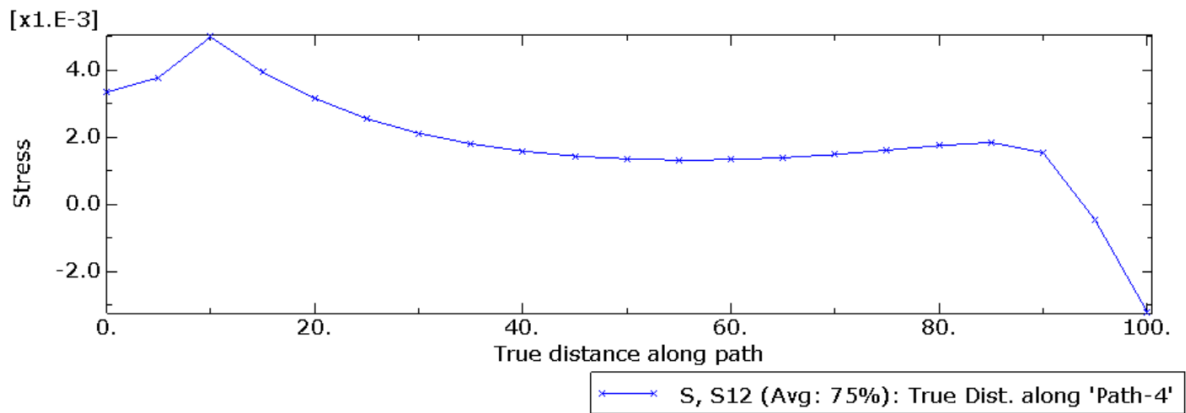


Figure 4.15: Shear distribution of S_{12} in orthotropic material at the top in bonded contact

4.5 Case 5 - Screwed connection

The last benchmark, is a steel part connected to the member part by two screws, see figure 4.16. To simplify the model in Abaqus, the screws are modelled as pipes without threads, and the screws are merged to the steel plates as one part. The diameter of the screws without threads is 20 mm, and the thickness of the steel plate is 20 mm. The length of the screws is set as the penetration length, 300 mm. The dimensions of the box member is $b \cdot h \cdot l = 350 \cdot 200 \cdot 1000 \text{ mm}^3$. When it comes to the contact between the screw pipes and the member part, this contact is modelled as tied, while the contact between the steel plate and member part is modelled as frictionless contact. The magnitude of the load applied is 100 kN distributed over the cross-section as a uniformly distributed load of 1.4286 MPa.

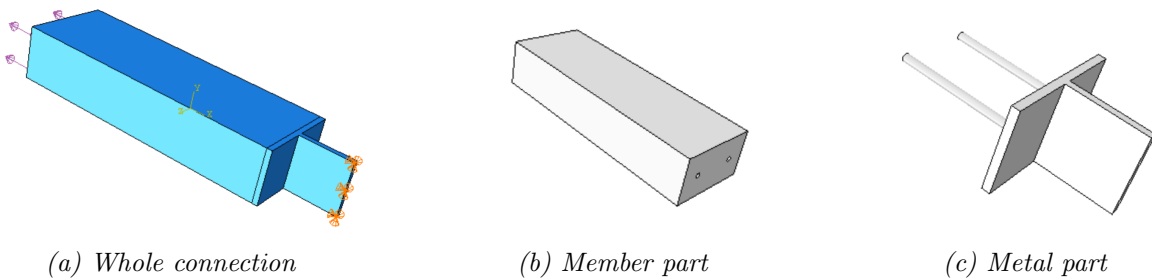


Figure 4.16: Benchmark, Case 5 - Connection

4.5.1 Theoretical capacity

The withdrawal capacity of connections with axially loaded screws is calculated with equation 3.20 given in section 3.3.1. Using GL32h, $n = 2$, $d = 20 \text{ mm}$ and $l_{ef} = 300 \text{ mm}$, $\alpha = 0^\circ$, $\rho_a = 400 \text{ kg/m}^3$ and a characteristic withdrawal strength parameter perpendicular to grain of $f_{ax,k} = 11.92 \text{ MPa}$ as input to equation 3.20, the withdrawal capacity is

$$F_{ax,\alpha,Rk} = 111.22 \text{ kN}$$

In figure 4.17 below, the withdrawal capacity is plotted for different angles, and it is found that the withdrawal capacity increases as the angle increases.

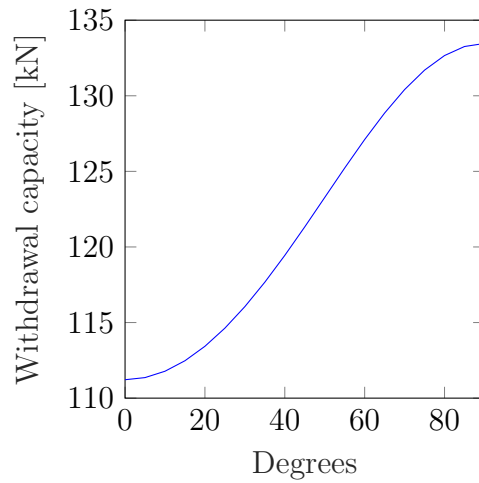


Figure 4.17: The withdrawal capacity increases as the angle increases

4.5.2 Results

The yield strength of the steel material in the rod is assumed to be 355 MPa. From the results in figure 4.18a and 4.18b for the connection with the isotropic and orthotropic member respectively, it shows that for both cases the highest Mises stress exceeds the yield stress. However, since it seems like the high stress concentrations appear on the outer surface of the rod and not inside the rod, this is neglected. Furthermore, the results shows that the stresses in the rod when connected to a member with an isotropic material are a bit higher than when connected to an orthotropic material.

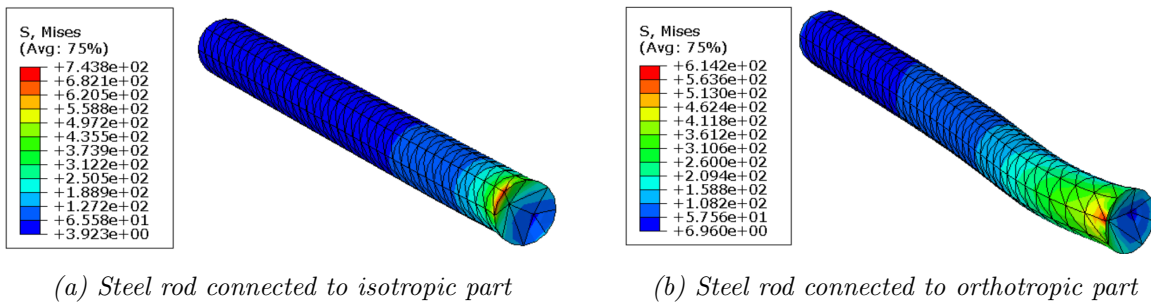


Figure 4.18: Mises stress in steel rod

5 Establishing a parametric finite element model

As written in section 1.5.1, current add-ons in Grasshopper does not provide the possibility to analyse solids in 3D. Abaqus was briefly introduced in section 1.5.2 and is a capable and advanced FEA tool. Setting up a model in Abaqus can be time consuming since one manually need to define all aspects of the model. Hence it is not well suited for making parametric models with slight changes in geometry. The aim is therefore to create a link between the Rhino/Grasshopper environment and Abaqus so that one can analyse solids parametrically.

One way of doing this is by making the geometry in Rhino/Grasshopper and thereafter exporting the geometry as a SAT-file and importing that into Abaqus. However, this is not very efficient as one still have to build the model in Abaqus. Another way of doing this is to build the parametric model in Rhino/Grasshopper and then run the analysis in Abaqus. This can be done by scripting an input text file which can be directly imported as a model and then run in Abaqus.

Mæhle (2017) created an extensive basis on exporting a model from Grasshopper through the INP-file to Abaqus in his master thesis. The focus has therefore been to implement and further develop his code and components. It is assumed that the reader has a general knowledge of FEA as the focus will be on explaining how the parametric model is set up to be run as a model in Abaqus. The resulting workflow is



5.1 The input file

The input file, or INP-file, is a text file. When a job for a model in Abaqus is submitted for analysis, the input file is generated for that model and this file is analysed. To see and modify the input file, a text editor can be used, and the format which the file is written in is ASCII (MIT, 2017). As it is time consuming setting up a model in Abaqus, it is desired to generate the INP-file in Grasshopper directly for the parametric model and then import the file to Abaqus for analysis. This will give a more effective workflow for making analyses for different dimensions of connector designs. A simple example which shows how an input file in Abaqus is structured is given below in listing 1. Importing the input file as a model in Abaqus, creates the model with geometry, boundary conditions and loading as shown in figure 5.1.

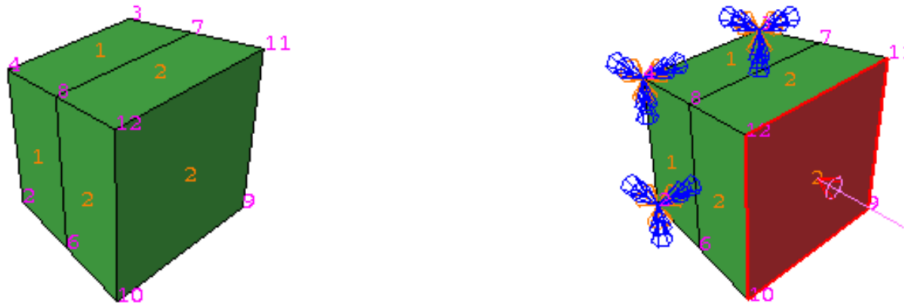
5.1 The input file

```
1 *Heading
2 GH_File
3 ** Job name: GH_Job Model name:
   GH_Model
4 *Preprint, echo=NO, model=NO,
   history=NO, contact=NO
5 ** PARTS
6 *Part, name=A
7 *Node
8 1, 0, -50, -50
9 2, 0, -50, 50
10 3, 0, 50, -50
11 4, 0, 50, 50
12 5, 50, -55, -55
13 6, 50, -55, 55
14 7, 50, 55, -55
15 8, 50, 55, 55
16 9, 100, -60, -60
17 10, 100, -60, 60
18 11, 100, 60, -60
19 12, 100, 60, 60
20 *Element, type=C3D8I
21 1, 1, 3, 4, 2, 5, 7, 8, 6
22 2, 5, 7, 8, 6, 9, 11, 12,
   10
23 *Nset, nset=Set-1, generate
24 1, 12, 1
25 *Elset, elset=Set-1, generate
26 1, 2, 1
27 *Orientation, name=Ori-1
28 1, 0, 0, 0, 1, 0
29 1, 0
30 **Section: A_section
31 *Solid Section, elset=Set-1,
   orientation=Ori-1, material=
   Steel,
32 *End Part
33 ** ASSEMBLY
34 *Assembly, name=Assembly
35 *Instance, name=A, part=A
36 *End Instance
37 *Nset, nset=fixed, instance=A
38 1,
39 2,
40 3,
41 4,
42 *Elset, elset=load-Surf, internal,
   instance=A
43 2,
44 *Surface, type=ELEMENT, name=load
45 load-Surf, S2
46 *End Assembly
47 ** MATERIALS
48 *Material, name=Steel
49 *Elastic
50 210000, 0.3
51 ** BOUNDARY CONDITIONS
52 ** Name: BC-1 Type: Displacement/
   Rotation
53 *Boundary
54 fixed, 1, 1
55 fixed, 2, 2
56 fixed, 3, 3
57 fixed, 4, 4
58 fixed, 5, 5
59 fixed, 6, 6
60 ** STEP: load
61 *Step, name=load, nlgeom=NO
62 Uniform Load
63 *Static
64 0.1, 1., 1e-05, 1.
65 ** LOADS
66 ** Name: load-Load Type: Pressure
67 *Dsload
68 load, P, 10
69 ** OUTPUT REQUESTS
70 *Restart, write, frequency=0
71 ** FIELD OUTPUT: F-Output-1
72 *Output, field, variable=PRESELECT
73 ** HISTORY OUTPUT: H-Output-1
74 *Output, history, variable=PRESELECT
75 *End Step
```

Listing 1: Example of an INP-file

5.1 The input file

First the node numbers and their coordinates are stated in the input file. The incompatible mode eight-node brick element (C3D8I) is assigned as the element type and the element numbers together with the nodes that make up the element comes next. In this example element number 1 consists of the nodes 1,3,4,2,5,7,8,6. All the nodes and elements makes up a set and the orientation and material is assigned for the whole set. Nodes 1,2,3 and 4 are fixed against displacements and rotation and a load of 10 MPa is applied to surface S2 of element 2.



(a) Two elements make up the model with node numbering and element numbering

(b) Model with boundary conditions and a surface pressure

Figure 5.1: The input file in listing 1 describes this model geometry with boundary conditions and loading

If one achieves to generate the INP-file for various geometries, this will open up the possibility of analysing solids parametrically in an efficient way.

5.2 FEM with Grasshopper components

In this section, descriptions of the grasshopper components used to create a parametric FE model, with an INP-file ready to be imported to Abaqus, are presented in tables along with more thorough descriptions of certain aspects of the components.

5.2.1 Creating the geometry

Rhino and Abaqus have different default right-handed Cartesian coordinate systems. Rhino have the Z-axis upwards, whereas Abaqus default coordinate system is rotated 90° around the X-axis, making the Y-axis being the upwards direction. This can be seen in figure 5.2. An issue may therefore occur when transferring geometry and conditions from Rhino to Abaqus. To avoid changing the setups of the programs, the issue is addressed by switching the Y- and Z-coordinates in Rhino such that the (X,Y,Z) coordinates in Rhino becomes the (X,Z,Y) coordinates in Abaqus.



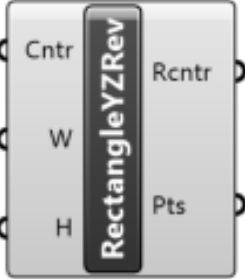



(a) In Rhino, the Z-axis is aligned upwards

(b) In Abaqus, the Y-axis is aligned upwards

Figure 5.2: Default coordinate systems in Rhino and Abaqus

Thus, the X-axis and the vertical axis are aligned equally in Rhino and Abaqus. However, the axis perpendicular to this plane has opposite directions, which results in a mirrored geometry. This imposes a challenge when sorting the nodes correctly so that Abaqus recognises elements with positive volumes. To address this issue, element nodes in Rhino are sorted counter clockwise, so that the points become sorted clockwise in Abaqus. It is also important to point out that while Rhino/Grasshopper begins numbering with 0, Abaqus begins enumerating with 1. In table 5.1, components that create and/or sort geometries are explained.

Table 5.1: Components that create and/or sort geometry

Description	Components
<p><i>RectangleYZRev</i> creates a rectangle in the YZ-plane from a centre point with chosen width and height. The output is a list of points sorted correctly which can further be used for meshing.</p>	
<p><i>SortPtsYZ</i> sorts a list of randomly ordered points primarily located in or near the YZ-plane, to a list of points counter clockwise. Complimentary components exist for the XZ-plane.</p>	
<p><i>PtsToSrf</i> creates a surface from a point list and can be convenient when for example assigning loads, boundary conditions or ties.</p>	
<p><i>GetVertices</i> extracts the vertices of a list of breps and sorts them. If the list of breps make up a closed shape, Closed is set as "True" and the first vertices are also added to the end of the list.</p>	

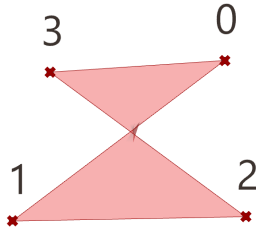
SortPts sorts the points by calculating the angle between the mean point of all the points and the points using the *Atan2* function, as seen in listing 2. In this way one can arbitrarily choose the points, without having to sort them first, see figure 5.3. This can be beneficial when creating larger models so that one does not have to manually sort the points in the correct order.

```

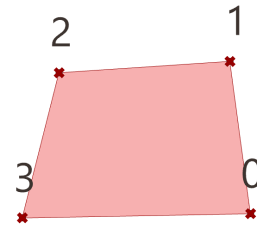
1   for (int i = 0; i < pointarray.Length; i++)
2     {angles[i] = Math.Atan2((pointarray[i].Z - cnt.Z), (pointarray[i].X -
   cnt.X)); //cnt is the central point}
3   Array.Sort(angles, pointarray);}

```

Listing 2: Sorting the points by using the *Atan2* function for points primarily located in or near the XZ-plane.



(a) Surface created from points in random order



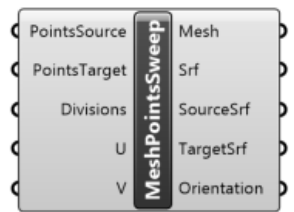
(b) Points sorted to get correct surface

Figure 5.3: SortPts sorts points automatically to reduce errors while creating new meshes from part in model

5.2.2 Making the mesh

In table 5.2, *MeshPointSweep*, a component which creates a mesh, is explained.

Table 5.2: MeshPointsSweep

Description	Component
<p><i>MeshPointsSweep</i> takes four corner source points and four corner target points, sorted in correct order, and creates a mesh between the points according to the assigned number of longitudinal and cross sectional divisions (u and v).</p>	

The different stages of the *MeshPointsSweep* code are illustrated in figure 5.4. It starts with four source points and four target points (5.4a) and generates lines between them (5.4b) with lengths that are divided in points according to the chosen number of divisions. From these points, surfaces are made in each division (5.4c). The nodes are then generated on the surfaces, first in the U-direction (5.4d) and then in the V-direction (5.4e) in compliance with the given input of the U- and V-divisions in the component. This is repeated for each surface until all the nodes are generated, creating $(U + 1) \cdot (V + 1) \cdot (Divisions + 1)$ nodes in total.

5.2 FEM with Grasshopper components

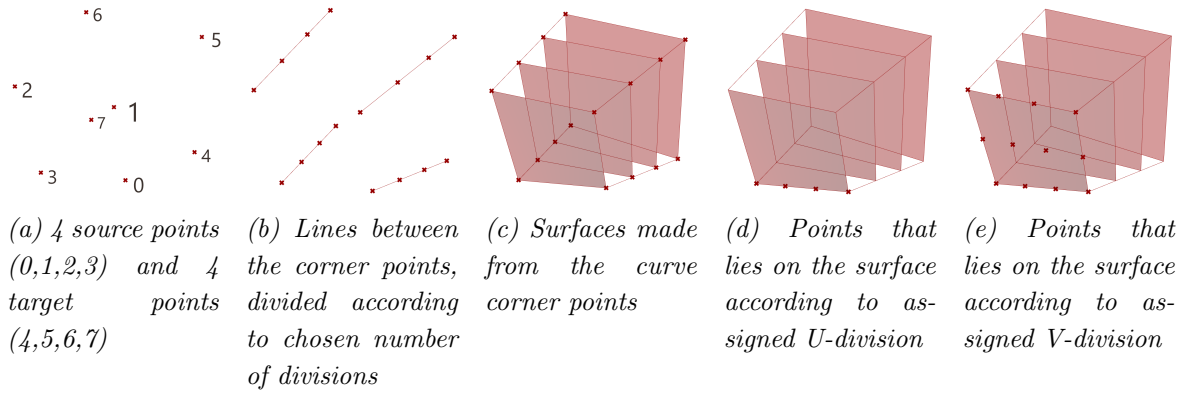


Figure 5.4: Stages of the *MeshPointsSweep* component

There are five outputs of the *MeshPointsSweep* component, which are illustrated in figure 5.5. *Mesh* consists of a data tree with the node list (5.5a, cross sectional surfaces that will make up the elements (5.5b, and a list of the number of divisions, number of nodes per division and the number of surfaces per division to be used further in the in the *AbaqusPart* component that will be described in table 5.7.

Srf are all the longitudinal surfaces (5.5c) which are sorted in a data tree so that the surfaces that are in the same plane are collected together. The *SourceSrf* and *TargetSrf* are the surfaces created from the source points (5.5d) and the target points (5.5e). These outputs can be practical when assigning which surfaces that will be loaded or restrained, as described in section 5.2.4. *Orientation* is the orientation of the mesh which will be further described in section 5.2.3.

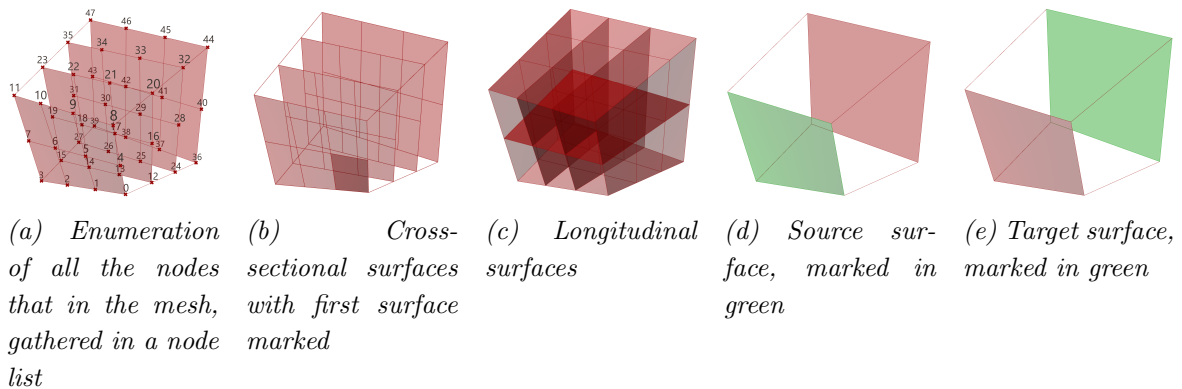


Figure 5.5: Output of the *MeshPointsSweep* component

5.2 FEM with Grasshopper components

An example of the mesh geometry and how the geometry looks like when it is imported in Abaqus can be seen in figure 5.6 and 5.7.

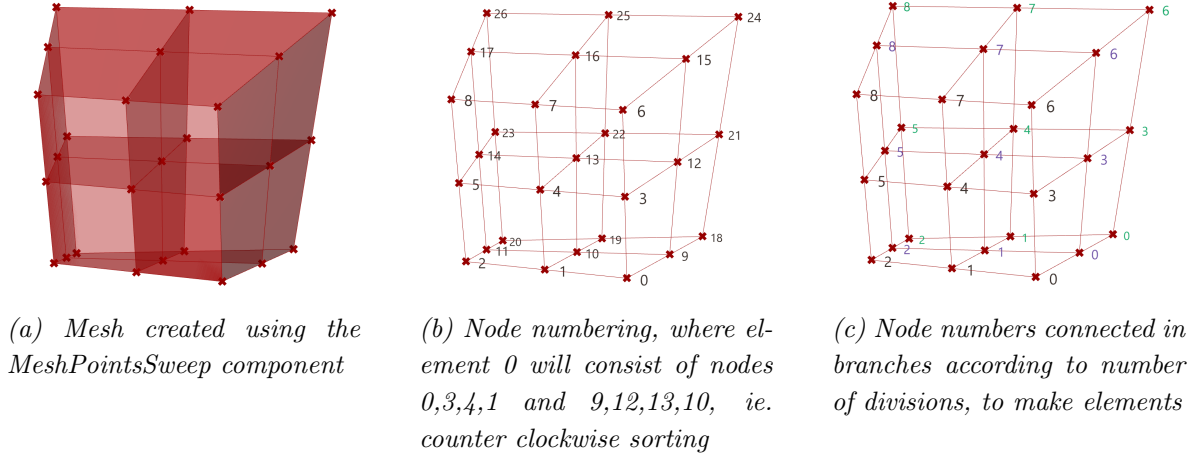


Figure 5.6: Geometry made in Grasshopper from 8 corner points, and assigned division of $2 \times 2 \times 2$, 8 elements in total

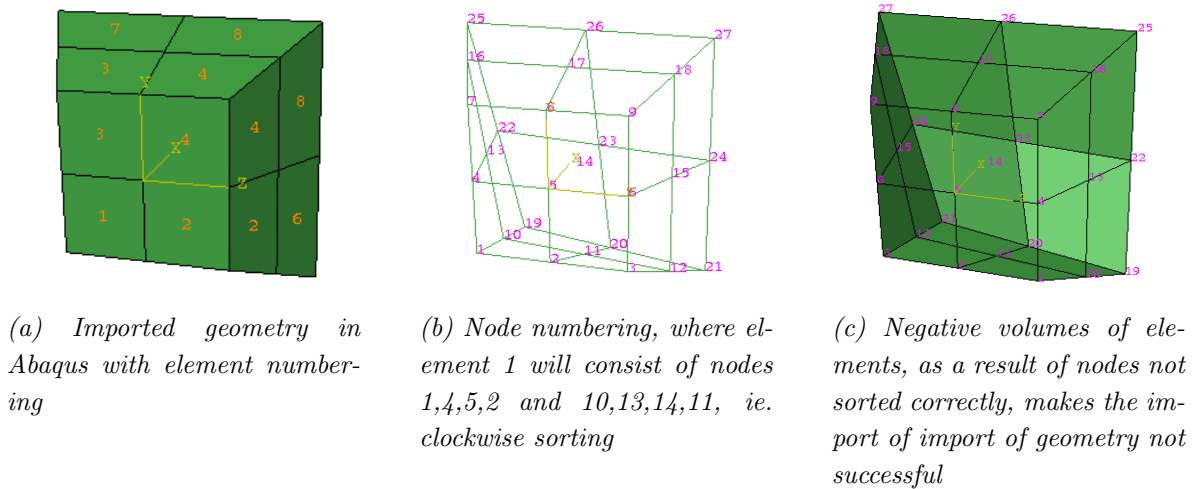
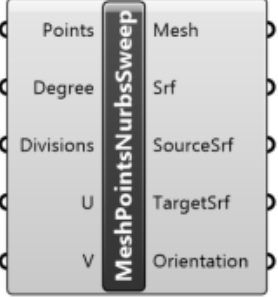


Figure 5.7: Imported, mirrored geometry in Abaqus. Note that Abaqus' numbering starts with 1, while Grasshopper starts with 0

In table 5.3 below, the *MeshPointsNurbsSweep* component is described, which is a further development of the *MeshPointsSweep* by use of NURBS curves.

5.2 FEM with Grasshopper components

Table 5.3: *MeshPointsNurbsSweep*

Description	Component
<p><i>MeshPointsNurbsSweep</i> is a further development of the <i>MeshPointsSweep</i> component which allows for more curved and complex geometry by using NURBS curves with chosen degree to approximate curves through a list of an arbitrary amount of points, as long as the points are sorted in one list sequentially in four and four corner points.</p>	

The component *MeshPointsNurbsSweep* makes the mesh similarly to the *MeshPointsSweep* component, but utilises NURBS curves to create edge curves, unlike *MeshPointsSweep* which create straight edge lines. The maximum degree of the NURBS curves are $(\text{Number of points} / 4) - 1$ as the list of points works as control points for the NURBS curves.

Figure 5.8 shows how the *MeshPointsNurbsSweep* component works and how one can easily adapt the mesh by increasing the NURBS curve degree and/or the longitudinal divisions.

In the following examples, the meshes are made coarsely to demonstrate how the mesh works and how the model can be run in Abaqus. The analysis results shown should therefore not be interpreted as final analysis results, but more as indications of stress distributions.

5.2 FEM with Grasshopper components

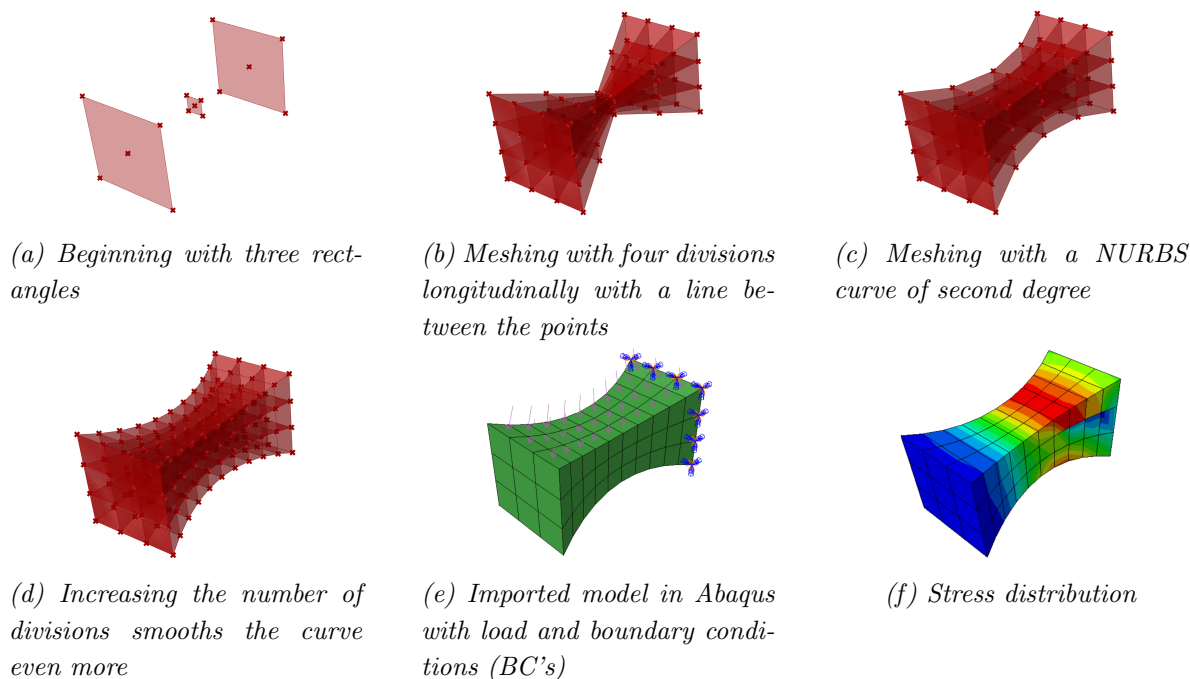


Figure 5.8: Example of making a more smooth mesh by approximating curves between corner points using NURBS curves in the *MeshPointsNurbsSweep* component

Figure 5.9 shows an example of how the *MeshPointsNurbsSweep* component can be used. A circle is made and the GH component *Perp Frames* is used which generates a number of equally spaced, perpendicular frames along a curve. Rectangles are made in the frames and the *GetVertices* component is used to extract the points to be used in the *MeshPointsNurbsSweep* component with *Closed* set to *True* to make a closed shape.

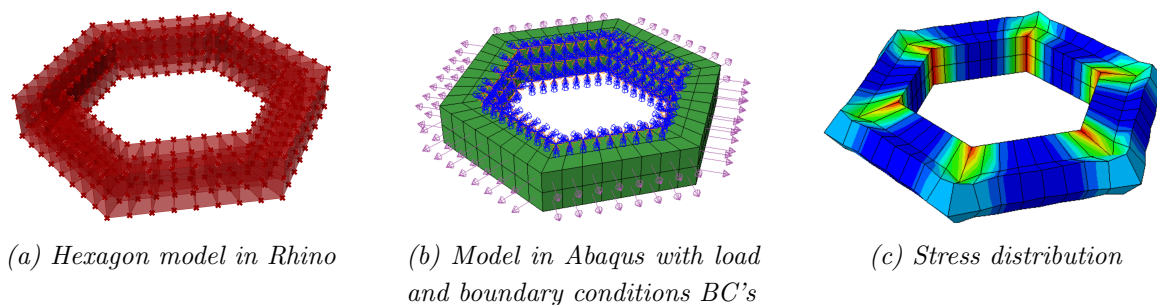


Figure 5.9: Hexagon mesh

By easily increasing the number of frames, the degree of the curve and the number of divisions in the same model one can get a circular mesh, as seen in figure 5.10.

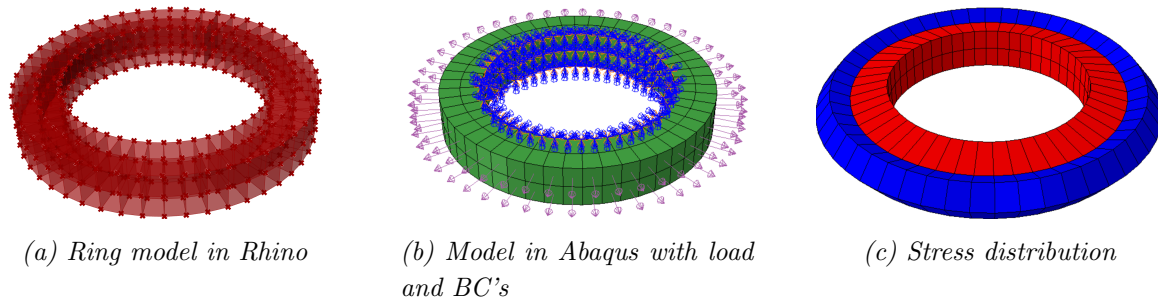


Figure 5.10: Ring mesh

The same procedure can be used to create a mesh from a geometry with varying cross-sections and rotations, as seen in figure 5.11.

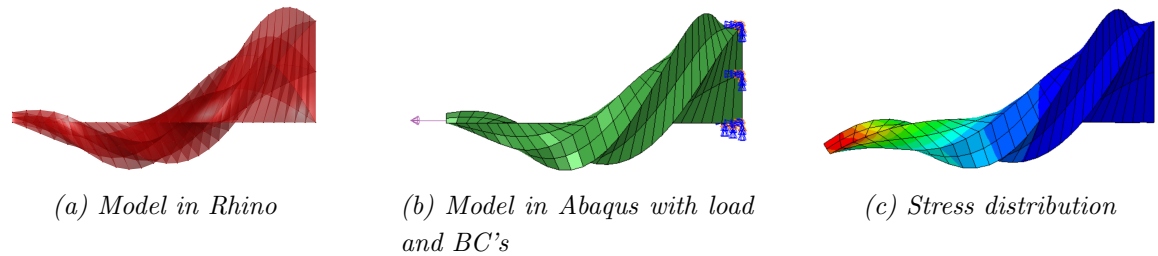


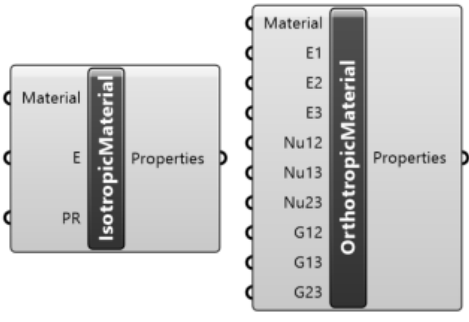
Figure 5.11: Twisted model

With the mesh components, it is possible to easily mesh various somehow rectangular geometries, and with the *MeshPointsNurbsSweep* component one can also mesh more curved and versatile geometry. However, as stated, the geometry has to be somehow rectangular and might therefore not be suitable for more complex geometry. In addition to this, if using the *MeshPointsNurbsSweep* component, it can be challenging to control the geometry as the NURBS curves approximates edge curves through the points and the shape can therefore change significantly when varying the degree or number of divisions.

5.2.3 Assigning materials and orientation

In table 5.4 below, the components for isotropic and orthotropic materials is described.

Table 5.4: Materials

Description	Component
<p><i>IsotropicMaterial</i> has steel as default material, but can take another isotropic material by its material properties as input.</p>	
<p><i>OrthotropicMaterial</i> has Norwegian spruce as default material, but can take another orthotropic material by its material properties as input.</p>	

Orthotropic materials, such as timber, have material properties that change according to the direction of the material. It is therefore important to assign the proper orientation to the parts with orthotropic materials in Abaqus, see figure 5.12. Orientation of the part is written in the input file as shown in listing 3.

```

1 *Orientation, name=Ori-1
2 1, 0, 0, 0, 1, 0, 0, 0, 0
3 1, 0

```

Listing 3: Example of how to assign the orientation of the part through the input file. Here the x-vector is the first direction, the y-vector is the second direction and the origin is (0,0,0)

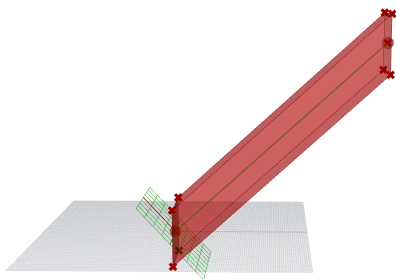
Where the second line has the coordinates of the vector along the first and second direction, as well as the coordinates of the origin point. The third line concerns the direction about which the additional rotation or rotations are given. In listing 3 the first direction is vector $[1,0,0]$, the second direction is vector $[0,1,0]$ and the origin point is $(0,0,0)$. The third axis is assigned automatically by calculating the vector cross-product of two others.

The orientations is assigned as part of the *MeshPointsSweep* and *MeshPointsNurbsSweep* components. To adjust for varying origin points and geometry, the orientation is assigned by making a vector between the mean points of the source points and target points, to make the first direction, see the script in listing 4. A normal plane is created from this vector and thereby the second direction is assigned.

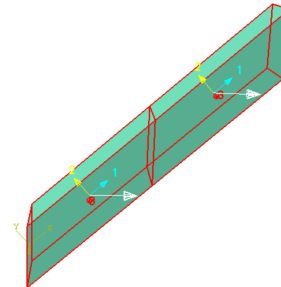
5.2 FEM with Grasshopper components

```
1 //orientation
2 List <string> orilist = new List<string>();
3 Vector3d vec1 = p2 - p1; //longitudinal direction of timber cross-
4 section central points = Direction 1 (x-axis). Created between the
5 average points (center points p1 and p2) of the source and target
6 points.
7 vec1.Unitize();
8 Plane nplan = new Plane(p1, vec1); //normal plane
9 Vector3d vec2 = nplan.XAxis; // Second axis (unitized)
10 double cx = p1.X; double cy = p1.Y; double cz = p1.Z; //center point
11 x,y,z
12 //coordinates of the first principal axis(x-axis)
13 double x1 = vec1.X + cx; double y1 = vec1.Y + cy; double z1 = vec1.Z
14 + cz;
15 //coordinates of the second principal axis(z-axis in Rhino, y-axis in
16 Abaqus)
17 double x2 = vec2.X + cx; double y2 = vec2.Y + cy; double z2 = vec2.Z
18 + cz;
19 //Add orientation (for orthotropic material)
20 orilist.Add("Ori-1");
21 orilist.Add("*Orientation, name=Ori-1");
22 orilist.Add(string.Format("{0}, {1}, {2}, {3}, {4}, {5}, {6}, {7},
23 {8}", x1, z1, y1, x2, z2, y2, cx, cz, cy)); //changed y z due to
24 abaqus/rhino different axis systems
25 orilist.Add("1, 0"); // 1,0. 1 means primary axis (x), 0 means no
26 rotation
27 Orientation = orilist;
```

Listing 4: Assign orientation of part by tangent vector between two central points and normal plane



(a) Rhino



(b) Abaqus model with correct orientation

Figure 5.12: Orientation of elements with orthotropic material

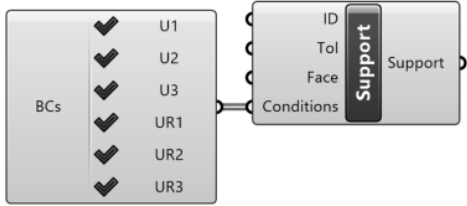
5.2 FEM with Grasshopper components

This method functions well, but the second and third axis might get interchanged due to how Rhino/Grasshopper defines perpendicularity of the normal plane. One should therefore confirm in the Abaqus model that the orientation is indeed created correctly, and the code could be developed to ensure the correctness of the second and third axis. One also have to make sure that one meshes the orthotropic parts in the first directions. Otherwise, the code can easily be extracted to be used for a separate component to set the orientation outside of the mesh component.

5.2.4 Boundary conditions and loads

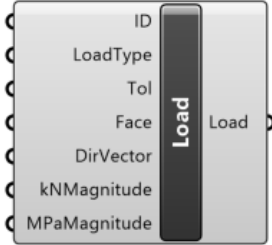
Boundary conditions and the loads are assigned to the model by choosing surfaces that the conditions will be applied to. Components for assigning boundary conditions are described in table 5.5.

Table 5.5: Boundary conditions

Description	Component
<p><i>BCs</i> and <i>Support</i> are components that are used with no modifications from Mæhle (2017). <i>BCs</i> creates a set of boundary conditions, by checking of the translational degrees of freedom and the rotational degrees of freedom that should be fixed. <i>Support</i> creates a support by assigning a surface <i>Face</i>, boundary conditions, and an <i>ID</i> name as inputs. The toleration <i>Tol</i> can also be set, or have the default value of 0.001 to determine how far the nodes can be located from the surface.</p>	

The *Support* component is used as an input to the *AbaqusPart*, where the component *AbaqusPart* will identify the nodes that lie on the surface with the given tolerance and make a node set with all the nodes so that they are assigned the correct boundary conditions. Furthermore, in table 5.6 the load component used for assigning load types and the components for possible load types are described.

Table 5.6: Load

Description	Component
<p><i>Load</i> is a further development of Mæhle (2017)'s component <i>UniformLoad</i>. It is possible to assign three different load types, as shown in figure 5.13; Uniform pressure, surface traction shear and surface traction general, to a designated surface <i>Face</i>. Uniform pressure is applied perpendicular to the surface, whereas the surface tractions are applied according to a direction vector <i>DirVector</i>. One can choose to input the total load in kN, where the load is divided over the area of the surface, or input the force directly in MPa. The output <i>Load</i> then works as an input to <i>AbaqusPart</i>, as will be explained in section 5.2.5.</p>	

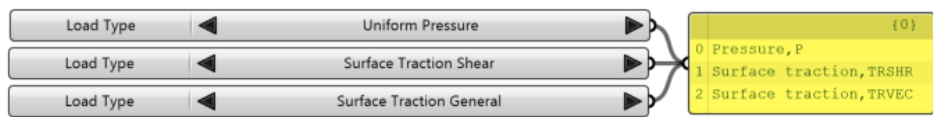


Figure 5.13: Possible Load types; Pressure and Surface traction

Figure 5.14 shows an example of the use of the three different load types.

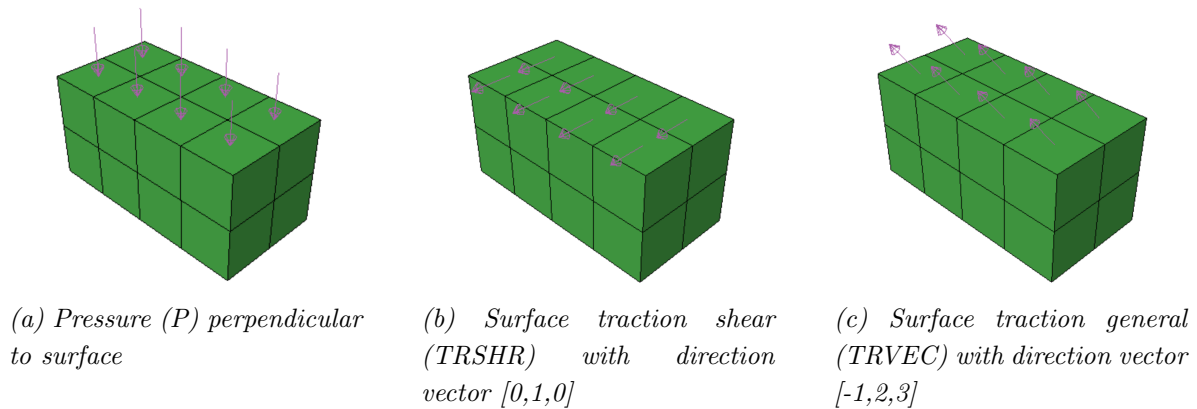


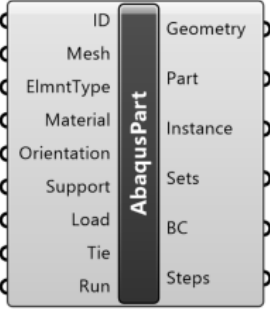
Figure 5.14: Examples using the different load types

As the BCs are assigned to nodes in the model, the load is assigned by identifying the elements that lie on the surface, and make an element set of which elements and their surface sides that will be subjected to loading. It is also possible to assign the BCs and load to several surfaces at once by assigning more surfaces as inputs to the components. By doing this, one have to assign as many ID's as there are surfaces.

5.2.5 Assembling the model

To assemble a single part, the component *AbaqusPart* is used as described in table 5.7, where the components described in the previous sections, work as input.

Table 5.7: *AbaqusPart*

Description	Component
<p><i>AbaqusPart</i> is a component that has the same set-up as Mæhle's (2017) component <i>PartSweep</i>, but is developed to work with the components written in this thesis. The component takes the mesh from <i>MeshPointsSweep</i> or <i>MeshPointsNurbsSweep</i>, the chosen material from either <i>IsotropicMaterial</i> or <i>OrthotropicMaterial</i>, the support from <i>Support</i>, the load from <i>Load</i>, and the element type as inputs and creates an Abaqus part with instances, steps, sets and boundary conditions as output.</p>	 <p>The diagram shows the <i>AbaqusPart</i> component as a central vertical bar with various inputs and outputs. On the left side, the inputs are: ID, Mesh, ElmntType, Material, Orientation, Support, Load, Tie, and Run. On the right side, the outputs are: Geometry, Part, Instance, Sets, BC, and Steps.</p>

To create a global node list, the component takes in the nodes from the mesh, or meshes, and remove the points that are duplicated, so that there won't be any nodes or elements that are overlapping. The vertices of the cross-sectional surfaces are thereby extracted and compared with the node list so that the nodes that makes up the different elements will be listed according to the global node list.

The *AbaqusPart* component identifies which nodes that are supported, by calculating the distance of the nodes to the supported surface. If the distance is smaller than a given tolerance, the node is added to the node set of the BCs. The element surfaces that are loaded or tied are identified by using a similar approach.

5.2 FEM with Grasshopper components

There are three Integration schemes of the hexahedral elements that can be chosen, as seen in figure 5.15, where it is possible to choose between full integration, reduced integration and incompatible modes.

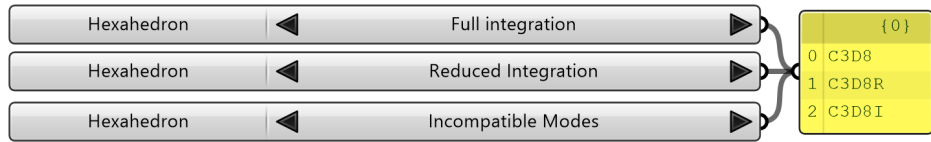


Figure 5.15: Possible element types; *C3D8*, *C3D8R* and *C3D8I*

To connect two different parts together, a tie constraint is used, which is established by using the *Tie* Component as described in table 5.8

Table 5.8: *Tie*

Description	Component
<p>The <i>Tie</i> component is used without any adjustments from Mæhle (2017). A tie constraint couples two separate surfaces from different parts together so that there is no relative motion between them. An <i>ID</i> have to be assigned as well as the <i>ID</i>'s of the <i>Master</i> part and the <i>Slave</i> part. The tie surface is assigned to <i>Face</i> so that the <i>AbaqusPart</i> can identify which elements that are included of the different parts in the tie constraint. The component has two outputs; one called <i>Part</i> which is an input to the <i>AbaqusPart</i> and one called <i>INP</i> which works as an input for the <i>INPAssembly</i></p>	<p>The diagram shows a vertical rectangular component labeled 'Tie' in the center. On the left side, there are five input ports labeled 'ID', 'Master', 'Slave', 'Tol', and 'Face' from top to bottom. On the right side, there are two output ports labeled 'Part' and 'INP' from top to bottom.</p>

The slave surface adjust itself according to the master, so it is recommended that the section with the highest mesh density is assigned as slave (Mæhle, 2017). This components is used in chapter 6 when making a connection between the timber members and the aluminium connection.

5.2 FEM with Grasshopper components

To create more complex model assemblies, it is practical to be able to join different meshes into the *AbaqusPart*, so that one does not need to create several *AbaqusPart*'s and *Tie* them together. To explain how this is done, an example with three simple meshes is given.

Figure 5.16a shows three meshes; 0, 1 and 2, where the meshes have different heights, V-divisions and longitudinal divisions. Mesh 0 has 1 V-division and 1 longitudinal division, mesh 1 has 2 V-divisions and 1 longitudinal division, whereas mesh 3 has 3 V-divisions and 2 longitudinal divisions. The meshes will together make a total of 9 elements.

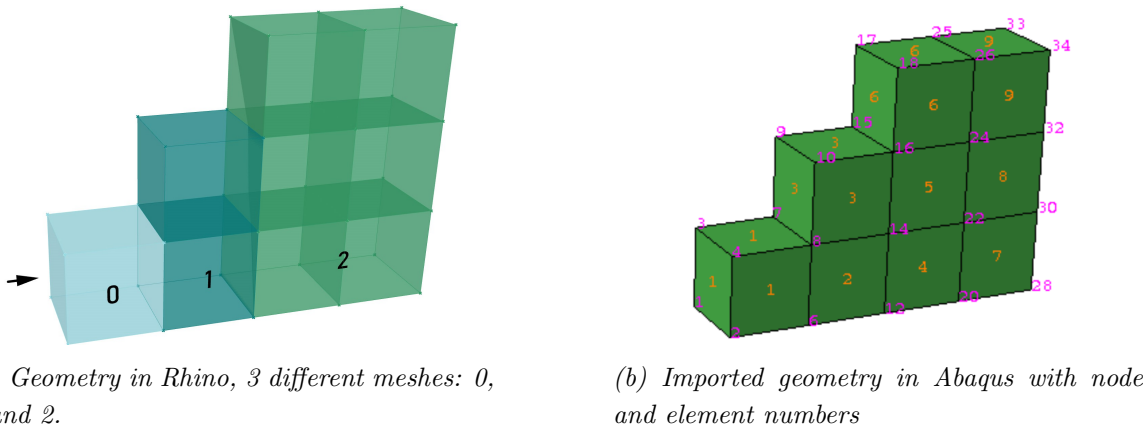


Figure 5.16: Example of joining three meshes together into one part

When the meshes are joined together in the *AbaqusPart* component, the cross-sectional surfaces will be put in the same list, and will be enumerated as illustrated in figure 5.17, giving a total of fifteen surfaces.

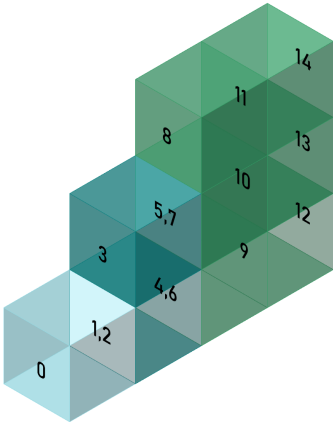


Figure 5.17: 15 surfaces numbered from 0-14

5.2 FEM with Grasshopper components

The data is sorted correctly by using the code in listing 5, so that the vertices that will make up the elements are gathered in a data tree according to the mesh number, division of the mesh and how many surfaces there are per division. The result can be viewed as a data tree in figure 5.18, where the stages of the code is shown clearly as tree branches, making a total of 15 branches which corresponds to the number of surfaces. When the element tree is sorted correctly, it will be used further in the AbaqusPart code for all the attributes that will successfully create the input file.

```
1  int div, numbr;
2  int startlocb = 0; //startindex of brep
3  int count = 0; //count to get correct assignment of div, numbr;
4  for (int j = 0; j < (Mesh.Branch(2, 0).Count() / 2) ; j++) //number
   of meshes
5  {
6      div = (int) Mesh.Branch(2, 0)[count]; //divisions j mesh
7      numbr = (int) Mesh.Branch(2, 0)[count + 1]; //number of surfaces in
   each division
8      for (int k = 0; k < (div + 1); k++)
9      {
10         for (int p = startlocb; p < (startlocb + numbr); p++)
11         {
12             Brep bb = (Brep) Mesh.Branch(1, 0)[p];
13             breps.Add(bb, new GH_Path(j, k));
14         }
15         for (int q = 0; q < numbr; q++)
16         {
17             Elements.AddRange(breps.Branch(j, k)[q].DuplicateVertices(),
   new GH_Path(j, k, q));
18         }
19         startlocb = startlocb + numbr; //make next location
20     }
21     count = count + 2; //to get next mesh's division and number of
   surfaces.
22 }
```

Listing 5: Joining several meshes into the same AbaqusPart

5.2 FEM with Grasshopper components

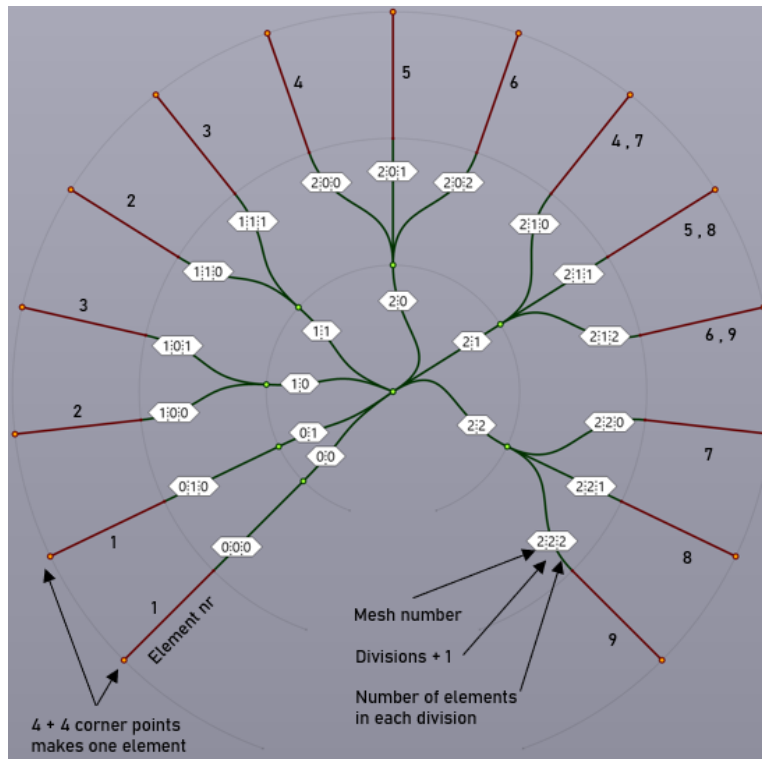


Figure 5.18: Grasshopper data tree of example

Last, but not least, the component `INPAssembly` in table 5.9, gathers the part or different parts and assembles the INP-file, a complete model text file which is ready to be imported to Abaqus.

Table 5.9: `INPAssembly`

Description	Component
<p><code>INPAssembly</code> takes the part, instances, steps, sets and boundary conditions from <code>AbaqusPart</code> as inputs, and creates the INP-file for the model, ready to be imported to abaqus, as output.</p>	<p>The screenshot shows the <code>INPAssembly</code> component interface. It features a vertical list of input parameters on the left, each with a dropdown arrow: ID, Job, Model, Part, Instance, Sets, BC, Material, Tie, and Steps. The component name 'INPAssembly' is displayed vertically in a dark bar, and the output 'INP' is shown on the right side of the component.</p>

5.2.6 Assembling all the components

To show in a simple way how some of the the components described can be connected in a GH assembly model, which gives the INP-file, a flowchart of a possible workflow was made, see figure 5.19.



Figure 5.19: A flowchart which shows the workflow of a GH script which has the INP-file as the last output.

In figure 5.20, an example on how the components can be connected together in GH to generate the INP-file for a finite element model, is given.

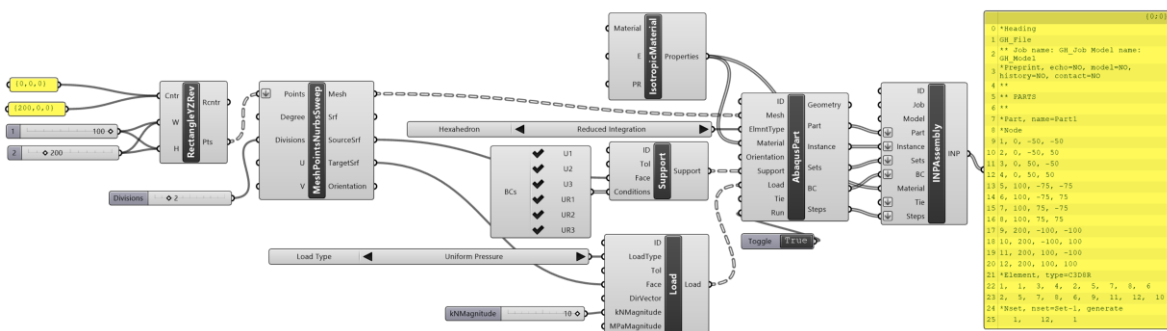


Figure 5.20: An example of assembling the different components to create a similar model to that of figure 5.1.

All the components are gathered in a separate GH file in appendix E.1. To show how the different components are used and how they are connected, a variety of functioning model assemblies can be found in a GH file in appendix E.2. The file includes some

5.2 FEM with Grasshopper components

simple examples, which are made to show the versatility of, and the possibilities with, the approach. The different model examples are seen in figure 5.21. Additionally, two of the model examples, namely the I-beam and the Shell, are elaborated further in appendix D.

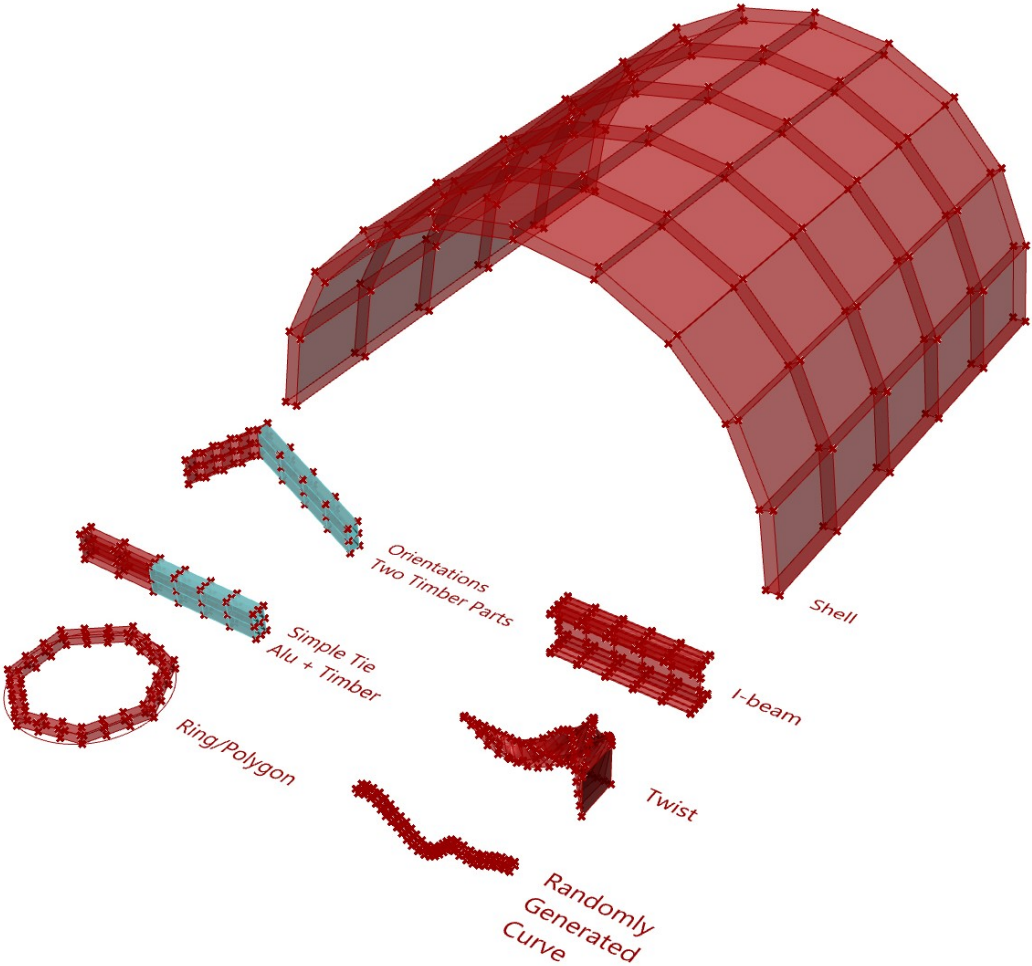


Figure 5.21: Model examples that are found in appendix E.2

6 Parametric finite element analyses of connectors

The custom GH components described in section 5.2 have been used to model and analyse simplified models of the GF and SR connector. The connector itself is modelled as one part with multiple meshes, whereas the timber members are modelled as separate parts due to their different orientations. The connector and timber members are tied together using a tie constraint. All analyses, except for the buckling analyses, have been made by building the model in GH and running the FEA in Abaqus. For the buckling analyses, the model have been built in GH, but the buckling step has been added to the model in Abaqus, since the approach does not cover buckling analysis yet. As mentioned in chapter 4, a linear elastic material model is used in all FEA in this thesis.

Elements used in all analyses are the 8-node trilinear element (Hex 8), which is the three-dimensional counterpart of the standard quadrilateral Q4 element. A shortcoming of these types of elements are that they exhibit parasitic or “false” shear strain. This may lead to shear locking where the finite element model will tend to “lock” as a lot of energy is required to sustain the false shear strain and the shear strain dominates completely. However, the effect of the parasitic shear strain depends greatly on the width/height ratio of the element (Bell, 2014, p. 385). The larger the ratio becomes, the risk of shear locking is greater. The additional shear stresses causes the element to reach equilibrium with smaller displacements. Hence it makes the element appear to be stiffer than it actually is and gives displacements smaller than they should be. It is therefore important to make sure that the width/height ratio is as small as possible to make the model more accurate.

To save computational time, reduced integration is used. Reduced integration tends to have a softening effect on an otherwise too stiff element as it dampens the effect of higher order terms (Bell, 2014, p. 221). However, the element has two zero-energy (hourglass) modes for this integration scheme. This problem can be addressed with hourglass control, which reintroduce the stiffness of the hourglass modes. Hence the modelling results can be quite accurate while reducing computational time.

6.1 Glued Finger connector

A simplified model of the GF connector was constructed, see figure 6.1a. Compared to the original design, the simplified connector do not contain the connection detail between the connector core and the gripper. In addition, the inner core is modelled with a hexagonal geometry, whilst the original geometry is irregular because of the different angles between the timber members. To analyse how the dimension of different geometrical parameters is impacting the structural behaviour of the connector, seven different parameters were at first analysed separately when applying shear in the vertical direction to the timber end. Due to symmetry, only one of the six connectors was part of these analyses, so both the behaviour of the connector centre and the five remaining connectors were not looked into at first. The result from this analysis are given in section 6.1.1. The parameters that was analysed are named in figure 6.1b below. The A1 parameter was analysed for both two inner splices and four. From the analysis results, an optimised solution for the GF connector is proposed, and the optimised solution of the whole simplified GF connector is analysed later in this chapter. When modelling the glued connection between the gripper and the timber part in Abaqus, this has been assumed and modelled as a tied contact.

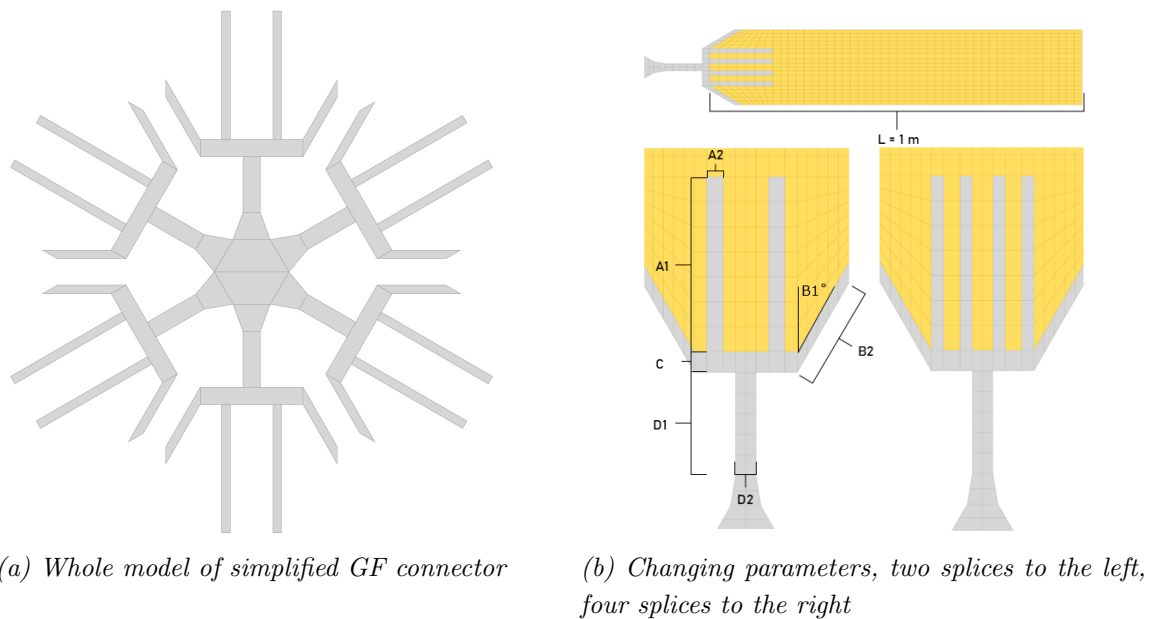


Figure 6.1: the GF connector

6.1.1 Changing parameters when applying shear to the timber end in one leg

To model one connector as realistically as possible, the part which is supposed to be connected to the inner core was applied fixed boundary conditions, see figure 6.2. The timber part was given the dimension $200 \cdot 200 \cdot 1000 \text{ mm}^3$, and applied a surface traction of 0.125 MPa at the tip surface, in the negative Z-direction, which sums up to a total force of 5 kN . This can be seen in figure 6.2. The connector itself is modelled as one part in aluminium and tied to the timber part. As the timber cross-section is assumed to be constant, changing the varying parameters of the connector itself might affect the dimensions of the remaining parameters. For example increasing the angle B1 or the length B2 makes the width of the mid plate (C) smaller.

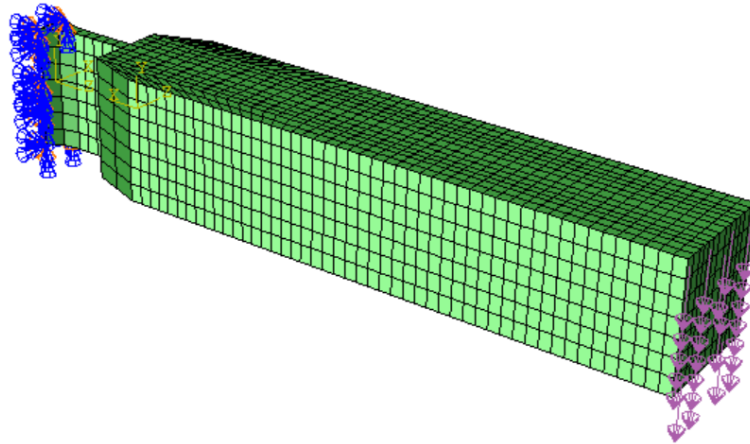


Figure 6.2: Applied load and boundary conditions to one connector

In the following, the results from the analyses of the simplified GF model is given. In these analyses it is not taken into account that the connector can collide with other connectors. The displacement percentage of change and Mises stress is compared with the volume percentage of change. It is desired to have the case with the lowest volume, displacement and Mises stress. This because the lowest volume means the lowest price, and the smallest displacement means the most stiff joint. An example, which shows how the result for one case is given in Abaqus, is shown in figure 6.3.

6.1 Glued Finger connector

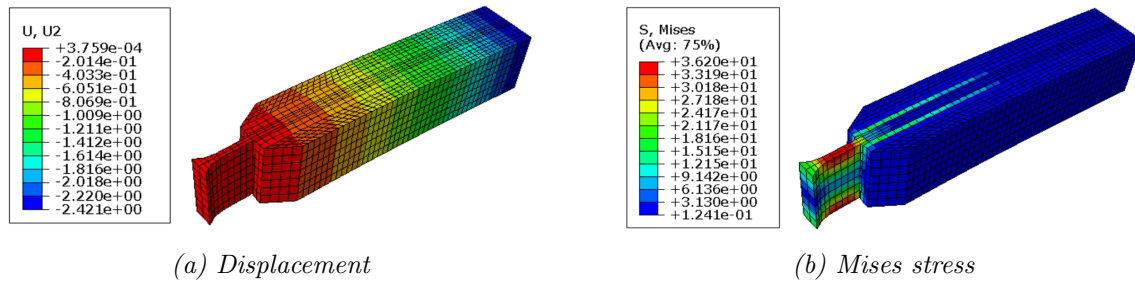


Figure 6.3: Demonstration of how FEA results are given in Abaqus

The first parameter which was done analyses of, was A1, which is the length of the inner splices. This was analysed for both two and four splices, and the difference in the results are given in figure 6.5. Here it is observed that the difference in displacement percentage of change and stresses is quite small and the volume percentage of change is high, so the change of volume will be the critical factor. Thus, as the volume percentage of change is over 50 % larger for four splices than for two splices, for a given length of A1, two splices will be the favourable design solution. In addition to this, it is observed that the two inner splices transfer most of the stresses. This can be seen in figure 6.4, where the exterior inner splices are not well visible as their stresses are low. The two exterior inner splices therefore seem to be redundant. It is a general observation that the closer the inner splices are to the centre, the larger the stresses in them becomes and the displacements decreases.

When it comes to the length of the splices, it is observed that the displacement percentage of change tend to flatten and that an increase of the length, maybe over 200 mm, will not have a significant impact on the displacement percentage of change compared to the increase in change of volume. However, it is strange that the Mises stress is constant when the displacement is decreasing, as a decrease in the displacement should lead to a decrease in the Mises stresses. Therefore, this case should be investigated further. It is also important to remember that the length of the splices affects the glue surface, such that it must be checked that the surface area which the timber part is connected to is larger than the necessary glue surface area.

6.1 Glued Finger connector

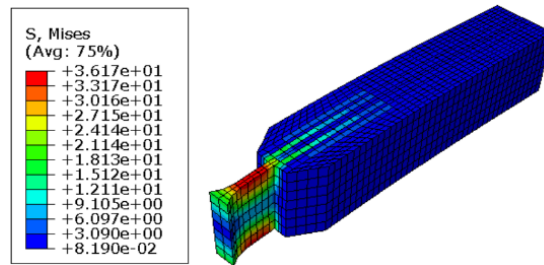


Figure 6.4: FEA Mises stress results of four splices with a length of 350 mm. The two inner splices transfer most of the stresses, making the two exterior inner splices appear to be redundant.

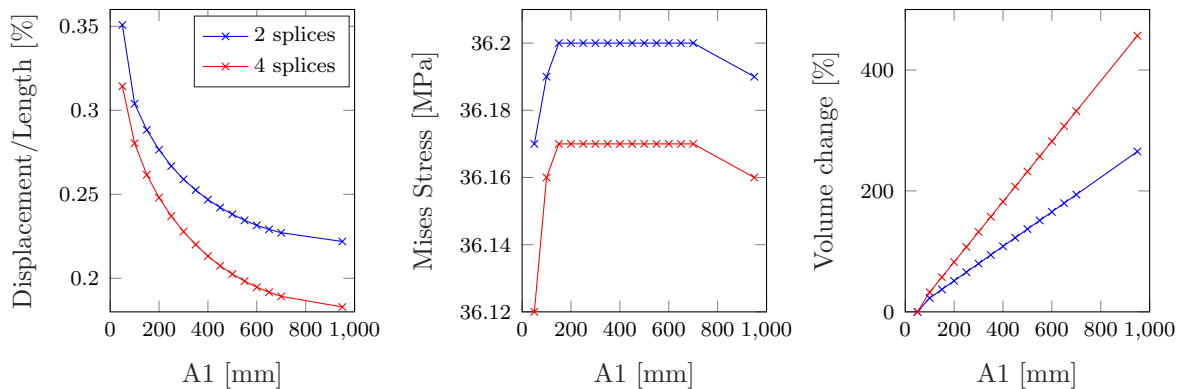


Figure 6.5: Length of inner splices

The second parameter that was analysed was A2, which is the width of the inner splices. In figure 6.6, the result from these analyses is shown. Here it is observed, that when increasing the width by 10 mm, the volume increases with around 17 %. Such as for A1, the displacement percentage of change and stresses have a small decrease when increasing A2. Therefore, a small width is preferable, maybe around 10-15 mm.

6.1 Glued Finger connector

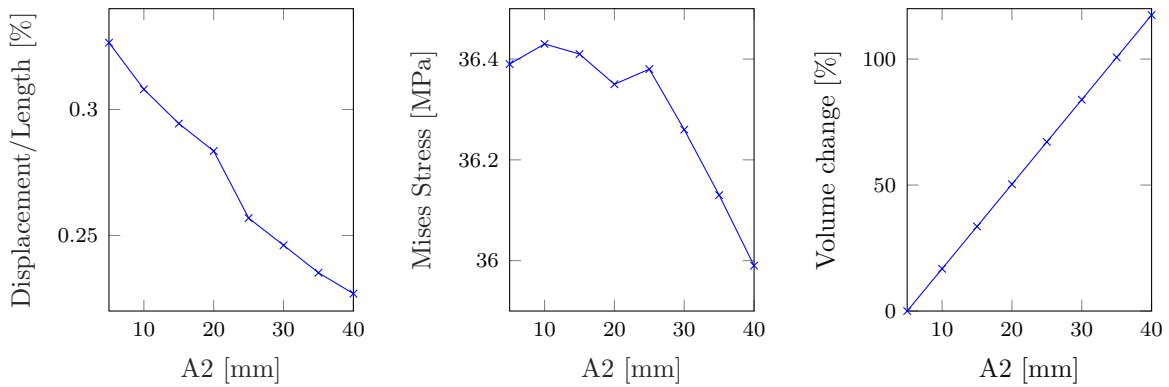


Figure 6.6: Width of inner splices

Furthermore, B1 was analysed, which is the angle between the outer and inner splices. The results are given in figure 6.7. Unlike A1 and A2, the change of volume is decreasing linearly when increasing B1. But this change of volume is much less than for A1 and A2. When increasing the angle by 5° , the volume is decreasing with around 2 %. Also, the displacement percentage of change and stresses also have small variations. Therefore, other factors may decide the angle, such as if the connectors are colliding for big angles, the glue surface area, or aesthetic arguments.

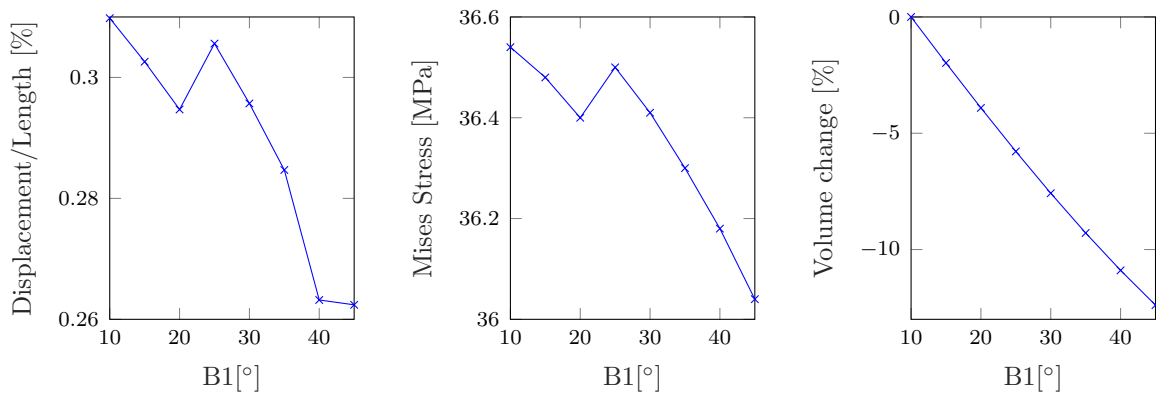


Figure 6.7: Angle between inner and outer splice

The next parameter that was analysed was B2, which is the length of the outer splices. This result can be found in figure 6.8. When increasing the length by 40 mm, the volume percentage of change increases with around 3.75 %. In addition, the Mises stress and the displacement percentage of change has quite small variations. But, there is a little jump from a B2 of 60 mm to a B2 of 80 mm, so a length of 80-100 mm may be a good solution for the outer splices.

6.1 Glued Finger connector

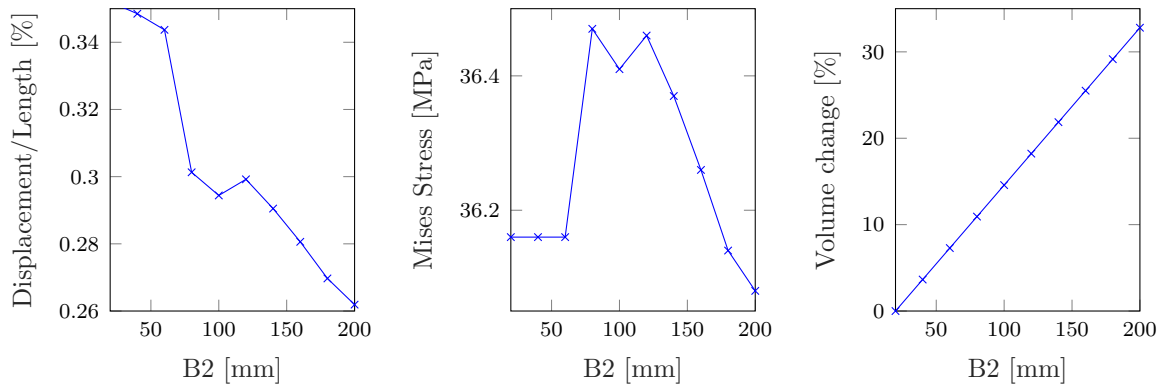


Figure 6.8: Length of outer splice

In addition, parameter C, which is the width of the mid plate that the splices are connected to, was analysed, see figure 6.9. Notice that when changing the dimension of C, the width of the outer splices also changes, but it seems like most of the transferring of stresses happens between the mid plate and the inner splices. It is observed that when increasing C with 5 mm, the volume change increases with around 13.5 %. Also, there is a jump in the displacement percentage of change from 25 mm to 30 mm, so maybe 30 mm will be a good value for C.

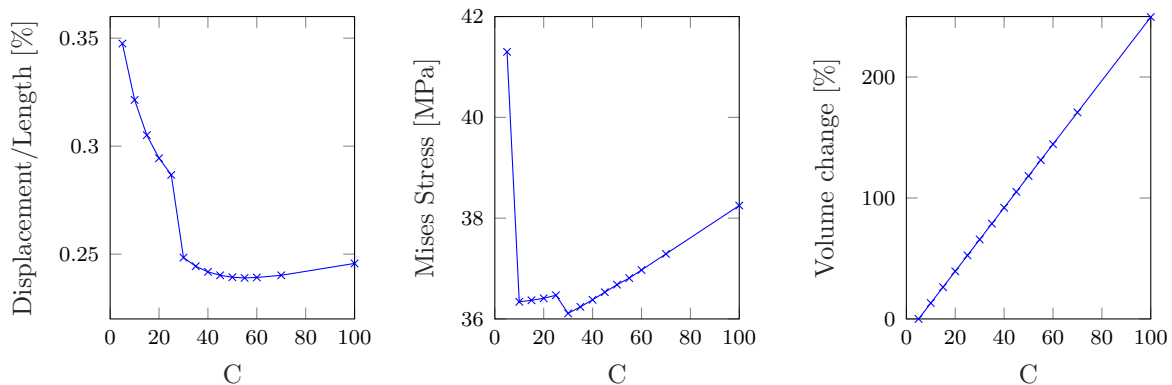


Figure 6.9: Width of mid plate

Next, the parameter that was analysed was D1, which is the length of the inner plate that is connected to the connector centre. Both the displacement, Mises stress and the volume is increasing when increasing the value of D1, as can be seen in figure 6.10. In this case, the variations in the displacement and Mises stress is larger than in the previous cases. The volume percentage of change is increasing with around 3 % when

6.1 Glued Finger connector

increasing D1 with 20 mm. To keep the displacement, Mises stress and volume low, the length of D1 should not be larger than 100 mm. Notice that it is also important that D1 is large enough so that the six connectors do not collide with each other.

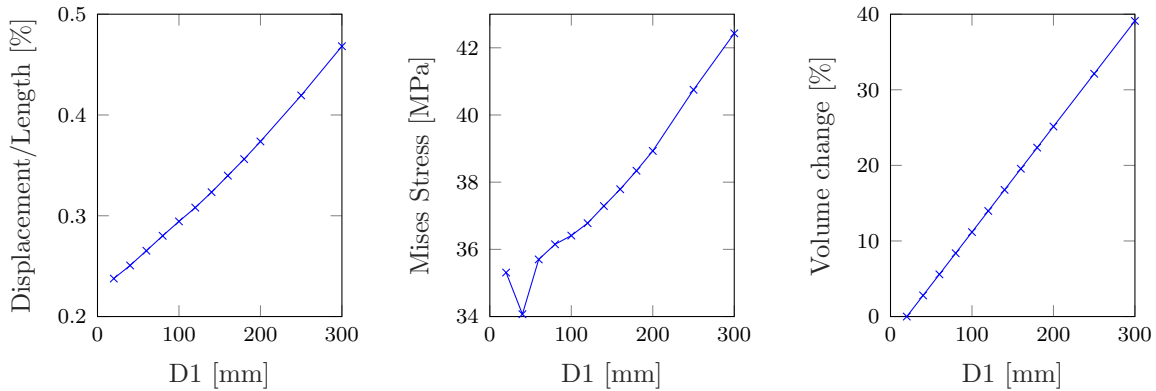


Figure 6.10: Length of inner plate

The last parameter that was analysed was D2, which is the width of the inner plate which is connected to the connector centre, see figure 6.11 for the result. The reason for the jump in the plot of D2 against the volume percentage of change, has to do with that the fixed part also had to increase its dimension as the width was increased over 35 mm. The variations in the Mises stress and the displacement percentage of change is also here larger than in previous cases. After 20 mm to 25 mm, the graphs for the displacement and stress tend to flatten. When increasing D2 with 5 mm, the volume change increases with 5 %, which is a quite low increase compared to some of the previous cases. Thus, 20 mm or 25 mm may be a good width of D2.

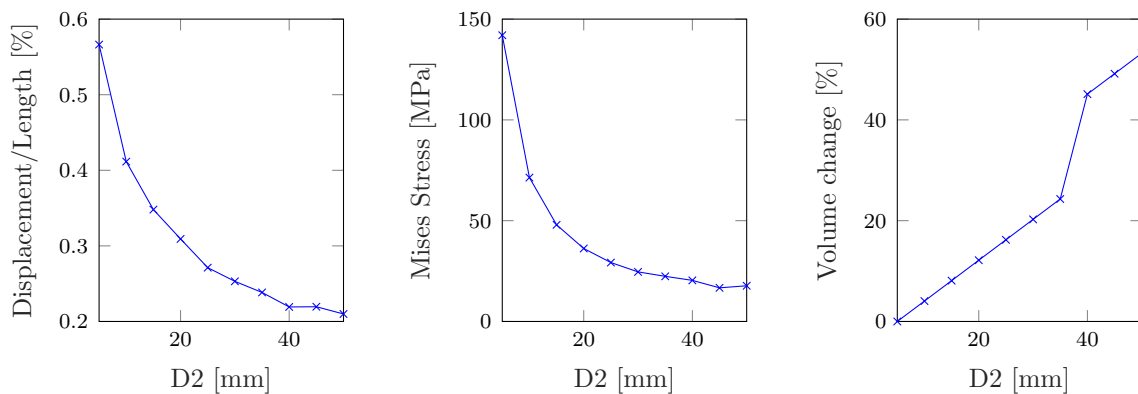


Figure 6.11: Width of inner plate

6.1 Glued Finger connector

To sum up the results and discussion, an optimised solution for the simplified GF connector is proposed. The values for the different parameters is given in table 6.1. This solution consists of two inner splices, which is the favourable number of splices according to the analyses. The values for B1 and D1 are determined by taking into account the possible collision of the six connectors, see figure 6.12 for the whole optimised GF connector. The necessary dimension of the hexagon in the centre is not analysed.

Table 6.1: Values which gives an optimised solution for the simplified GF connector

A1	A2	B1	B2	C	D1	D2
[mm]	[mm]	[°]	[mm]	[mm]	[mm]	[mm]
200	10	20	100	30	100	25

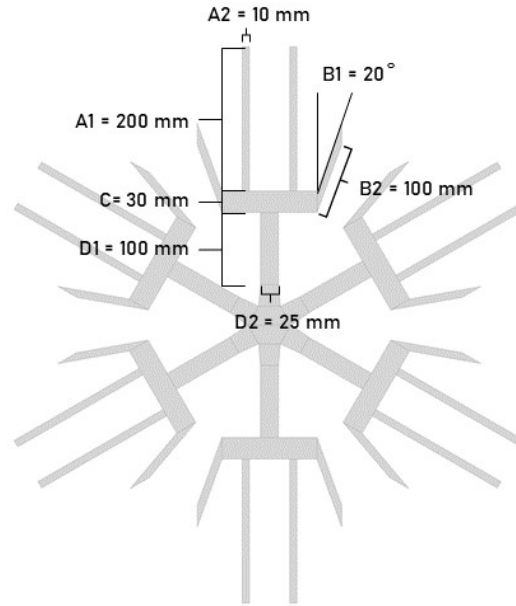


Figure 6.12: Whole GF connector with proposed geometry as stated in table 6.1. As seen, the connectors do not collide.

The glue surface of this connector was calculated to be $350 \cdot 10^3 \text{ mm}^2$. Comparing this to the estimated necessary glue surface that was calculated in section 3.2, with a value of $43 \cdot 10^3 \text{ mm}^2$, it is found that the glue surface is 8 times more than necessary.

This proposed connector design was also analysed, and the result for the displacement and the Mises stress is given in figure 6.13.

6.1 Glued Finger connector

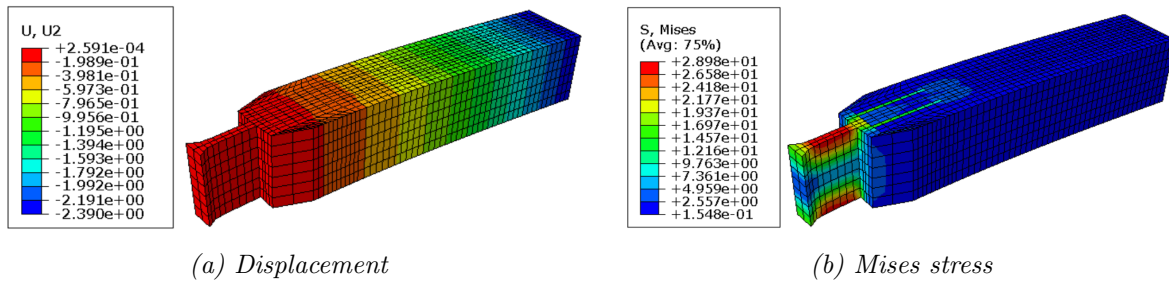


Figure 6.13: Displacement and Mises stress in the optimised GF connector

6.1.2 Shear force in horizontal direction

The same uniformly distributed load of 0.125 MPa was also applied to the same tip surface, but now in the horizontal direction for the optimised connector design of one GF connector. See figure 6.14 for analysis result of displacement and Mises stress with the new load condition.

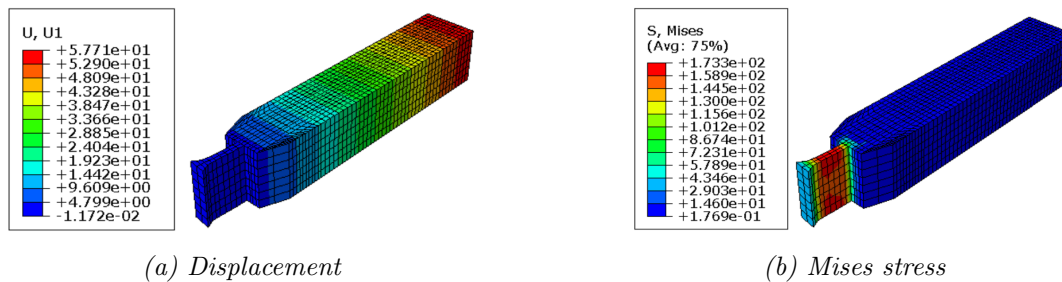


Figure 6.14: Displacement and Mises stress in the proposed solution of simplified GF connector with shear force applied in the horizontal direction

From the result, it is shown that the maximum Mises stress is very high, when applying the same shear load in the horizontal direction, compared to in the vertical direction. The maximum Mises stress is 173.3 MPa which is just lower than the yield stress of the chosen aluminium alloy which is 180 MPa. To lower the Mises stress, one could increase the area that takes up shear in the horizontal direction, by inserting plates perpendicular to the inner plate. For example one could change the cross section to an I-profile.

6.1.3 Eccentricity

The Mises stress in a case with pure compression was checked by applying a pressure of 2.75 MPa, see figure 6.15. This corresponds to a load of 110 kN distributed on the timber end surface with an area of $200 \cdot 200 \text{ mm}^2$. Then, to introduce eccentricities, which causes moments, the same load of 110 kN was distributed over an area translated 50 mm in the vertical direction, see figure 6.16, and horizontal direction, see figure 6.17, respectively.

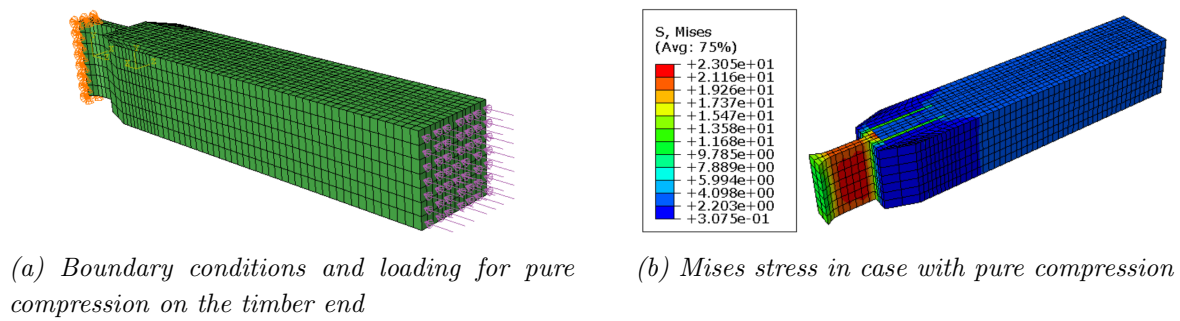


Figure 6.15: GF connector applied to pure compression

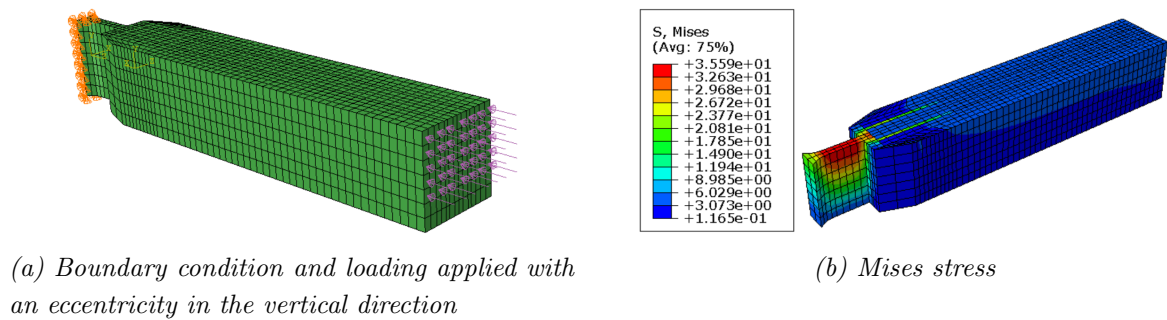


Figure 6.16: GF connector with eccentricity in the vertical direction

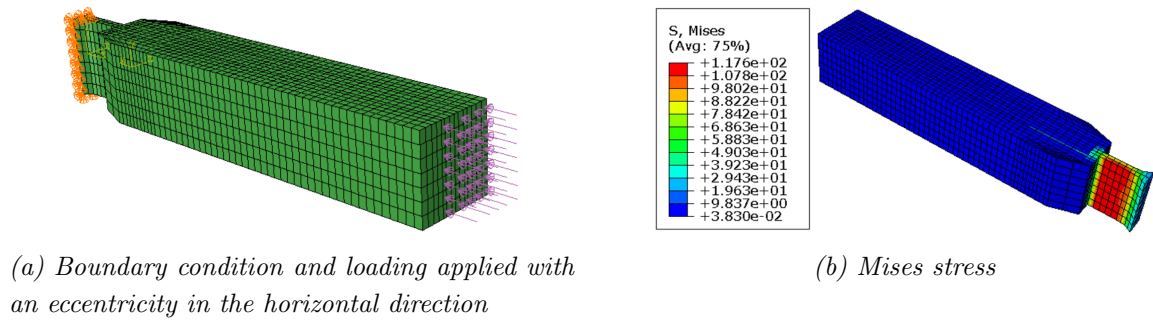


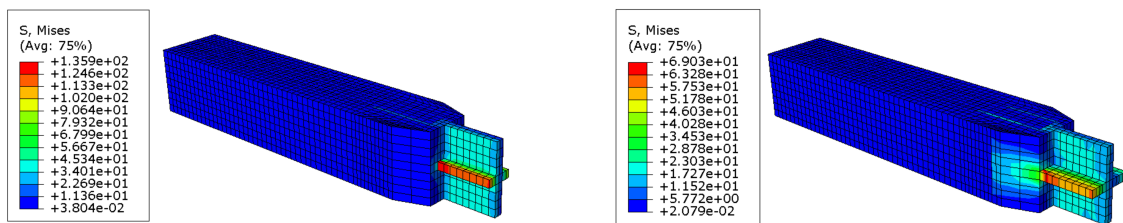
Figure 6.17: GF connector with eccentricity in the horizontal direction

6.1 Glued Finger connector

From the Mises stress results in the figures above, it can be seen that the Mises stress when applying the load with an eccentricity in the vertical direction is 54 % bigger than the Mises stress for pure compression. Furthermore, when applying the load with an eccentricity in the horizontal direction, the Mises stress is 410 % bigger than the Mises stress for pure compression, which is a significant difference. The connector is therefore vulnerable to eccentric loads, which might be a problem for gridshells with varying geometry.

To combat this, it is crucial to increase the bending stiffness by increasing the second moment of area about the weak axis. A common way to do this is by using for instance I-beams, where the slender webs handles the shear forces and the flanges handles the bending. For the GF connector, one could increase the width of the whole inner plate, but it could be more efficient to insert plates perpendicular to the inner plate, for example in the top and bottom, like the I-profile. To save material, one could instead insert plates in the middle of the cross-section. Both would be efficient for eccentric loads in the horizontal direction, but the most efficient for the eccentric loads in the vertical direction, would be plates in the top and bottom.

It is the eccentricity in the horizontal direction which is critical. Therefore, it was investigated how a plate inserted in the middle affected the Mises stress for the case with an eccentricity in the horizontal direction, see figure 6.18. As seen, when introducing plates in the middle, the stress distribution changes, and when the width increases, the maximum stress decreases significantly. This could therefore be an efficient way to deal with eccentricities.



(a) When introducing stiffening plates, the stress distribution changes

(b) When increasing the plate width, the maximum stress decreases

Figure 6.18: GF connector with stiffening plates

When increasing the width of the additional plate to be equal to the length of the mid plate, the Mises stress increase in the outer splices, see figure 6.18b.

6.1.4 Buckling capacity of inner plates

To find the buckling capacity of the inner plate in one leg, the optimised metal part was connected to a small timber part, with a length of 250 mm, width of 200 mm and height of 350 mm, and made a buckling analysis of. A pressure of 1 MPa was applied to the ends of the timber part, see figure 6.19 for boundary condition and applied loading.

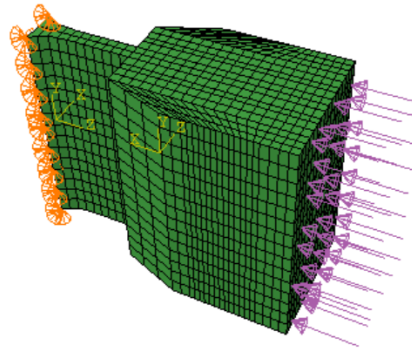


Figure 6.19: Boundary conditions and loading for buckling analysis of one leg

As can be seen in figure 6.20a, the lowest positive eigenvalue that generated buckling in the inner part was found to be 58.562 MPa. This means that the buckling capacity for the inner parts is 58.562 MPa. This is distributed over an area of $200 \cdot 350 \text{ mm}^2$, which means that it can be summed up to an axial compression load of 4099.43 kN. The buckling modes in figure 6.20b and 6.20c, have different buckling shape and the lowest positive eigenvalue for those shapes are given in these figures.

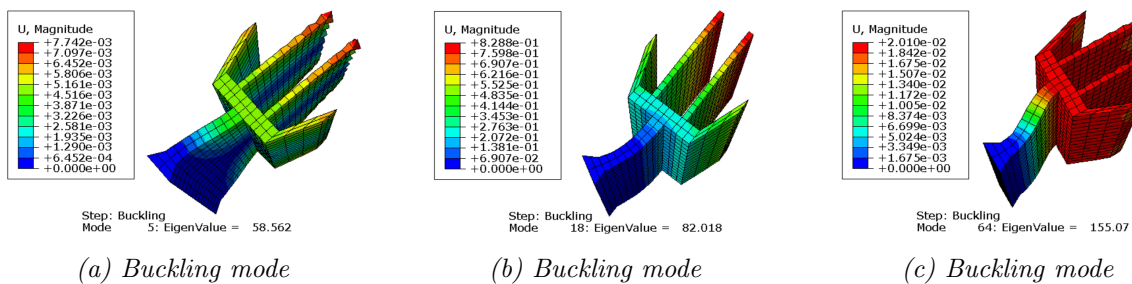


Figure 6.20: Buckling modes

To increase the buckling load, one could insert a plate perpendicular to the inner plate in the middle, as suggested when dealing with eccentricities, or one could increase the width of the inner plate. The first option will be the most volume efficient solution.

6.1.5 Applying compression load to all timber members in connector

To get a better understanding of how the stresses are distributed in one connector as a whole, all the six grippers assembled together with the timber members, as can be seen in figure 6.21, was analysed.

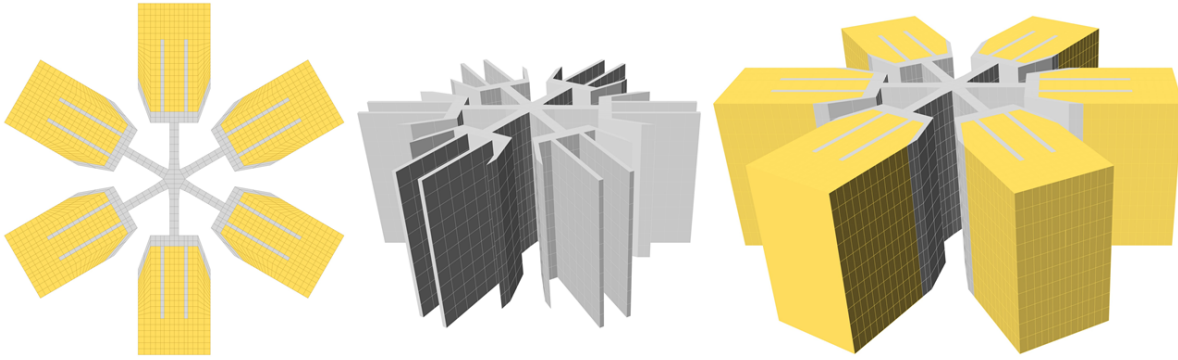


Figure 6.21: GF whole connector

According to Seifi (2019), because of the doubly curved geometry of gridshell structures, the internal forces are mainly in-plane. Therefore, at first, the parametric connector model, with the optimised dimensions from table 6.1, was only subjected to pressure at the ends of the timber members. The pressures applied to the timber members in the six different grippers, was calculated from the axial forces working on the connector which is subjected to the maximum axial force in the gridshell, given by Brun (2019). These are given in table 6.2, and can also be found in figure 6.22. To achieve stability of the connector, the inner splices of the gripper with the lowest pressure, was applied fixed boundary condition. The connector was analysed for two different widths of the hexagon, first a width of 60 mm was analysed, and then a width of 100 mm. The results can be found in figure 6.23.

6.1 Glued Finger connector

Table 6.2: Pressures applied to the ends of the timber members, calculated from connector number 1125 which are subjected to biggest axial force

Member	Axial load [kN]	Pressure [MPa]
3036	109.66	1.57
3038	34.59	0.49
3111	30.34	0.43
3157	108.82	1.55
3082	39.99	0.57
3037	32.70	0.47

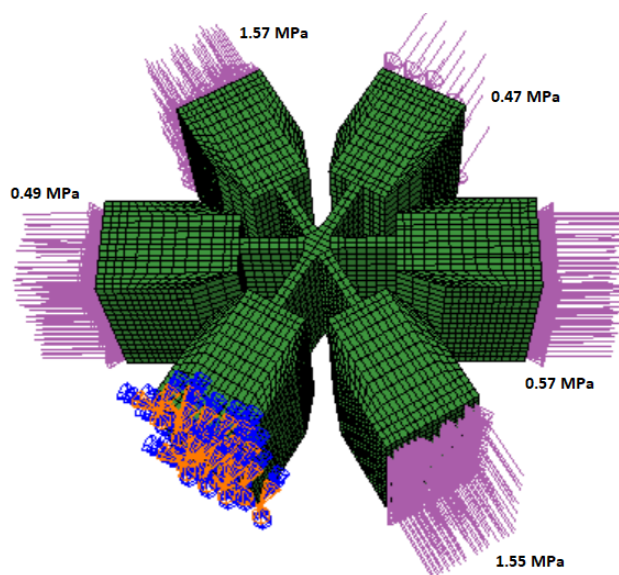
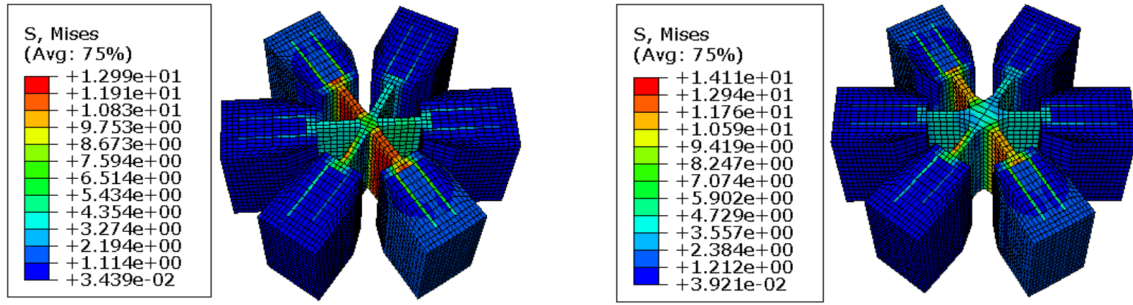


Figure 6.22: Whole GF connector applied to different pressures on the ends of the timber members

6.1 Glued Finger connector



(a) Mises stress in whole GF connector with 60 mm width of hexagon, applied to different pressures at the ends of the timber members

(b) Mises stress in whole GF connector with 100 mm width of hexagon, applied to different pressures at the ends of the timber members

Figure 6.23: Mises stress in whole simplified GF connector applied to pressure

From the results, it is shown that when applying pressure to the ends of the timber parts and changing the width of the hexagon, the maximum Mises stress is about the same. For the connector with a hexagon width of 60 mm, the maximum Mises stress is 12.99 MPa, whilst for the connector with a hexagon width of 100 mm, it is 14.11 MPa. However, the maximum Mises stress is located in the inner plates of the connectors which is applied a fixed boundary condition. If comparing the Mises stresses in the inner plates of the connectors which is applied the two highest pressure loads, the maximum Mises stress is 11.91 MPa for the connector with a hexagon width of 60 mm, whilst for the connector with a hexagon width of 100 mm, it is 11.76 MPa. In addition, it can be seen that most of the load are transferred through the inner splices and almost nothing through the outer splices. Therefore, the question on whether these are necessary should be discussed. It seems at least like the dimension of the outer splices, if they are included, can be minimised.

6.1.6 Applying shear load to all timber members in connector

In addition, to get a better understanding of the structural behaviour of the connectors, the same connector model was only subjected to surface tractions at the ends of the timber members. The surface traction applied to the six different timber members, was calculated from the shear forces working on the connector, which is subjected to the maximum shear force in the gridshell, given by Brun (2019). These are given in table 6.3, and can also be found in figure 6.24. To achieve stability of the connector, the top hexagonal surface in the centre of the connector, was applied fixed boundary condition. This case was also analysed for two different widths of the hexagon, first a width of 60 mm was analysed, and then a width of 100 mm, as for the case with compression. The results can be found in figure 6.25.

6.1 Glued Finger connector

Table 6.3: Surface tractions applied to the ends of the different timber members, calculated from connector number 1 which are subjected to the biggest shear force

Member	Shear load [kN]	Surface traction [MPa]
90	0.66	0.009
3	-1.20	-0.017
2	-5.82	-0.083
1	-0.92	-0.013
87	-1.32	-0.019
147	-0.71	-0.010

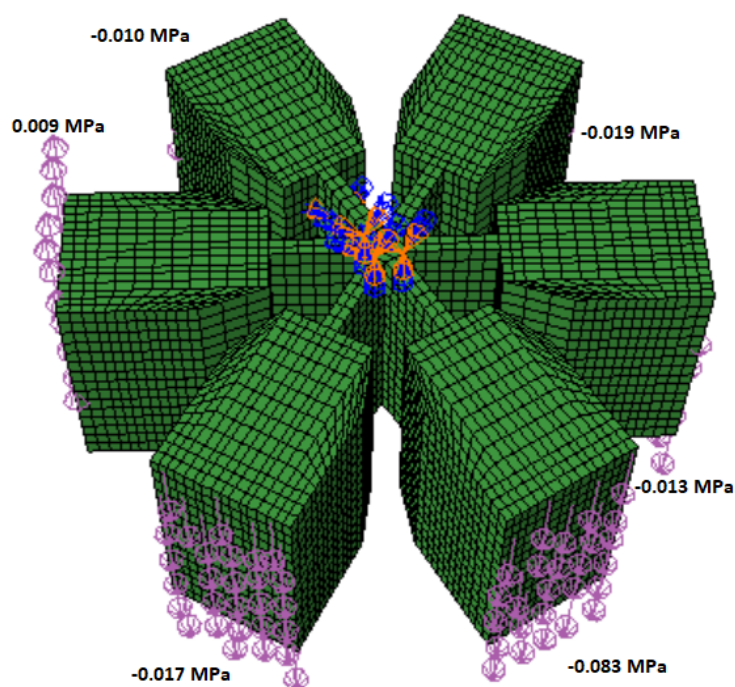


Figure 6.24: Whole GF connector applied to different surface tractions at the ends of the timber parts

6.1 Glued Finger connector

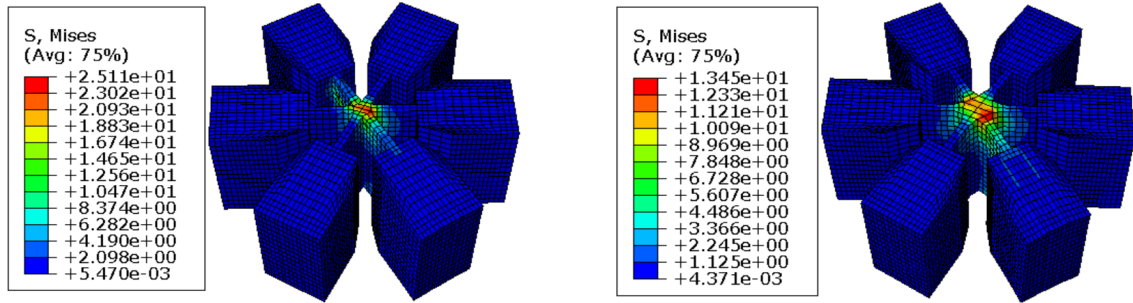


Figure 6.25: Mises stress of connectors applied to surface traction

From the results, it is shown that when applying shear to the ends of the timber parts and changing the width of the hexagon, the maximum Mises stress is decreasing with almost 50 % when increasing the width of the hexagon in the core by 40 mm. For the connector with a hexagon width of 60 mm, the maximum Mises stress is 25.11 MPa, whilst for the connector with a hexagon width of 100 mm, it is 13.45 MPa.

6.1.7 Buckling capacity of inner plates in whole connector

To find the buckling capacity of the whole optimised connector, five timber ends was applied a uniform compression load of 1 MPa. The last timber end was applied a fixed boundary condition, as can be seen in figure 6.26.

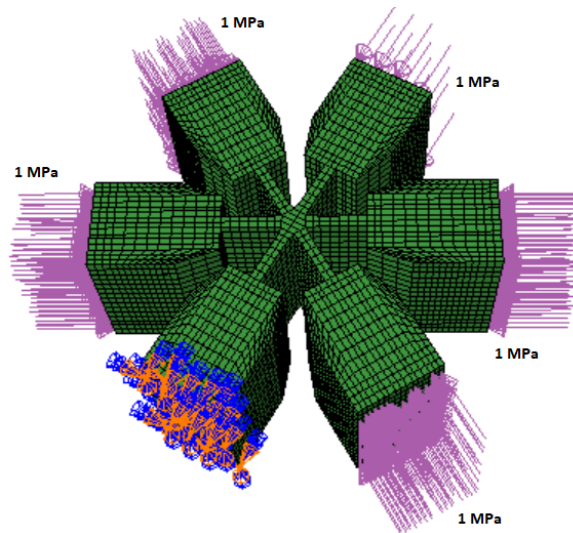


Figure 6.26: Applied loading for checking the buckling capacity of the whole connector

6.1 Glued Finger connector

As can be seen in figure 6.27a, the lowest positive eigenvalue that generated buckling in the inner part of the whole connector was found to be 14.697, which is much lower than for one connector. This is distributed over an area of $200 \cdot 350 \text{ mm}^2$ and corresponds to an axial compression load of 1028.79 kN. However, this buckling mode, in addition to the buckling mode with another buckling shape in figure 6.27b, has buckling of the inner part of the connector which is fixed. Therefore, buckling modes that generated buckling in the inner plate of the others connectors which were not fixed, was also investigated. The lowest positive eigenvalues of different buckling shapes for such buckling modes, are given in figure 6.28.

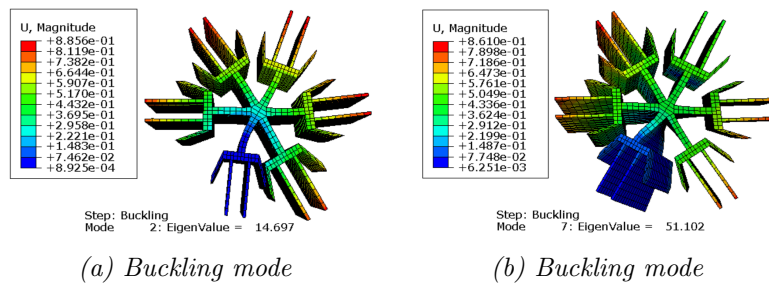


Figure 6.27: Buckling modes with buckling of fixed leg

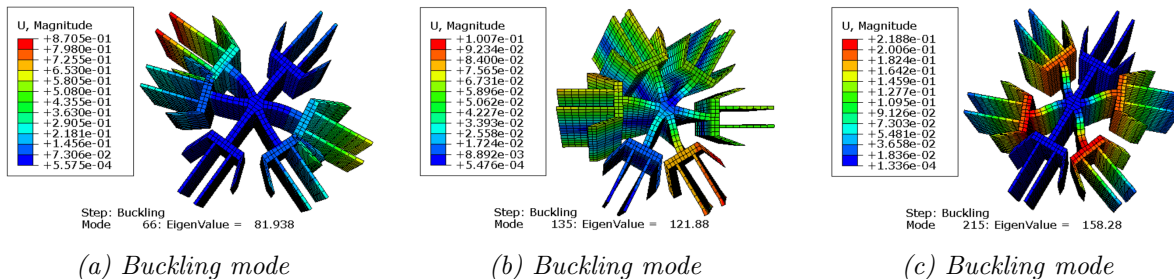


Figure 6.28: Buckling modes

To prevent buckling of the inner plates the best way of doing this is to increase the moment of inertia around the weak axis. This can be done either by increasing the width of the inner plates, such that the plates gets less slender, or by changing the cross section of the plates, to stiffer geometries. A good solution could be to insert plates perpendicular to the existing plates as was suggested for the eccentricity problem in section 6.1.3.

6.2 Split Ring connector

A simplified model of the original SR connector design is constructed to investigate the possible stress distribution in this connector as well, see figure 6.29.

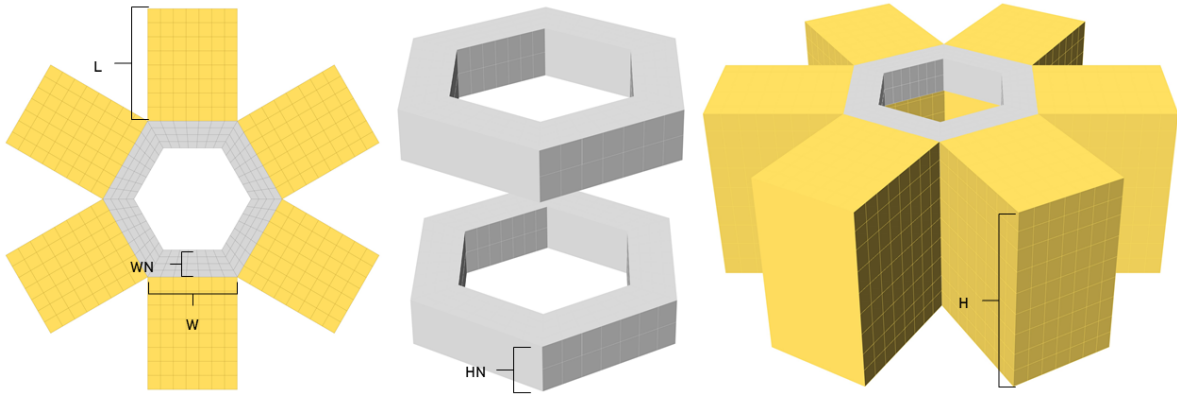


Figure 6.29: Simplified SR connector with parameters

The top and bottom split rings are modelled as two parts and not four as in the original design. Also, the four threaded rods for each member are not included. However, the connection between the aluminium part and the timber parts is modelled as tied in to columns, where the four threaded rods are supposed to be, see figure 6.30 below.

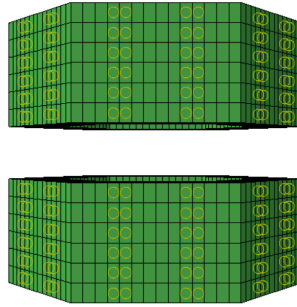


Figure 6.30: The yellow circles marks the surfaces that are tied in a tied connection

According to table 3.1 and 3.2, $e_2 = 1.2 \cdot d_0$ and $d_0 = d + 2$, for bolts with a diameter between M16-M24. For a plate with one bolt row, the minimum height is therefore $2 \cdot e_2$. For a bolt of size M24, as used in section 3.3.4, the minimum height is therefore

$$h_{min} = 2 \cdot 1.2(24 + 2)mm = 62.4mm$$

Hence, the height of one split ring should at least be 62.4 mm.

6.2.1 Eccentricity

As for the GF connector, it is interesting to look at how the SR connector handles eccentricities. Thus, the whole connector was applied the same compression loads as in table 6.2 and shown in figure 6.31. The fixed boundary condition was applied to the timber member with the lowest pressure. The dimensions of the width and height of both hexagon rings was 55 mm and 140 mm, respectively, as found when comparing the volumes of both connectors, which is explained in section 6.3.2.

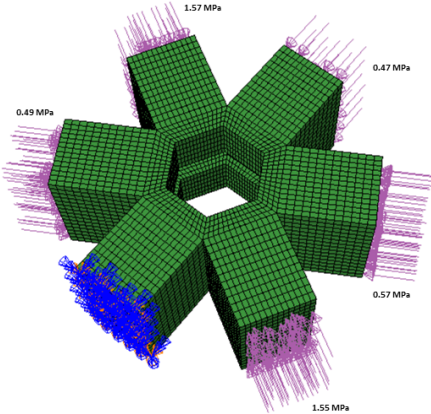
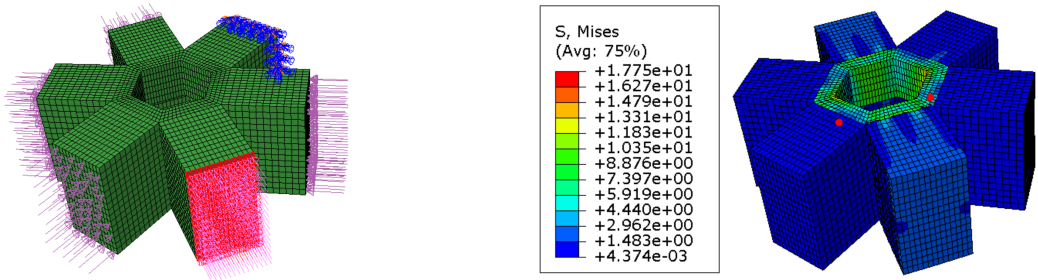


Figure 6.31: SR connector applied to different pressures on the ends of the timber members

The eccentricities were introduced by distributing the same load over a smaller area in the designated direction. The timber member applied the highest axial load of 110 kN, corresponding to a pressure of 1.57 MPa distributed over an area of 200·350 mm², was applied eccentricities. For the connector applied pure compression, see figure 6.32, the maximum stress is 17.75 MPa and is located along the bottom, inner corners of the hexagon of the members next to the largest load. Due to symmetry, the bottom hexagon have the same stress distribution as the upper one.



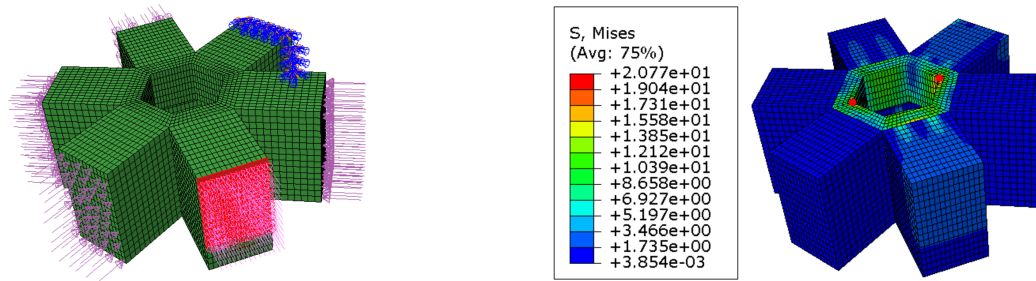
(a) BCs and loading for pure compression on the timber end

(b) Mises stress. Red marks shows the locations of the maximum stress.

Figure 6.32: SR connector with pure compression

6.2 Split Ring connector

For the eccentricity in the vertical direction, the maximum stress is 14.5 % bigger than for pure compression, and the location of the maximum stress is shifted upwards, since the load is shifted upwards, as seen in figure 6.33. However, since the bottom hexagon is subjected to less stress, so there are less stresses in the bottom hexagon.

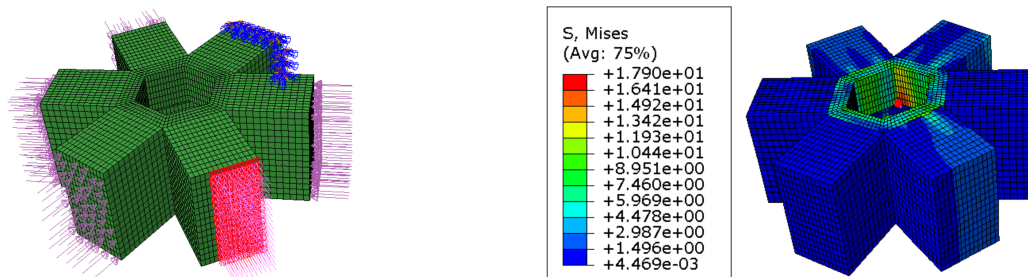


(a) Boundary condition and loading applied with an eccentricity in vertical direction

(b) Mises stress. Red marks shows the locations of the maximum stress.

Figure 6.33: SR connector with eccentricity in the vertical direction

For the eccentricity in the horizontal direction, as seen in figure 6.34, the value of the maximum stress is about the same as for pure compression, but the location is shifted to the following corner from the two other cases.



(a) Boundary condition and loading applied with an eccentricity in the horizontal direction

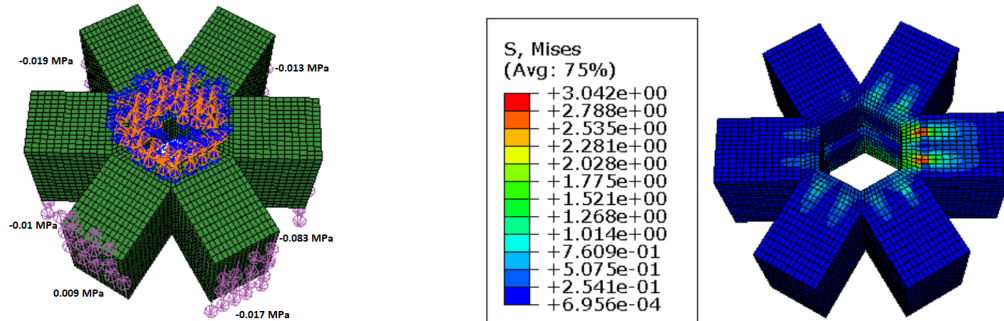
(b) Mises stress. Red mark shows the locations of the maximum stress.

Figure 6.34: SR connector with eccentricity in the horizontal direction

Since the SR connector has a hollow hexagonal geometrical shape with constant wall thickness and encircles a circle, it was anticipated that the eccentric axial loads would not influence the behaviour significantly. Such cross sections are known for being resistant against warping and for having good bending stiffness around both axes as the material is moved away from the centre of area.

6.2.2 Applying shear load to all timber members in connector

In addition, the whole SR connector was subjected to only surface tractions at the ends of the timber members. The surface traction applied to the six different timber members, was the same that are given in table 6.3, and can also be found in figure 6.35a. To achieve stability of the connector, the inside of the top split ring, was applied fixed boundary condition. The resulting Mises stresses are given in figure 6.35.



(a) Boundary condition and shear loading (b) Mises stress in SR connector applied to shear

Figure 6.35: Whole simplified SR connector applied to shear

From the result, it is found that the maximum stress appears in the tied connection in the leg which is applied the highest shear load.

6.3 Comparing necessary volumes of Glued Finger and Split Ring connector

To reduce costs, one aim to keep the volume of the connector down while ensuring that the connector has enough structural capacity. To compare the two different connector designs, the connectors were analysed with different load combinations; compression loads according to table 6.2 in section 6.3.1, identical compression load in all members in section 6.3.2 and identical shear load in all members in section 6.3.2. The volume of the connectors were then adjusted in the parametric model with the aim of making the maximum stress reach 90 % of the yield stress of 180 MPa. The volume of the SR connector was calculated by including the threaded rods by using the diameter and penetration length found in section 3.3.4.

6.3.1 Compression loads according to table 6.2

At first, it was tried to use the loads from table 6.2 and then decrease the volume of both the GF connector and the SR connector, to try to find the necessary volume to reach a Mises stress of 90 % of the yield stress. The result for each connector can be found in figure 6.36.

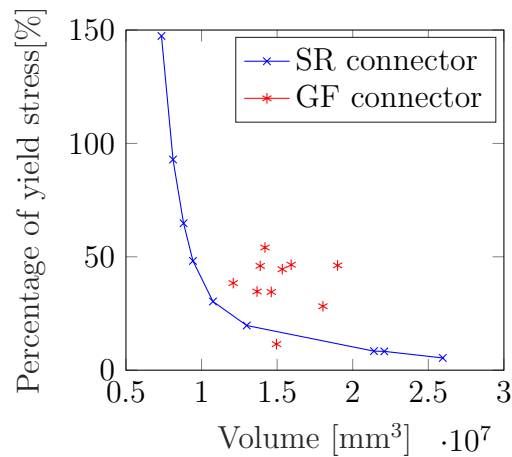


Figure 6.36: Comparison of GF and SR connector when decreasing the volumes

From the result, it can be seen that for the SR connector, at first when decreasing the volume, the increase in the Mises stress is quite small. But, when the volume approaches the value of $1 \cdot 10^7 \text{ mm}^3$, then the rate of change gets steeper and a little decrease in the volume will result in reaching 90 % of the yield stress. However, for the GF connector, not always a decrease in the volume led to increase in the Mises stress, it depended on which parameters that was decreased, and how much.

6.3.2 Identical compression load applied to all members

To be able to compare the connectors, the compression load that is necessary for inducing a Mises stress of around 90 % of the yield stress in the optimised GF connector was found. This was found to be 20 MPa when applying it to five timber ends, and when fixing one timber end, see figure 6.37. The SR connector was applied the same load and boundary condition, and the geometry of the connector which give a Mises stress of around 90 % of the yield stress was found, see figure 6.38. The dimensions of the width and height of the resulting connector, was 55 mm and 140 mm, respectively.

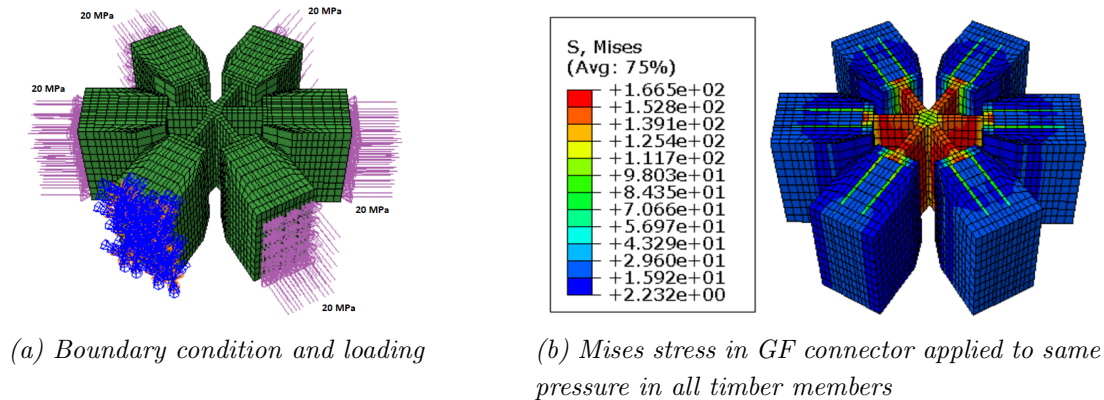


Figure 6.37: Pressure of 20 MPa applied to all timber members in the GF connection

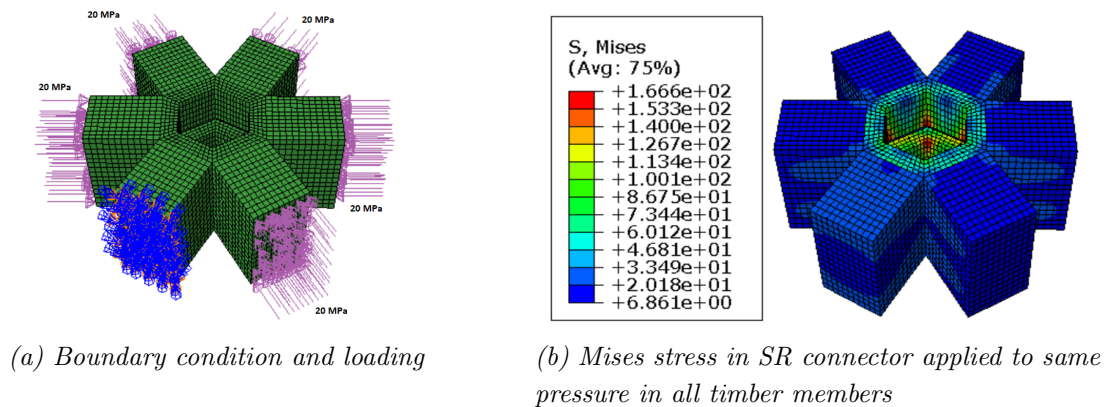


Figure 6.38: Pressure of 20 MPa applied to all timber members in the SR connection

The volume of the optimised GF connector is $37.09 \cdot 10^6 \text{ mm}^3$, whilst the volume of the SR connector is $21.67 \cdot 10^6 \text{ mm}^3$. This means that for the same compression load applied to the connectors, the GF connector needs 1.7 times the volume of the SR connector, for both connectors to not have higher Mises stress than 90 % of the yield stress. For

6.3 Comparing necessary volumes of Glued Finger and Split Ring connector

the GF connector the highest stress concentrations are located in the inner plates and the mid plates, whilst for the SR connector they are located in the inner corners of the hexagon shaped split rings.

6.3.3 Identical shear load applied to all members

In addition, one more comparison was performed, where the shear load that is necessary for inducing a Mises stress of around 90 % of the yield stress in the optimised GF connector was found. This was found to be 2 MPa when applying it to all the six timber ends and when fixing the top core surface, see figure 6.39. The SR connector was applied the same load, but here the boundary condition was fixed on the inside of the top SR connector, and the geometry of the connector which give a Mises stress of around 90 % of the yield stress was found, see figure 6.40. The dimensions of the width and height of the resulting connector, was 25 mm and 65 mm, respectively.

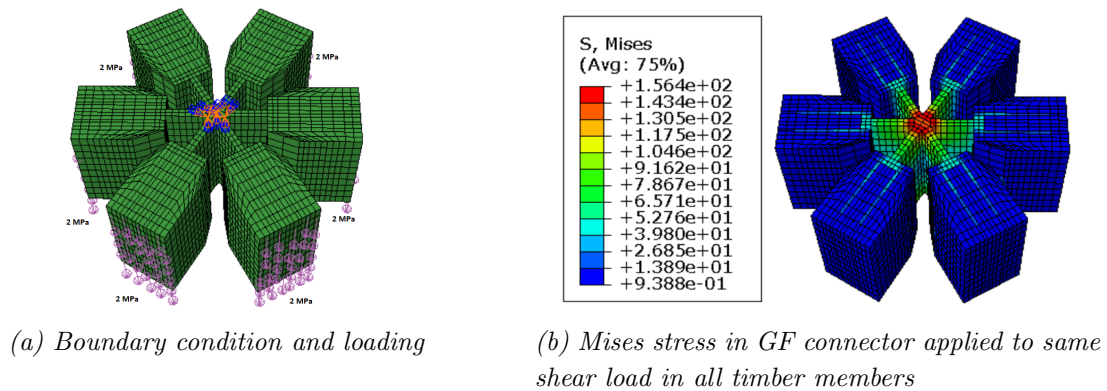


Figure 6.39: Shear load of 2 MPa applied to all timber members in GF connection

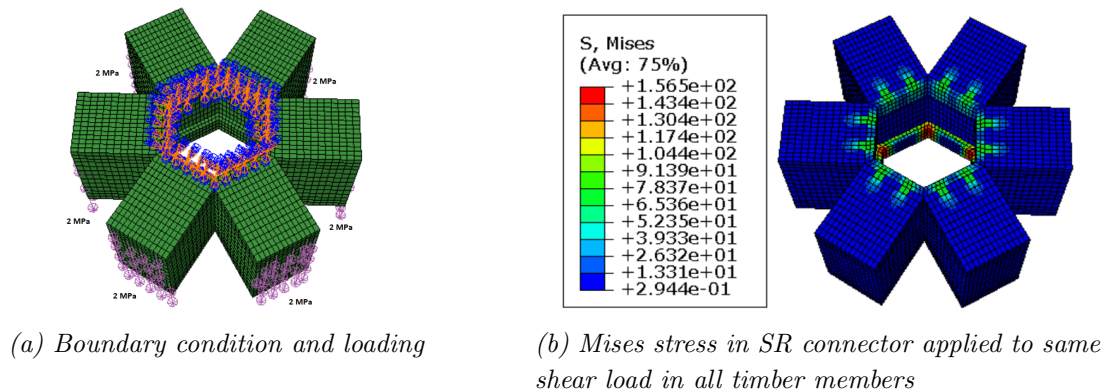


Figure 6.40: Shear load of 2 MPa applied to all timber members in SR connection

6.3 Comparing necessary volumes of Glued Finger and Split Ring connector

The volume of the optimised GF connector is $37.09 \cdot 10^6 \text{ mm}^3$, whilst the volume of the SR connector is $8.89 \cdot 10^6 \text{ mm}^3$. This means that for the same shear load applied to the connectors, the GF connector needs 4.17 times the volume of the SR connector, for both connectors to not have higher Mises stress than 90 % of the yield stress. For the GF connector the highest stress concentrations are located in the core of the connector, whilst for the SR connector they are located in the corners of the bottom hexagon shaped split ring.

6.4 Comparing rotational stiffness of Glued Finger and Split Ring joints

In previous years, for discrete single-layer free form surfaces, the problem has not been to know how to perform the structural design, but rather how to develop connector designs that provides sufficient rotational stiffness (Lopez et al., 2011). Thus, the rotational stiffness of both the GF and SR joints is estimated and compared in this section.

6.4.1 Rotational stiffness of Glued Finger joints

To estimate the rotational stiffness of the GF joints, one leg of the optimised simplified connector was looked at. The timber cross-section was set to $200 \cdot 350 \text{ mm}^2$ and had a length of 1 m. The timber end was applied a load of 5 kN which corresponds to a surface traction of 0.071 MPa, see figure 6.41.

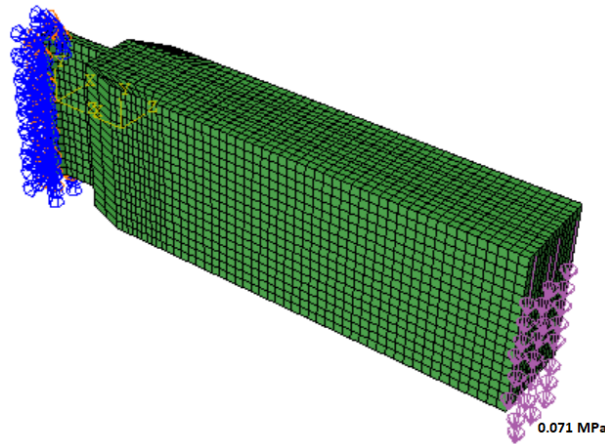


Figure 6.41: Loading and for estimating rotational stiffness of GF joints

The displacement along the length in the centre of the timber cross-section was plotted, see figure 6.42.

6.4 Comparing rotational stiffness of Glued Finger and Split Ring joints

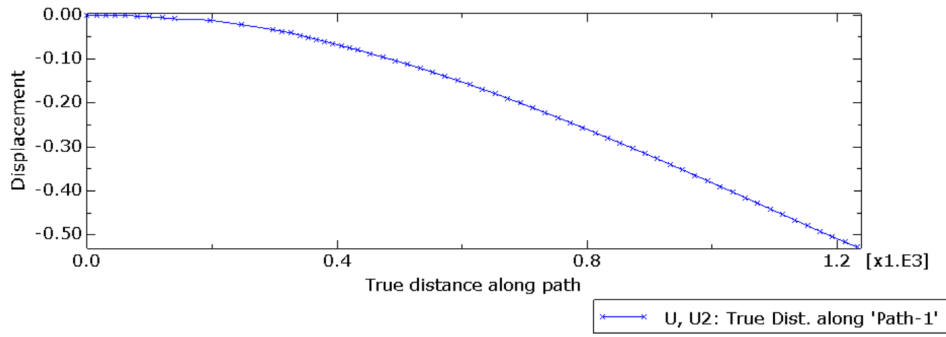


Figure 6.42: Plot of displacement in the middle of one leg of the GF connector

It is a general observation that the plot of the displacement at first has a linear shape before it gets curved and then linear again. In addition, many engineers will argue that the displacement value at the transition point from the curved shape to the linear shape at the end, is the value which will give the best estimation of the rotational stiffness of the joint. Thus, this was assumed as the best value for the estimation of the rotational stiffness.

To find a rough estimation of the rotational stiffness of the joint, the displacement was taken from figure 6.42, where the displacement U_2 at the transition point is 0.27 mm. The length of the timber beam is 1 m and the length of the joint is 0.19 m. Thus, the rotational stiffness, S_j is calculated as

$$S_j = \frac{M}{\Phi} = \frac{F \cdot L}{U/L} = \frac{5kN \cdot 1.19m}{0.27mm/813.06mm} = 17917.80kNm/rad \quad (6.1)$$

Using the classification criteria from section 5.2.2.5(1) (Standard Norge, 2009a) with the modulus of elasticity for timber in the longitudinal direction, which is 10000 MPa, and the second moment of inertia of the timber beam, one obtain the following value

$$\frac{S_j}{E \cdot I/L} = 2.98$$

Hence, the connection is semi-rigid since it is over 0.5 (pinned), but below 8 (rigid). The result can be found in table 6.4 below.

Table 6.4: Estimated rotational stiffness of GF connector

U2	L	S_j
[mm]	[mm]	[kNm/rad]
0.27	813	17917

6.4.2 Rotational stiffness of Split Ring joints

To estimate the rotational stiffness of the SR joints, one leg of the connector was looked at. The height of each Split Ring was 140 mm, and the width of each Split Ring was 55 mm, which was the resulting geometrical values from section 6.3.2. The timber cross-section was set to 200·350 mm² and had a length of 1 m. The timber end was applied a load of 5 kN which corresponds to a surface traction of 0.071 MPa, see figure 6.43a. The fixed boundary condition was applied on the inside of both top and bottom ring.

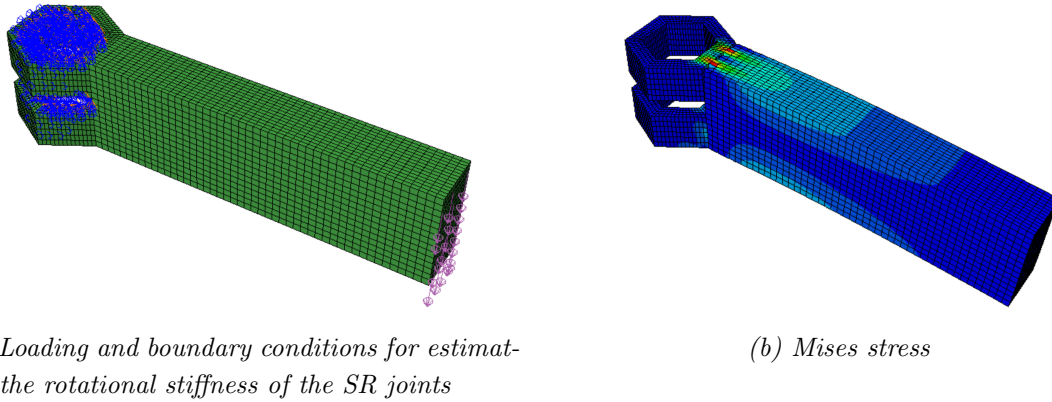


Figure 6.43: Model to estimate the rotational stiffness of SR joints

The displacement along the length in the centre of the timber cross-section was plotted, see figure 6.44

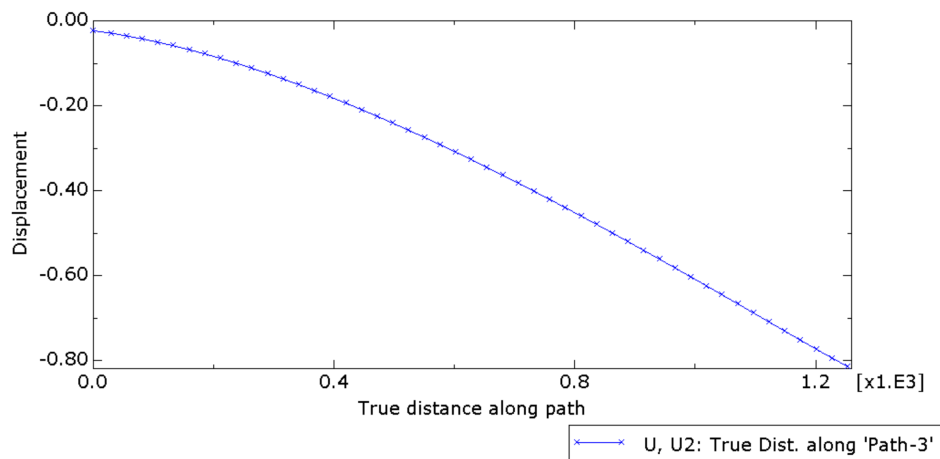


Figure 6.44: Plot of displacement in the middle of one leg of the SR connector

6.4 Comparing rotational stiffness of Glued Finger and Split Ring joints

As for the GF connector, the transition point between the curved part of the plot and the linear at the end, was assumed as the best value for the estimation of the rotational stiffness. From the plot it is found that this transition point has a displacement value of -0.46 mm.

The rotational stiffness of the joint was roughly estimated, by using the length of the timber beam of 1 m as the length.

$$S_j = \frac{M}{\Phi} = \frac{F \cdot L}{U/L} = \frac{5kN \cdot 1.0m}{0.46mm/810.96mm} = 8814.78kNm/rad \quad (6.2)$$

Using the classification criteria from section 5.2.2.5(1) (Standard Norge, 2009a) with the modulus of elasticity for timber in the longitudinal direction, which is 10000 MPa, and the second moment of inertia of the timber beam, one obtain the following value

$$\frac{S_j}{E \cdot I/L} = 1.23$$

Hence, the connection is semi-rigid since it is over 0.5 (pinned), but below 8 (rigid). The result can be found in table 6.5 below.

Table 6.5: Estimated rotational stiffness of SR connector

U2	L	S_j
[mm]	[mm]	[kNm/rad]
0.46	811	8815

6.4.3 Comparing rotational stiffness of Glued Finger and Split Ring joints

From the result of the rotational stiffness for both connectors, it was found that the GF connector provides a higher rotational stiffness than the SR connector, with twice as high rotational stiffness, see figure 6.6.

Table 6.6: Comparing rotational stiffnesses of the GF and SR connector

S_{j,GF}	S_{j,SR}	S_{j,GF}/S_{j,SR}
[kNm/rad]	[kNm/rad]	[—]
17917	8815	2.03

6.4 Comparing rotational stiffness of Glued Finger and Split Ring joints

To compare the rotational stiffnesses of the Glued Finger and the Split Ring joints, the displacements for both connectors was also plotted against each other, see figure 6.45. The dashed lines represent straight lines from the initial point, through the transition point, to the end point. The transition point is the point where the displacement curve becomes linear. To calculate Φ , the displacement from the initial point to the transition point was divided by the true distance to the transition point. It is observed that the SR joint’s displacement plot is initially curved, whereas the GF connector’s displacement plot is initially more linear. This is because the GF connector has aluminium splices that aligns along the beginning of the timber beam that reduces the displacements. The SR model is modelled without the threaded rods, which would probably lead to a less steep displacement curve. One could therefore argue that the SR joint’s rotational stiffness is a bit higher in reality.

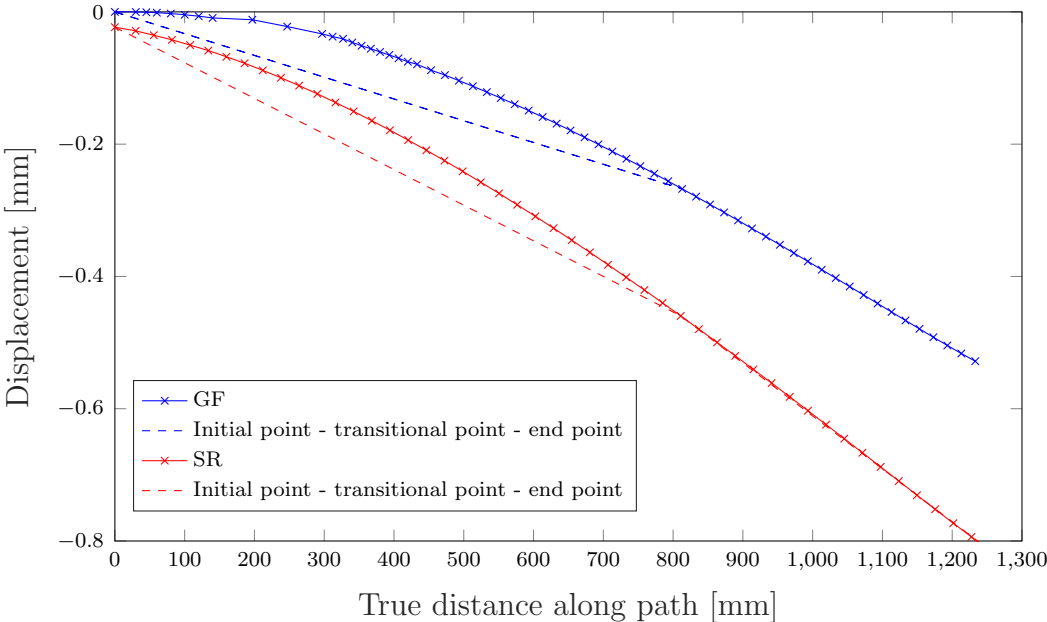


Figure 6.45: Comparison of displacements, where the dashed lines represent straight lines from the initial point, through the transition point, to the end points.

7 Discussion

In this chapter, the result from the problems addressed in this master thesis will be discussed. This includes choice of material in connector design, the efficiency and functionality of the parametric workflow, the structural behaviour of the GF and SR connector, and a comparison of the connector designs.

7.1 Choice of material - steel vs. aluminium

In section 3.1, the difference in weight between a connector design, used in a timber gridshell, in steel and aluminium was investigated. For the investigated connector design, it was found that the steel connector weighed 1.74 times the weight of the connector in aluminium with a equally design. However, a question that should be asked is if it is advantageous to have more lightweight connectors in gridshell structures. It is reasonable to think that for a timber gridshell consisting of thousands of connectors, the higher weight of the connector will increase the weight of the total structure significantly and affect the structural behaviour of the gridshell. In addition, the necessary cross-section, for a solid rectangular geometry, was calculated for both steel and aluminium from the given forces in chapter 2. The necessary cross-section of aluminium was found to be around 40-45 % bigger than the necessary cross section in steel. This, together with that the density of steel is about three times the density of aluminium, using aluminium may not give a significant reduction in the weight compared to using steel, for all connector designs.

7.2 The efficiency and functionality of the parametric workflow

The GH components that are developed, or further developed, during the work of this thesis, can successfully generate parametric FEA by constructing INP-files to be imported as models in Abaqus. The approach is versatile, and can be used to analyse solids parametrically. There are many possibilities, both geometrically, material wise and regarding loads and boundary conditions. It can be more efficient to set up and change the model in Grasshopper and purely run the analysis in Abaqus, as one does not have to go through all the modules in Abaqus step by step. For people that have no experience with Abaqus, but some experience with Rhino/Grasshopper, it can be a more intuitive and effective way to set up a FE model. However, there are certain issues and limitations that will be addressed and discussed in this section.

When the model is set up, one can easily adjust the parameters that are needed. In this way the model adapts itself accordingly and one can quickly run a new FEA. However, if the geometry is complex with many different parameters and parts, setting up the model for it to be fully parametric can become time consuming and the model can end up being quite comprehensive. In this way it can be quite difficult to control all the inputs and outputs to assure that the model is working and that the wires in grasshopper are assigned correctly, since one will end up with numerous wired inputs and outputs. For example, the whole GH assembly of the GF connector can be seen in figure 7.1, where it is observed that the model is quite extensive with a substantial amount of wires.

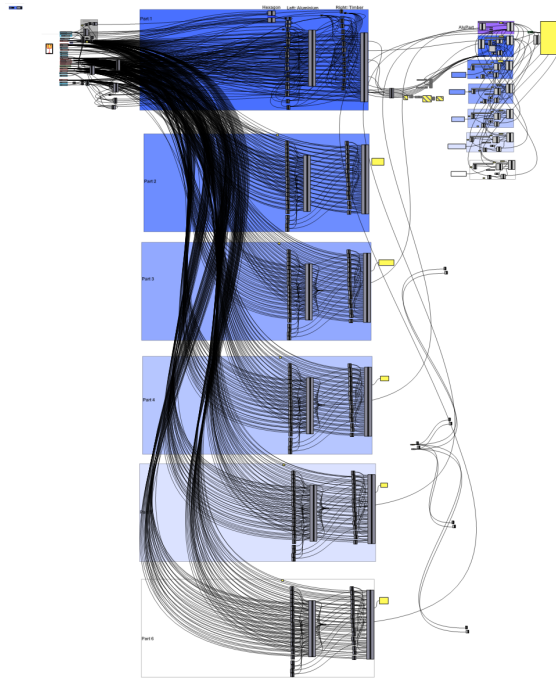


Figure 7.1: Whole Grasshopper assembly model for the GF connector

This is in large part because the mesh has to be consistent to get correct analysis results. By consistent, it means that when different meshes are somehow connected, the nodes of the meshes have to coincide, so that the nodes of one mesh are not placed in between the nodes of the other meshes. This can be seen in figure 7.2. For the whole GF connector, a total of $30 \cdot 6 = 180$ meshes was made to ensure consistent meshing and for the model to be fully parametric.

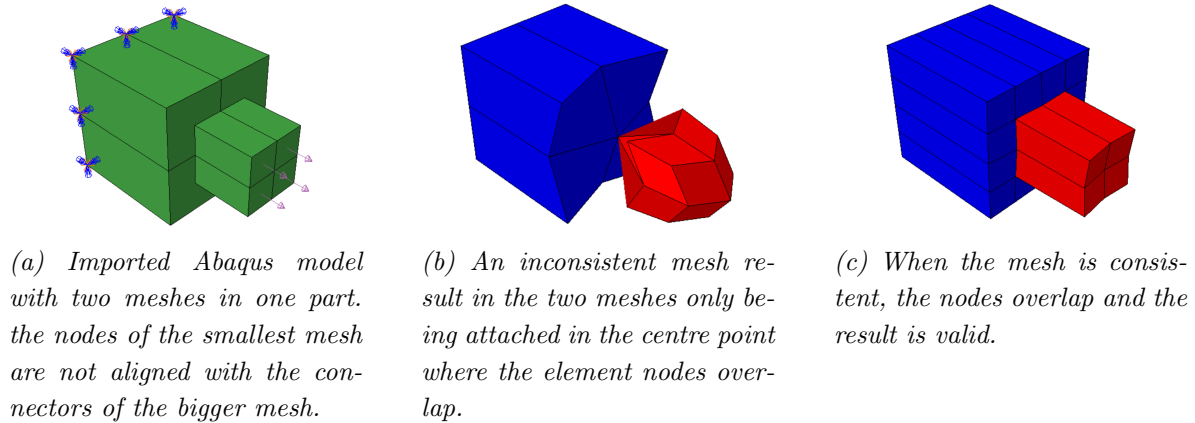


Figure 7.2: Example of an inconsistent and consistent mesh

For models with a large amount of elements, it can take several minutes for the code to run. This is due to the fact that the code runs through the whole node list to compare which nodes that should be assigned to the node sets, element list, element sets and so on. The effectiveness of the code could therefore be looked further into.

At present, the approach is restricted to 8 node hexahedral elements. However, it should not be too complicated to extend the code to work with hexahedral elements consisting of more nodes. It could also be interesting to look at how to mesh, or assign, other types of elements, to make the approach more versatile. Considering the often complex geometries of joints, such as bolt holes, bolts and so on, it is necessary to improve or adapt the mesh components to develop the approach. The current mesh components meshes through geometries where four vertices somehow can be extracted. This works well for many cases, but imposes issues for certain geometries and limits the approach as a whole.

7.3 Structural behaviour of Glued Finger connector

The results from the finite element analyses in Abaqus shows that for the simplified GF connector, when applied to compression, the stresses are mainly transferred through the inner splices, the mid plate and the inner plate. An increase in the size of the core, will not have a significant effect on the Mises stress when applying compression. When it comes to shear, it looks from the results that the inner plates and the core is taking up most of the stresses. When increasing the size of the core, the maximum Mises stress will have a significant reduction.

To look at how the GF connector is behaving when applying both moment and axial load, analyses with eccentricities was performed. From the result it was found that the bending stiffness about the vertical axis was little, as the maximum Mises stress became high compared to for the analysis with pure compression. The bending stiffness about the horizontal axis was not that high compared to the case with pure compression.

When looking at buckling of the inner plate in the GF connector, several buckling modes were found. For the buckling case with one leg of the GF connector, the buckling load was found to be 4100 kN. This is a quite high value, but since large forces can be induced in gridshells, efforts should be made to increase the buckling capacity. When looking at the buckling load of all legs in the whole connector, it was found to be 1029 kN. This result should be discussed since this buckling happened in the leg which was fixed, and it is therefore a question whether this result can be realistic or not. As it is impossible to model the boundary and loading condition similar to as in reality, the connector should have a design which prevents buckling.

7.4 Structural behaviour of Split Ring connector

From the analysis results in section 6.2 it has been showed that when applying only compression to the simplified SR connector, the maximum Mises stress are located in two of the bottom corners in the top ring, and two of the top corners in the bottom ring, symmetrically. Else, the stresses are pretty uniformly distributed in the split rings.

When applying only shear to the whole SR connector, it is reasonable to think that the stresses induced will mainly be transferred from the threaded rods to the rings. Since that the threaded rods was modelled in a simplified way by using tied contact in two columns in each side of the rings in the shear analysis, it is difficult to predict from the result how the stress distribution will be in reality. For the leg which is applied the maximum shear load, the maximum Mises stress appears in the tied connection between the timber and aluminium. The rest of the stresses in the corresponding side of the rings are located mostly at the top of the top ring and at the bottom of the bottom ring. However, the Mises stresses have quite low values, compared to when applying compression.

To induce a moment and axial load simultaneously, eccentricities have also been applied to one of the legs in the SR connector. As stated in section 6.2.1, it was found from the analysis results that when applying the eccentricity in the vertical direction, the maximum Mises stress became 14.5 % bigger than for pure compression. Whilst when

applying eccentricity in the horizontal direction, the stresses was equal to the stresses for pure compression. Therefore, the hexagonal shape of the split rings provides good bending stiffness in both directions, which is suitable for gridshells as they have varying loading conditions and angles between members. It was also tried to perform a buckling analysis of the SR connector, but without obtaining any informational results. However, buckling of a final design of the SR connector should be checked.

7.5 Comparing the designs of Glued Finger and Split Ring connector

When comparing the designs of the two connectors, several aspects should be considered. For instance, how stresses are distributed for different load cases, how the design is handling eccentricities and buckling, if the connections are easy to assemble at construction site, the rotational stiffnesses of the joints and how volume efficient the designs are.

Considering the stress distribution in the connectors, the two different connection types should be discussed. Though it is not made an analysis of what will happen in the connection between the threaded rods and the aluminium split rings, it is reasonable to think that sharp stress peaks may arise in the area where those parts are connected and where the bolt heads are pushing against the split rings. For the glued connection in the GF connector, sharp stress peaks in the bonded contact may arise if a stiff adhesive is chosen. However, if choosing a soft bonding type, this can be avoided and a more even shear stress distribution can be obtained. Another problem that has not been analysed is the connection between the connector core and the grippers. It is reasonable to think that high stress peaks may arise in this area.

Furthermore, when considering that the connector designs must handle eccentricities and be resistant against buckling, the GF connector design was found to be the most unstable. A suggestion on how to better the design according to this problem was suggested in section 6.1.3, where a plate was inserted perpendicular to the inner plate in the middle to accomplish higher bending stiffness about the weak axis of the inner plate. It was suggested to insert it in the middle to get the most volume efficient solution, but another option may be to insert plates at the top and bottom so that the cross-section of the inner plates becomes an I-profile. However, inserting a plate at the middle of the inner plate will make the design more stable against buckling, compared to an I-profile. Inserting plates perpendicular to the inner plate will also create more shear area to take up shear forces in the horizontal direction, which is beneficial as the

Mises stress became almost as high as the yield stress when applying horizontal shear to one leg.

Looking at the volume efficiency, which was done in section 6.3, it was found that when applying a compression load of 20 MPa, which induces a maximum Mises stress of 90 % of the yield stress in the optimised GF connector, the necessary volume of the SR connector, including threaded rods, was 58 % of the total volume of the optimised GF connector. When doing the same analysis for shear, the necessary volume of the SR connector is only 24 % of the optimised GF volume. This means that it is the case with compression that should be looked at, and the volume difference is significant as the volume of the GF connector is almost twice as big as the volume for the SR connector. The reason why the volume of the GF connector is so high is that it consists of many parts, where all have the same height as the height of the timber beam. Therefore, as it is observed that most of the stresses are taken up by the inner splices and almost no stresses by the outer splices, the question on whether these are necessary should be looked at. As discussed previously, it seems at least like the dimension of the outer splices, if they are included, can be minimised. However, as seen in figure 6.18b, when inserting a plate perpendicular to the middle of the inner plate and increasing the width of the additional plate to be equal to the length of the mid plate, the Mises stress increases in the outer splices.

Also, the rotational stiffness of the two types of joints is vital to investigate. The rotational stiffness of the joints in the GF connector is found to be twice as high as the rotational stiffness of the joints in the SR connector. On the other hand, the threaded rods is neglected in the analysis, so it reasonable to think that the rotational stiffness will be higher for the SR joints in reality.

Another important aspect that must be considered, is the practicality when assembling the structure at building site. Looking first at the GF connector, as stated in section 1.4.1, the thought is that all the grippers will be the same and the connection to the timber part can be prefabricated, while it is the connector cores with the inner plates that will be unique for all connectors in the gridshell. Furthermore, for the SR connector, the threaded rods are supposed to be prefabricated into the timber members, and the split rings are supposed to be unique for all connectors in the gridshell. This means that for the SR connector it need to be produced twice as many unique parts as for the GF connector. When it comes to assembling the gridshell with SR connectors, it will probably be more complicated as it is four parts that are supposed to connect

7.5 Comparing the designs of Glued Finger and Split Ring connector

all the six timber members, and two and two rings are supposed to be bolted together by six screws each. Whilst for the GF connector it is only one part that is supposed to connect the six timber members, and this will happen either by self-locking or by six screws. Thus, the GF connector can be argued for having the most practical solution for assembling.

8 Conclusion

Concerning the topic of parametric structural analysis and development of aluminium connectors in timber gridshells, conclusions can be drawn regarding both the approach to analyse the connectors parametrically, as well as the results of the analyses.

The parametric FE approach

The method of generating the INP-file in Grasshopper and import the whole model and run the FEA in Abaqus, proved to be successful with many possibilities. Mæhle (2017) created an extensive basis which have been implemented, altered and further developed to ease and expand the meshing functionality, add several different meshes into one part, add the possibility of having orthotropic materials with orientations and different type of loads. By using the components, one can model various geometries and easily adjust the parameters. However, there are certain issues and limitations that should be addressed. For complex geometries, setting up the model can be quite comprehensive. This is in large part because the mesh has to be consistent to get correct analysis results. Furthermore, the mesh components are currently limited to geometries which somehow has four corner points. In addition to this, for very fine meshes with a great amount of elements, it can take several minutes for the code to run as the code runs through the whole node list until it reaches the correct node to be assigned to the correct set.

Comparing the Glued Finger and Split Ring connector

When it comes to the structural design performed in section 3.2 and 3.3, Eurocode 5 do not provide sufficient information for designing the two connection types structurally. Therefore, both connections should be tested experimentally, as the equations used for the structural design of the SR connection with threaded rods are only assumed to be valid and are not validated experimentally, and the structural design of the glued GF connection is based on a lot of assumptions.

Summing up the arguments in the discussion about the GF connector and the SR connector, it is concluded from the results that the SR connector is the most volume efficient design. As it is found that the outer splices of the GF connector is taking up a small amount of stresses, the necessity of these should be discussed and investigated further. When it comes to which of the currently connector designs that counteracts eccentricities best and are most resistant against buckling, it is found from the results to be the SR connector, because of its high bending stiffness about both axes. However,

for the GF connector, it is proposed to insert plates perpendicular to the middle of the inner plates, to make the connector resistant against buckling and to handle eccentricities well.

Furthermore, the GF connector is argued to be the most practical design when assembling the structure at building site, as it consist of less parts which connects the timber members together. In addition, according to the analyses of the rotational stiffness, it is found that the GF connector provides higher rotational stiffness than the SR connector. However, it is reasonable to think that the original SR connector will provide a higher rotational stiffness in reality as the threaded rods were neglected in the simplified model of the SR connector.

Looking at stress distribution in both connectors, when applying shear to the GF connector, it is found that the stresses are concentrated in the core of the connector. To increase the shear capacity, increasing the size of the core is found to be a good solution. However, for the SR connector, the highest stresses are concentrated in the inner corners of the bottom ring. For compression applied to the GF connector, the highest stresses are located in the middle of the mid plate and the inner plates. On the other hand, for the SR connector the highest stresses are located at the inner corners of the connector, when applied to compression.

9 Recommendations for further work

To investigate further the topic of parametric structural analysis and development of aluminium connectors in timber gridshells, several recommendations can be made:

The parametric FE approach

- The Grasshopper components established are limited to 8 node elements as they are now. However, the mesh components should be quite easy to adapt with some extra coding, to create other hexahedral elements.
- It is important to assign timber parts the correct orientation. As the components are now, the orientations are not always correct when importing the model to Abaqus, so sometimes one have to manually change the orientation. Thus, this is something which could be looked further into.
- The current mesh components can only mesh between geometries with four corner points. Therefore, certain geometries can not be meshed which is a limitation factor of the components. A good idea is therefore to look at the possibility to develop components which can mesh more complex geometries.
- The load component are now only suited for uniformly distributed loads, so developing this to work for point loads as well could be interesting.
- As the components are now, the geometry and the FE model must be created simultaneously. Therefore, it would be beneficial if components, that easily generate the mesh from a given geometry, could be developed.
- It could also be interesting to program tools which automatically import and run the FEA in Abaqus without having to manually import the input file and run the analysis.
- A problem which often arises is that the total mesh can become inconsistent if the separate meshes are not modelled with node locations that are aligned to eachother. Thus, it could be looked at how to make it easier to make consistent meshes.
- To decrease the computational time, it can be beneficial to develop the *AbaqusPart* component further to create elements without having to iterate through the whole node list.

- The buckling step has been added to the model in Abaqus for buckling analyses, since the approach does not cover buckling analysis yet. Thus, how this can be included in GH components can be further investigated.

The Glued Finger and Split Ring connector

- The structural behaviour of the two connector designs, should be investigated further. As stated in the discussion about the stress distribution of the GF connector, the connection between core and the grippers has not been addressed in this thesis. As it is reasonable to think that high stress peaks may arise in this area, this is a vital part of the design and should be investigated. Also, the connection between the threaded rods and the split rings in the SR connector, has not been sufficiently analysed in this thesis, and should also be investigated.
- For the GF connector, the design should be updated to increase its bending stiffness to avoid buckling and minimise rotations due to eccentric loads. When it has been updated it should be reanalysed.
- The relevance of the outer splices should also be looked at, since they are only taking up a small amount of stresses.
- As Eurocode 5 do not provide sufficient information for designing the two connection types structurally, both the SR and GF connection should be tested experimentally. This includes experimental tests of how much spacing that is required between the threaded rods and the required distance to the end in the SR connector.
- It should be also investigated if the SR connector design could be further developed in a way which increases its efficiency and practicality when assembling the structure at building site.

Bibliography

- Arup (2013), 'Canary Wharf Crossrail station ©Arup'. Photo: ©Arup.
- Bell, K. (2014), *An engineering approach to finite element analysis*, Fagbokforlaget.
- Brun, H. K. (2019), *British Museum grid shell analysis*, NTNU. Project.
- Chilton, J. and Tang, G. (2016), *Timber gridshells: architecture, structure and craft*, Routledge.
- Cmglee (2011), 'Herbert Backstage Pass'. CC BY-SA. Retrieved 24-04-20.
URL: https://commons.wikimedia.org/wiki/File:Herbert_Backstage_Pass_cmglee_67.jpg
- Dassault Systèmes (2014), 'Abaqus 6.14 Online Documentation: Abaqus/CAE User's Guide'.
- Dassault Systèmes (2020), 'Abaqus/CAE: Complete solution for Abaqus finite element modeling, visualization and process automation'. Retrieved 21-04-20.
URL: <https://www.3ds.com/products-services/simulia/products/abaqus/abaquscae/>
- Davidson, S. (2020), 'Grasshopper: Algorithmic modeling for Rhino'. Retrieved 21-04-20.
URL: <https://www.grasshopper3d.com/>
- Dome of Visions (2013), 'Dome of visions: Nu også for studerende'. Photo: Paul Nybo Andersen. Retrieved 02-06-20.
URL: <http://domeofvisions.dk/dome-of-visions-nu-ogsaa-for-studerende/>
- Dome of visions (2017), 'Dome of Visions 3.0 / Atelier Kristoffer Tejlgaard'. Photo: Kristoffer Tejlgaard. Retrieved 02-06-20.
URL: <http://domeofvisions.dk/the-architecture/dome-3-0/>
- Dunn, A. (2005), 'British Museum Great Court roof'. CC BY-SA. Retrieved 17-05-20.
URL: <http://www.andrewdunnphoto.com/>
- Dyvik, S. H., Manum, B., Mork, J. H. and Luczkowski, M. (2019), 'Structural aluminium in architecture - the history and future of aluminium as a structural material'.
- ETA Danmark A/S (2013), 'European Technical Approval ETA-12/0114'.

BIBLIOGRAPHY

- ETA Danmark A/S (2016), ‘European Technical Approval ETA-11/0030’.
- Fondazione Renzo Piano (n.d.), ‘IBM Padiglione itinerante’. Photo: ©Gianni Berengo Gardin. Retrieved 04-06-20.
URL: <https://www.fondazionerenzopiano.org/it/project/ibm-padiglione-itinerante/#section-images-498>
- Harris, R. (2011), ‘Design of timber gridded shell structures’, *Proceedings of the Institution of Civil Engineers*, 164(2), pp.105–116. .
- Harris, R., Gusinde, B. and Roynon, J. (2012), ‘Design and construction of the pods sports academy, scunthorpe, england’, *WCTE: World conference on Timber Engineering* .
- Karamba3D (2020), ‘Karamba3D: Parametric Engineering’. Retrieved 21-04-20.
URL: <http://karamba3d.com/>
- Labonnote, S. (2015), ‘Trondheim gridshell 2015’. Retrieved 03-06-20.
URL: <https://www.ntnu.edu/kt/research/csdg/research/trondheim-gridshell>
- Labonnote, S. (2016), ‘PrintShell 2016’. Retrieved 03-06-20.
URL: <https://www.ntnu.edu/kt/research/csdg/research/printshell>
- Lopez, A., Puente, I. and Aizpurua, H. (2011), ‘Experimental and analytical studies on the rotational stiffness of joints for single-layer structures, Engineering Structures volume 33’.
- Malo, K. A. (2018), Anisotropy in Wooden Materials, Technical report, Norwegian University of Science and Technology (NTNU). NTNU TKT4212 Timber Structures 2, Lecture notes.
- Mazzolani, F. M. (2008), ‘Design of Aluminium Structures’.
- MIT (2017), ‘Writing the input file only’. Retrieved 03-05-20.
URL: <https://abaqus-docs.mit.edu/2017/English/SIMACAECAERefMap/simacae-c-anajobmanwritebtn.htm>
- Monasterio, M., Goñi, J. and Cabañas, A. (2018), ‘Development of a bolted system for timber gridshells’, *Proceedings of the IASS symposium 2018 Boston, Creativity in structural design* .

BIBLIOGRAPHY

- MX3D (2020), ‘Connector for Takenaka’. Photo: ©Leonard Fäustle. Retrieved 03-06-20.
URL: <https://mx3d.com/projects/takenaka-connector/>
- Mæhle, H. R. (2017), The parametric design of adaptive joints, Master’s thesis, Norwegian University of Science and Technology (NTNU), Department of Structural Engineering.
- Müller, U. (2010), *Introduction to Structural Aluminium Design*, Dunbeath: Whittles Publishing.
- Otarawanna, S. and Dahle, A. K. (2011), *Fundamentals of aluminium metallurgy, chapter 6: Casting of aluminium alloys*, Woodhead Publishing.
- R. McNeel & Associates (2020), ‘Rhinoceros: design, model, present, analyze, realize’. Retrieved 21-04-20.
URL: <https://www.rhino3d.com/>
- Rossi, P. (2005), ‘Dettaglio del British Museum (Londra 2005)’. Public domain. Retrieved 17-05-20.
URL: [https://commons.wikimedia.org/wiki/File:Dettaglio_del_British_Museum_\(Londra_2005\).jpg](https://commons.wikimedia.org/wiki/File:Dettaglio_del_British_Museum_(Londra_2005).jpg)
- Seele (2014), ‘Canary wharf crossrail station’. Photo: Nigel Young.
URL: <https://seele.com/references/canary-wharf-crossrail-station>
- Seifi, H. (2019), ‘Topology Optimisation and Additive Manufacturing of Structural Nodes of Gridshell Structures’.
- Seifi, H., Javan, A. R., Lin, X. and Xie, Y. M. (2020), ‘An innovative and inexpensive experimental setup for testing connections in gridshell structures’.
- Shivkumar, S., Wang, L. and Apelian, D. (1990), ‘The lost-foam casting of aluminum alloy components. JOM 42, 38–44’. Retrieved 14-02-20.
URL: <https://doi.org/10.1007/BF03220435>
- Stamatopoulos, H. (2016), Withdrawal Properties of Threaded Rods Embedded in Glued-Laminated Timber Elements, PhD thesis, Norwegian University of Science and Technology (NTNU), Department of Structural Engineering.
- Stamatopoulos, H. (2019), Joints based on glue. NTNU TKT4212 Timber Structures 2, Lecture notes.

- Stamatopoulos, H. and Malo, K. A. (2015*a*), Characteristic withdrawal capacity and stiffness of threaded rods, Technical report, Norwegian University of Science and Technology (NTNU).
- Stamatopoulos, H. and Malo, K. A. (2015*b*), Withdrawal capacity of threaded rods embedded in timber elements, Technical report, Department of Structural Engineering, Norwegian University of Science and Technology (NTNU).
- Standard Norge (2009*a*), ‘NS-EN 1993-1-8:2005+NA:2009. Eurocode 3: Design of steel structures. Part 1-8: Design of joints’.
- Standard Norge (2009*b*), ‘NS-EN 1999-1-1:2007+A1:2009+NA:2009. Eurocode 9: Design of aluminium structures. Part 1-1: General structural rules’.
- Standard Norge (2010*a*), ‘NS-EN 1706:2010. Aluminium and aluminium alloys, Castings, Chemical composition and mechanical properties’.
- Standard Norge (2010*b*), ‘NS-EN 1706:2010. Aluminium and aluminium alloys, castings, chemical composition and mechanical properties’.
- Standard Norge (2010*c*), ‘NS-EN 1995-1-1:2004+A1:2008+NA:2010. Eurocode 5: Design of timber structures. Part 1-1: General common rules and rules for buildings’.
- Standard Norge (2015), ‘NS-EN 1993-1-1:2005+A1:2014+NA:2015. Eurocode 3: Design of steel structures. Part 1-1: General rules and rules for buildings’.
- Standard Norge (2018), ‘NS-EN 1090-2:2018. Execution of steel structures and aluminium structures. Part 2: Technical requirements for steel structures’.
- Stephan, S., Sánchez-Alvarez, J. and Knebel, K. (2004), ‘Reticulated structures on free-form surfaces’.
- Vallée, T., Tannert, T. and Fecht, S. (2017), ‘The journal of adhesion - Adhesively bonded connections in the context of timber engineering - A review’.
- Vallée, T., Tannert, T. and Hehl, S. (2011), ‘Experimental and numerical investigations on full-scale adhesively bonded timber trusses. Mater Struct 44, 1745’.
- Westmuckett Hawkes Ltd (2010), ‘Scunthorpe Sports Academy’. Retrieved 02-06-20.
URL: <http://www.westmucketthawkes.com/about-us/>
- Worsfold, T., Bryant, M. and Crack, J. (2018), ‘Design of canary wharf elizabeth line station and crossrail place oversite development’, *The Structural Engineer* .

Appendices

A Comparing connectors in aluminium and steel

A.1 Detailed calculation of necessary aluminium cross-section

Here, the detailed calculations from chapter 2.1 are given. A width of 30 mm is assumed to find the necessary cross-section, which gives the following expressions for the design resistances:

$$N_{Rd} = \frac{h \cdot 30\text{mm} \cdot 180\text{MPa}}{1.1} = \frac{h \cdot 5400\text{N/mm}}{1.1}$$

$$M_{y,Rd} = \frac{\frac{30\text{mm} \cdot h^2}{6} \cdot 180\text{MPa}}{1.1} = \frac{900\text{N/mm} \cdot h^2}{1.1}$$

$$M_{z,Rd} = \frac{\frac{(30\text{mm})^2 \cdot h}{6} \cdot 180\text{MPa}}{1.1} = \frac{27000\text{N} \cdot h}{1.1}$$

Inserting these expressions in equation 2.1, gives the following equation:

$$\left(\frac{68600\text{N}}{\frac{h \cdot 5400}{1.1}} \right)^2 + \left[\left(\frac{15.79 \cdot 10^6 \text{Nmm}}{\frac{h^2 \cdot 900}{1.1}} \right)^{1.7} + \left(\frac{0.45 \cdot 10^6 \text{Nmm}}{\frac{h \cdot 27000}{1.1}} \right)^{1.7} \right]^{0.6} \leq 1.0$$

Solving this equation for h, gives a necessary height of 141 (140.92) mm. The necessary cross-section is $A = b \cdot h = 30\text{mm} \cdot 141\text{mm} = 4230\text{mm}^2$.

In the end, it need to be checked that $V_{Ed} \leq 0.5 \cdot V_{Rd}$. By inserting the necessary values in equation 2.5 for the shear design resistance, the following expression is obtained:

$$V_{Rd} = 0.8 \cdot 4230\text{mm}^2 \cdot \frac{180\text{MPa}}{\sqrt{3} \cdot 1.1} = 319.70\text{kN}$$

This gives the following

$$V_{Ed} = 3.04\text{kN} < 0.5 \cdot V_{Rd} = 159.85\text{kN}$$

The criteria is thus found to be fulfilled.

A.2 Detailed calculation of necessary steel cross-section

Here, the detailed calculations from section 2.2 are given. A width of 30 mm is assumed to find the necessary steel cross-section, which gives the following expressions for the design resistances:

$$N_{Rd} = \frac{h \cdot 30mm \cdot 355MPa}{1.05} = \frac{h \cdot 10650N/mm}{1.05}$$

$$M_{y,Rd} = \frac{\frac{30mm \cdot h^2}{4} \cdot 355MPa}{1.05} = \frac{2662.5N/mm \cdot h^2}{1.05}$$

$$M_{z,Rd} = \frac{\frac{(30mm)^2 \cdot h}{4} \cdot 355MPa}{1.05} = \frac{79875N \cdot h}{1.05}$$

Inserting these expressions in equation 2.7, gives the following equation:

$$\left(\frac{68600N}{\frac{h \cdot 10650N/mm}{1.05}} \right)^2 + \left(\frac{15790000Nmm}{\frac{2662.5N/mm \cdot h^2}{1.05}} \right) + \left(\frac{450000Nmm}{\frac{79875N \cdot h}{1.05}} \right) \leq 1.0$$

Solving this equation for h, gives a necessary height of 82.23 mm. The necessary cross-section is $A = b \cdot h = 30mm \cdot 82.23mm = 2466.9mm^2$.

In the end, it need to be checked that $V_{Ed} \leq 0.5 \cdot V_{Rd}$. If this is verified there should be no reduction of the resistances defined for axial force and bending. By inserting the necessary values in equation 2.11 for the shear design resistance, the following expression is obtained:

$$V_{Rd} = A_v \cdot \frac{f_{yk}}{\sqrt{3} \cdot \gamma_{M0}} = 2466.9mm \cdot \frac{355MPa}{\sqrt{3} \cdot 1.05} = 481.4kN$$

This gives the following

$$V_{Ed} = 3.04kN < 0.5 \cdot V_{Rd} = 240.7kN$$

The criteria is thus found to be fulfilled.

B Structural design of timber-to-metal connections

B.1 Difference in weight of connector in aluminium and steel

In this section, the calculation of the estimation of the difference in weight of a connector in aluminium and steel is given. First, the calculation of the weight of a connector in aluminium is given and then the weight calculation of a connector in steel. The problem was described in section 3.1, and the calculation is done in Excel.

Capacity of connection with laterally loaded bolts + weight calculation		
		Yield moment: M _{y,Rk} : 59477.7 Nmm
		Embedment strength: f _{h,k} : 28.9 N/mm ²
Parameters	Value	
d	12	mm
t metal plate	20	mm
rho_k (GL32c)	400	kg/m ³
t ₁	70	mm
t ₂	180	mm
d ₀	13	mm
rho_alu	2700	kg/m ³
f _{t,0,k}	19.5	N/mm ²
k _{mod}	0.8	
gamma_m	1.3	
f _{v,k}	3.5	N/mm ²
# rows	2	
alpha_v	0.5	
f _{ub}	310	N/mm ²
A _{bolt}	113.1	mm ²
gamma_m2	1.25	
t _{ef} (d)	29.86	mm
L _{net,t}	48	mm
L _{net,v}	648	mm
n	5	
n _{ef}	3.352	
A _{net,t}	3360	mm ²
A _{net,v} (inner)	45360	mm ²
A _{net,v} (outer)	34900.3	mm ²
A _{net,v} (tot)	115160.6	mm ²
# Shear planes	4	
F _{v,Ed}	145750	N
b_wood	120	mm
h_wood	350	mm
b_alu	62.4	mm
l_alu	145.6	mm
Final aluminium plate dimension:		
b _{min}	200	mm
l _{min}	271.2	mm
V bolts	39584.1	mm ³
V alu plates:	1084800.0	mm ³
V hexagonal:	2078461.0	mm ³
V total:	17570362.6	mm ³
m total:	47.44	kg
Thick cross-section: (Johansens eq.)	Outer members: (single shear)	F _{v,Rk} (c): 24245.8 N F _{v,Rk} (d): 11224.2 N F _{v,Rk} (e): 10439.4 N (rope effect neglected)
	Inner members: (double shear)	F _{v,Rk} (l): 31173.1 N F _{v,Rk} (m): 10439.4 N (rope effect neglected)
	One bolt:	F _{v,Rk} : 41757.4 N F _{v,Rd} : 25696.9 N
	Necessary # of bolts:	5.7 6.0
	# bolts in one row:	3
Shear resistance: (one bolt)	F _{v,Rd} :	56096.3 N
	Necessary # of bolts:	2.6 4
	#bolts in one row	2
Splitting grain: (all bolts)	F _{v,ef,Rd} :	172282.1 N
	# bolts in one row:	5
Block Shear: (all bolts)	F _{v,Rd} :	173626.8 N
	# bolts in one row:	5
bolt resistance, all: 560962.8 N		
Spacings:	Wood part:	a1: 60 mm a2: 48 mm a3,t: 84 mm a4,c: 36 mm
	Alu part:	e1: 15.6 mm e2: 15.6 mm p1: 28.6 mm p2: 31.2 mm

Figure B.1: Weight calculation of aluminium connector

B.1 Difference in weight of connector in aluminium and steel

Capacity of connection with laterally loaded bolts + weight calculation		
	Yield moment	M _{y,Rk} 76745.4 Nmm
	Embedment strength:	f _{h,k} : 28.9 N/mm ²
Parameters	Value	
d	12	mm
t metal plate	20	mm
rho_k (GL32c)	400	kg/m ³
t ₁	70	mm
t ₂	180	mm
d ₀	13	mm
rho_steel	7850	kg/m ³
f _{t,0,k}	19.5	N/mm ²
k _{mod}	0.8	
gamma_m	1.3	
# rows	2	
f _{ub}	400	N/mm ²
A _{bolt}	113.1	mm ²
f _{v,k}	3.5	N/mm ²
Shear planes	4	
t _{ef} (d)	30.11	mm
L _{net,t}	48	mm
L _{net,v}	648	mm
n	5	
n _{ef}	3.352	
A _{net,t}	3360	mm ²
A _{net,v} (inner)	45360	mm ²
A _{net,v} (outer)	35061.9	mm ²
A _{net,v} (tot)	115483.7	mm ²
F _{v,Ed}	145750	N
b _{wood}	120	mm
h _{wood}	350	mm
b _{steel}	62.4	mm
l _{steel}	145.6	mm
Final steelplate dimension:		
b _{min}	129	mm
l _{min}	271.2	mm
V bolts:	39584.1	mm ³
V steel plate:	699696.0	mm ³
V hexagonal:	864691.7	mm ³
V total:	10521576.1	mm ³
m total:	82.59	kg
Thick cross-section: (Johansens eq.)	Outer members:	F _{v,Rk,(c)} : 24245.8 N
	(single shear)	F _{v,Rk,(d)} : 11559.9 N (rope effect neglected)
		F _{v,Rk,(e)} : 11858.3 N (rope effect neglected)
	Inner members:	F _{v,Rk,(l)} : 31173.1 N
	(double shear)	F _{v,Rk,(m)} : 11858.3 N (rope effect neglected)
	One bolt:	F _{v,Rk} : 46836.3 N
		F _{v,Rd} : 28822.4 N
	Necessary # of bolts:	5.1 6
	# bolts in one row:	3
Shear resistance:	F _{v,Rd} :	72382.3 N
(one bolt)	Necessary # of bolts:	2.0 4
	# bolts in one row:	2
Splitting grain:	F _{v,ef,Rd} :	193236.6 N
(all bolts)		
	# bolts in one row:	4
Block Shear:	F _{v,Rd} :	174113.9 N
(all bolts)		
	# bolts in one row:	5
	bolt resistance, all	723822.9 N
Spacings:	Wood part:	a1: 60 mm
		a2: 48 mm
		a3,t: 84 mm
		a4,c: 36 mm
	Steel part:	e1: 15.6 mm
		e2: 15.6 mm
		p1: 28.6 mm
		p2: 31.2 mm

Figure B.2: Weight calculation of steel connector

B.2 Necessary glue surface in Glued Finger connector

In this section, the calculation of the estimation of the necessary glue surface and splice lengths is given. The problem was described in section 3.2, and the calculation is done in Excel.

Necessary glue area and splice length		
Parameters	Value	
b	350	mm
t ₁	48	mm
E ₁	11200	N/mm ²
A ₁	16800	mm ²
t ₂	14	mm
E ₂	70000	N/mm ²
A ₂	4900	mm ²
d _g	1	mm
G _{glue}	500	N/mm ²
F _{Ed}	167287.5	N
Gamma	500	
alpha	0.549	(<= 1)
tau _f	3	N/mm ²
L_{inner}	44.50	mm
L _{outer}	22.25	mm

F_{Ed} one side of one inner splice:	33457.5 N
Omega:	1.689
F_{max}:	33457.5 N
Necessary glue area: (all splices)	77867.3 mm ²

Figure B.3: Necessary glue surface and splice lengths in GF connector

B.3 Diameter and penetration length of threaded rods in Split Ring connector

In this section, the calculation of the estimation of the diameter and penetration length of the threaded rods in the SR connector is given. The problem was described in section 3.3, and the calculation is done in Excel.

Necessary diameter and penetration length of threaded rods in SR connector			
Parameters	Value		
alpha	10	degrees	
CS height	350	mm	
CS width	200	mm	
n	2	(# rods in one row)	
n_ef	1.87		
f_ax,k	11.92	N/mm ²	
rho_a	400	kg/m ³	
rho_k	400	kg/m ³	
d	22.1	mm	
d_ef	24.32	mm	
A_s	383.82	mm ²	
L	498.6	mm	
f_u,k	310	N/mm ²	
f_y,k	260	N/mm ²	
gamma_M2	1.25		
gamma_M	1.3		
k_mod	0.8		
E	70000	N/mm ²	
gamma_M1	1.1		
k_90	1.71		
N_pl,k	99794.4	N	
kappa_c	0.792		
k	0.768		
lambda_k	0.589		
N_ki,k	288143.9	N	
I	11723.46	mm ⁴	
k_v,alpha,k	101.17		
# rows	2		
e_0	217.36	mm	

Characteristic yield moment:	M_y,Rk	373129.7	Nmm
Embedment strength:	f_h,alpha,k	20.5	N/mm ²
Design shear capacity:	F_v,Rd	22143.3	N (for two rods)
Design withdrawal capacity:	F_ax,alpha,Rd	67712.2	N
Design tensile capacity:	F_tens,Rd	85669.7	N
Design buckling capacity:	F_ki,Rd	57494.5	N
Design axial capacity:	F_ax,Rd	107288.6	N (for two rods)
Design shear load:	F_v,Ed	1520	N (for two rods)
Design axial load:	F_ax,Ed	106944.3	N (for two rods)
Failure criterion:		1.00	(must be <1)

Spacings:	r	66.32	mm (3d)
	s	44.21	mm (2d)
	x	86.57	mm
Maximum height:	h	350.00	mm (350mm=max)
	a2	44.21	mm
	a2,CG	66.32	mm
Maximum width	w	176.85	mm (200mm=max)

Figure B.4: Estimated calculations of diameter and penetration length of threaded rods in SR connector

C Benchmarks - comparing structural behaviours

Here, more detailed tables and additional figures from the benchmarks in chapter 4 are given.

C.1 Case 1 - Cantilever

Table C.1: Cantilever stresses for orthotropic material

Mesh	Elements	S11 [MPa]	S22 [MPa]	S33 [MPa]	S12 [MPa]
1x1x10	10	2.67316	0.01135	0.06493	-0.09500
2x2x20	80	2.85515	0.09847	0.09530	-0.09002
3x3x30	270	3.09318	0.13294	0.11089	-0.09189
4x4x40	640	3.25799	0.15313	0.12016	-0.09836
5x5x50	1250	3.39387	0.16777	0.12709	-0.10433
6x6x60	2160	3.50967	0.17901	0.13256	-0.11056
7x7x70	3430	3.61235	0.18825	0.13717	-0.11645
8x8x80	5120	3.70517	0.19607	0.14115	-0.12206
9x9x90	7290	3.79034	0.20290	0.14470	-0.12736
10x10x100	10000	3.86934	0.20896	0.14790	-0.13238
11x11x110	13310	3.94320	0.21444	0.15084	-0.13713
12x12x120	17280	4.01271	0.21944	0.15355	-0.14163
14x14x140	27440	4.14096	0.22833	0.15848	-0.14997
16x16x160	40960	4.25755	0.23611	0.16287	-0.15758
20x20x200	80000	4.46439	0.24937	0.17053	-0.17100
25x25x250	156250	4.68706	0.26306	0.17866	-0.18528
30x30x300	270000	4.88137	0.27466	0.18569	-0.19754

Table C.2: Cantilever stresses for isotropic material

Mesh	Elements	S11 [MPa]	S22 [MPa]	S33 [MPa]	S12 [MPa]
1x1x10	10	2.59708	-0.11800	0.59000	-0.10000
2x2x20	80	2.80000	0.57000	0.91500	-0.02530
3x3x30	270	2.99983	0.82800	1.06750	-0.01520
4x4x40	640	3.15787	0.97700	1.15232	-0.03580
5x5x50	1250	3.29985	1.08199	1.22000	-0.06000
6x6x60	2160	3.43161	1.16516	1.26991	-0.09010
7x7x70	3430	3.55590	1.23485	1.31663	-0.11800
8x8x80	5120	3.67409	1.29566	1.35912	-0.14600
9x9x90	7290	3.78703	1.35010	1.39862	-0.17200
10x10x100	10000	3.89534	1.39977	1.44000	-0.20000
11x11x110	13310	3.99949	1.44569	1.47118	-0.22100
12x12x120	17280	4.09987	1.48857	1.50501	-0.24400
14x14x140	27440	4.29058	1.56719	1.56889	-0.28700
16x16x160	40960	4.46960	1.63842	1.62867	-0.32600
20x20x200	80000	4.79877	1.76498	1.74000	-0.40000
25x25x250	156250	5.16747	1.90235	1.86256	-0.47000
30x30x300	270000	5.49970	2.02366	1.97495	-0.53500

Table C.3: Comparison of cantilever displacement

Mesh	Elements	U2 [mm] Isotropic	U2 [mm] Orthotropic
1x1x10	10	-1.49649	-1.58000
2x2x20	80	-1.49191	-1.57984
3x3x30	270	-1.49600	-1.58779
4x4x40	640	-1.49828	-1.59134
5x5x50	1250	-1.49963	-1.59319
6x6x60	2160	-1.50051	-1.59426
7x7x70	3430	-1.50111	-1.59495
8x8x80	5120	-1.50155	-1.59541
9x9x90	7290	-1.50187	-1.59574
10x10x100	10000	-1.50213	-1.59598
11x11x110	13310	-1.50233	-1.59616
12x12x120	17280	-1.50249	-1.59631
14x14x140	27440	-1.50274	-1.59651
16x16x160	40960	-1.50292	-1.59666
20x20x200	80000	-1.50316	-1.59683
25x25x250	156250	-1.50333	-1.59695
30x30x300	270000	-1.50344	-1.59702

C.2 Case 2 - Column

Table C.4: Column stresses for orthotropic material

Mesh	Elements	S11 [MPa]	S22 [MPa]	S33 [MPa]	S12 [MPa]
1x1x10	10	-0.01000	-0.00066	-0.00044	0.00000
2x2x40	160	-0.01049	-0.00067	-0.00044	-0.00015
3x3x50	450	-0.01077	-0.00069	-0.00045	-0.00020
4x4x80	1280	-0.01126	-0.00071	-0.00046	-0.00029
5x5x80	2500	-0.01161	-0.00072	-0.00047	-0.00034
6x6x118	4248	-0.01194	-0.00074	-0.00048	-0.00037
8x8x154	9856	-0.01252	-0.00076	-0.00050	-0.00043
10x10x200	20000	-0.01310	-0.00079	-0.00052	-0.00049
13x13x250	42250	-0.01376	-0.00082	-0.00054	-0.00054
16x16x323	82688	-0.01445	-0.00085	-0.00056	-0.00059
20x20x400	160000	-0.01516	-0.00089	-0.00059	-0.00064

Table C.5: Column stresses for isotropic material

Mesh	Elements	S11 [MPa]	S22 [MPa]	S33 [MPa]	S12 [MPa]
1x1x10	10	-0.01000	-0.00429	-0.00429	0.00000
2x2x40	160	-0.01085	-0.00441	-0.00441	-0.00050
3x3x50	450	-0.01132	-0.00458	-0.00458	-0.00076
4x4x80	1280	-0.01235	-0.00484	-0.00484	-0.00113
5x5x80	2500	-0.01308	-0.00506	-0.00506	-0.00134
6x6x118	4248	-0.01374	-0.00526	-0.00526	-0.00150
8x8x154	9856	-0.01496	-0.00565	-0.00565	-0.00175
10x10x200	20000	-0.01624	-0.00605	-0.00605	-0.00201
13x13x250	42250	-0.01764	-0.00652	-0.00652	-0.00223
16x16x323	82688	-0.01923	-0.00703	-0.00703	-0.00250
20x20x400	160000	-0.02082	-0.00757	-0.00757	-0.00274

Table C.6: Comparison of buckling coefficient

Mesh	Elements	Buckling Coefficient	
		Isotropic	Orthotropic
1x1x10	10	2059.6	2010.3
2x2x40	160	2057.7	1994.9
3x3x50	450	2028.6	1920.2
4x4x80	1280	2008.7	1874.4
5x5x80	2500	1993.6	1841.4
6x6x118	4248	1981.8	1816.2
8x8x154	9856	1963.5	1778.4
10x10x200	20000	1949.1	1750.3
13x13x250	42250	1933.3	1719.2
16x16x323	82688	1920.2	1695.1
20x20x400	160000	1907	1670.5

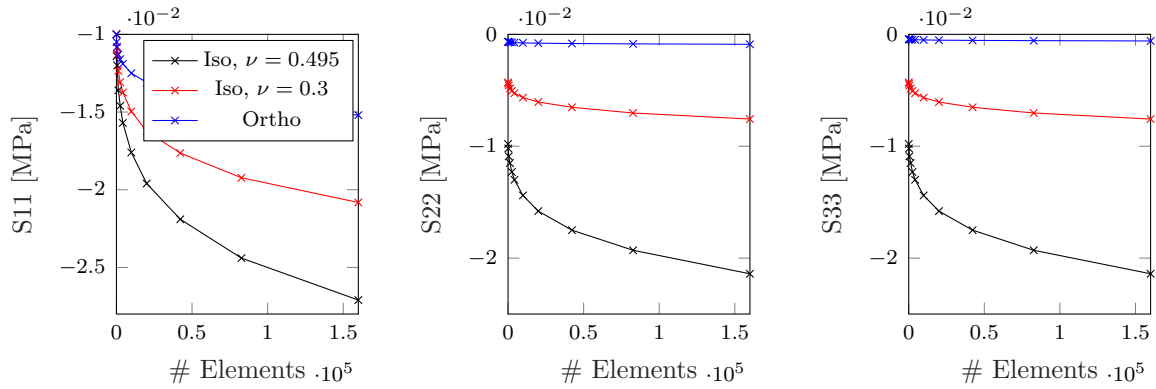


Figure C.1: Principal stresses case 2

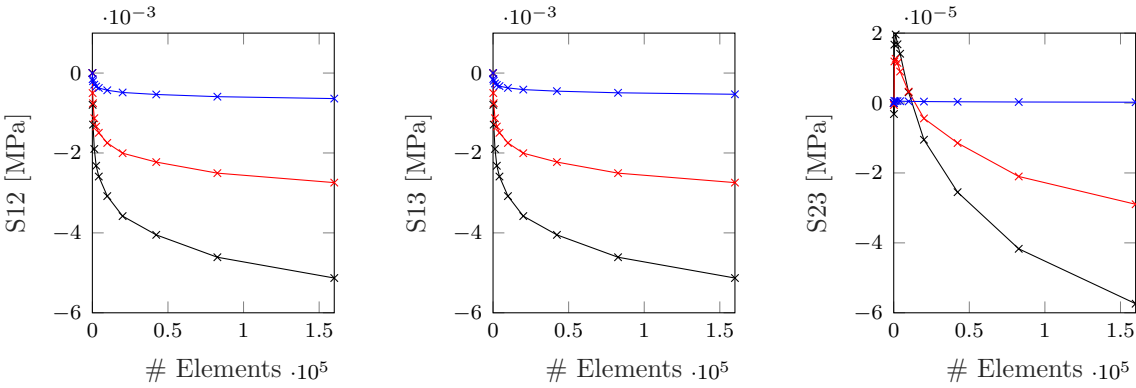


Figure C.2: Shear stresses case 2

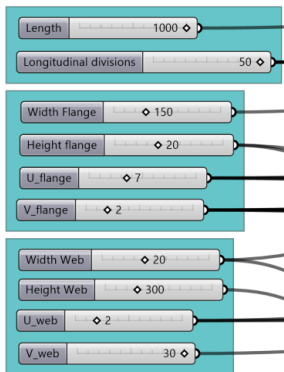
D Parametric FEM model examples

The parametric FE model examples that can be found in appendix E.2 are gathered in a separate GH file. The model examples are sorted in groups with headings to easily distinguish the different examples. To save computation space, parts of the assemblies have temporarily been *disabled*, and should be *enabled* before generating the INP file. To run the code and create the input file, the *boolean toggle*, marked in red, have to be set to *true*.

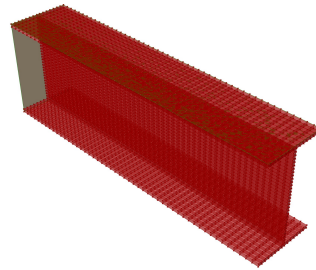
Two of the parametric FE model examples are elaborated further; the I-beam and the shell model. The rest can be viewed and further explored in the attached GH file.

D.1 I-Beam

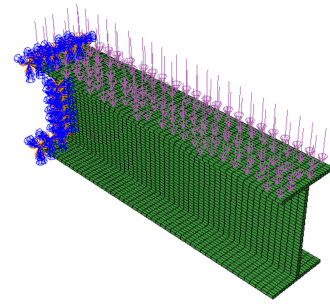
A cantilever I-beam have been modelled parametrically where a total load of 10 kN have been distributed over the top flange surface. By changing the width and height of both the flanges and the web, the length of the beam, size of the mesh, the load and boundary conditions, the model can easily be adapted, see figure D.1.



(a) Geometrical parameters

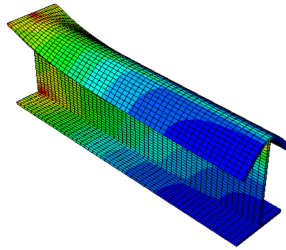
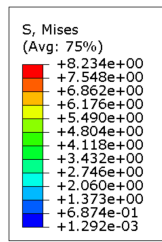


(b) Geometry in Rhino

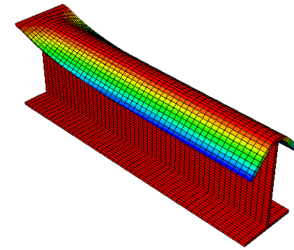
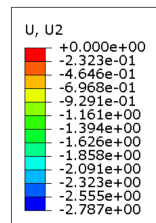


(c) Imported model in Abaqus with Load and BC's

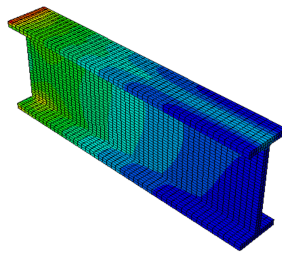
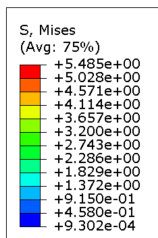
D.1 I-Beam



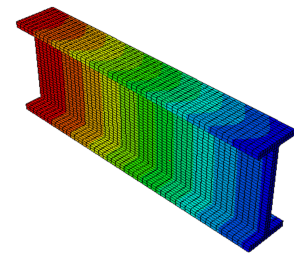
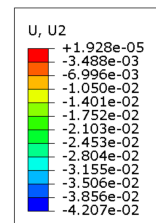
(d) Mises distribution of a slender I-profile with deformation



(e) Vertical displacements of the same I-beam



(f) When decreasing the web's width and increasing the thickness of both the flange and webs, the stress is more evenly distributed

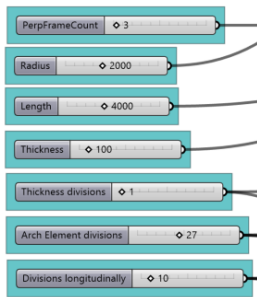


(g) The displacements are also more evenly distributed

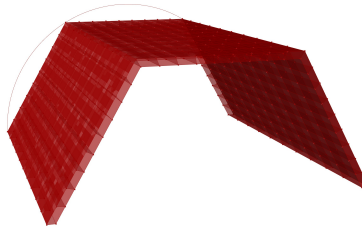
Figure D.1: I-Beam

D.2 Shell

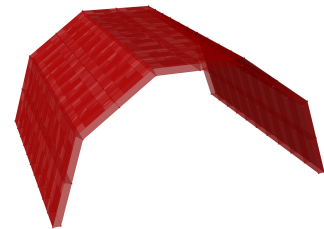
A shell have been modelled, from an *Arc* curve, with an arbitrary number of divisions. In addition, a pressure of 1 MPa have been applied on top of the roof in various ways as seen in figure D.2. It is possible to change numerous parameters such as the radius, the length and the thickness. To show different configurations and results, and to save computational time, a coarse mesh has been used. It should be noted that *Shell elements* should be used to model shells more properly, which is out of scope of this approach.



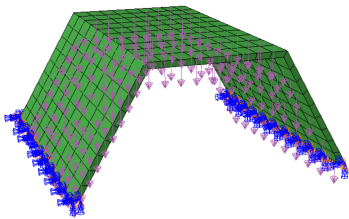
(a) Geometrical parameters



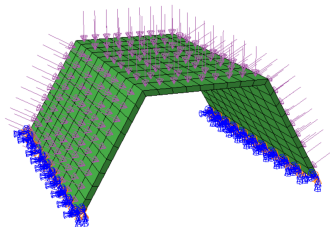
(b) Shell created from an arc divided in three



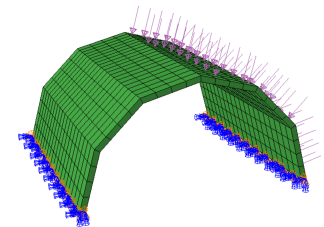
(c) Shell created from an arc divided in five



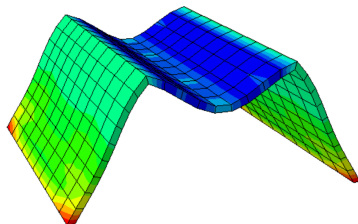
(d) Surface traction working downwards



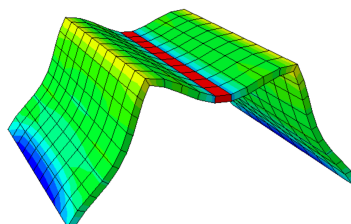
(e) Uniform pressure



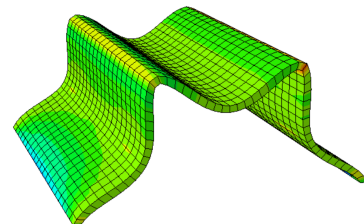
(f) Uniform pressure over half the roof



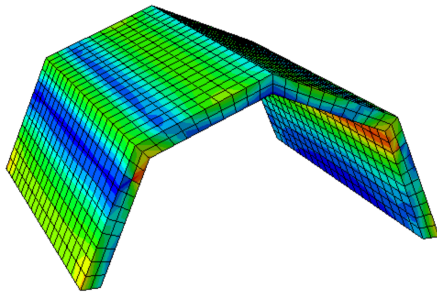
(g) Surface traction downwards Mises stresses



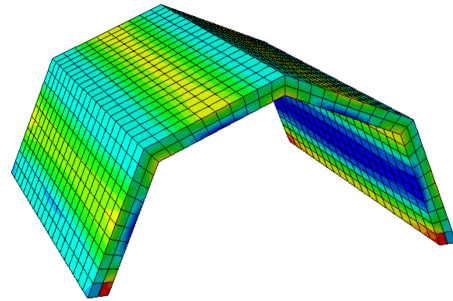
(h) Uniform pressure: Mises stresses. A coarse mesh result in



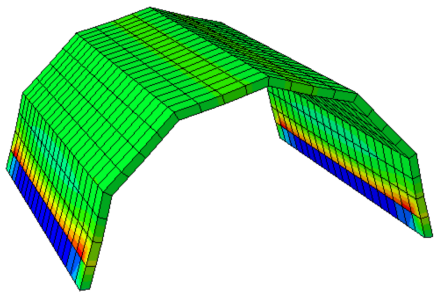
(i) Finer Mesh



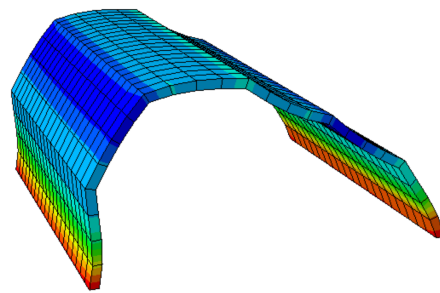
(j) Surface traction: Mises stresses



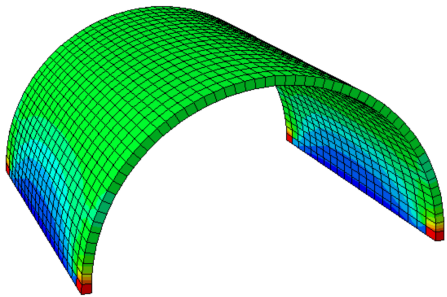
(k) Uniform pressure: Mises stresses



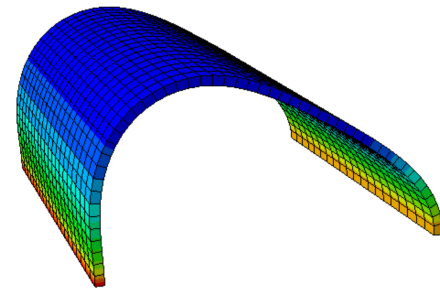
(l) Uniformly distributed load over the whole shell



(m) Uniformly distributed load over half of the shell



(n) Uniformly distributed load over the whole, circular shell



(o) Uniformly distributed load over half of circular shell

Figure D.2: Parametric FE Shell model

E Grasshopper files attached

Grasshopper files that are attached as a ZIP-file

E.1 Components

E.2 ModelExamples.gh

E.3 GFConnector.gh

E.4 SRConnector.gh

